Monitoring and Analysis of Manufacturing Processes in Automotive Production

Volume 7

ISBN 978-3-96595-021-4
e-ISSN (PDF) 2629-3161

Bibliographic information published by the Deutsche Nationalbibliothek
The Deutsche Nationalbibliothek lists this publication in the Deutsche Nationalbibliographie; detailed bibliographic data are available on the internet at
https://portal.dnb.de/opac/simpleSearch?query=2629-316

RAM-Verlag
Stüttinghauser Ringstr. 44
D-58515 Lüdenscheid
Germany
RAM-Verlag@t-online.de
https://www.ram-verlag.eu

Editorial Board

Chairman of the Editorial Board:

Members of the Editorial Board:

V. Sklabinskyi, I. Pavlenko, J. Pitel'

Monitoring of Hydrodynamics and Mass Transfer in Vortex Flows

Abstract

The monograph aims at monitoring of hydrodynamics and mass transfer in two-phase gas-droplet vortex flows in spraying countercurrent mass transfer apparatuses. Up-to-date methods of mass transfer in vortex gas-droplet flows and approaches for rational designing vortex apparatuses are presented. The development of innovative designs of mass transfer equipment is presented. Based on experimental studies and practical experience, methods for evaluating the hydraulic and mass transfer characteristics have been proposed. Particular attention is paid to intensifying hydrodynamic and mass transfer processes in equipment for chemical technology. The scientific results have been achieved within the research project Creation of new granular materials for nuclear fuel and catalysts in the active hydrodynamic environment" (State reg. no. 0120U102036).

Keywords

process innovation, hydrodynamics, mass transfer, vortex flow, energy efficiency

V. Sklabinskyi
Sumy State University, Sumy, Ukraine

I. Pavlenko
Sumy State University, Sumy, Ukraine

J. Pitel'
Technical University Kosice, Slovakia, SK

Contents

Preface

The energy crisis of the late 20th and early 21st centuries, constantly increasing requirements for product quality, a sharp increase in the cost of materials, and a number of environmental disasters drew society's attention, governments worldwide to strengthen requirements for cleanliness of industrial emissions. Simultaneously, problems arose that created the preconditions for the emergence of innovative directions in the development of mass transfer equipment.

Basically, the search for new ways of development aims to create mass transfer equipment with an increase in the efficiency of using the working volume by 2–3 times or more, compared with traditional column equipment, where plate or packed contact elements are commonly used.

Along with the improvement of mass transfer equipment, the search for ways of organizing the movement of flows in mass transfer equipment and the consequent monitoring continues. Today, it becomes possible to carry out highly efficient mass transfer processes with a simultaneous decrease in the dimensions of apparatuses and an increase in their productivity.

Over the past decade, many publications on the study of vortex flow in mass transfer devices have been increased. Mainly, publications recommended by the authors of the monograph are summarized in References.

Also, the number of designs of various vortex devices has significantly increased, which created the conditions for the contact between gas and liquid phases under their vortex movement. Particularly, Sumy State University successfully carries out research works on vortex flows and innovative designs of mass transfer equipment.

Remarkably, the increased interest in vortex flows in mass transfer equipment is substantiated by the possibility of a significant intensification of mass transfer processes. This is

because mass transfer processes in vortex flows are carried out in relatively small volumes of working chambers. This fact allows one to increase the size of the mass transfer apparatus and reduce costs for designing, manufacturing, and exploitation of vortex mass transfer apparatuses.

Hydrodynamic features of the vortex flows highlight two main factors for intensifying mass transfer processes. The first one concerns the possibility of performing a finely dispersed spraying of a liquid phase due to high relative velocities of phases. As a result, a significant increase in the interfacial surface is achieved. Accordingly, mass transfer processes are accelerated.

The second factor is creating the developed turbulent two-phase flow in the entire volume of a vortex mass transfer chamber. This allows one to increase the intensity of internal circulation currents in droplets and accelerate the renewal of the interfacial surface.

The monograph is devoted to the theoretical and experimental study of hydrodynamic and mass transfer processes' monitoring in two-phase gas-droplet vortex flows within a single spraying stage. In an entire volume of a vortex chamber, gas moves from the periphery to the center, and liquid – from the center to the periphery. The main attention is paid to methods of intensifying hydrodynamic and mass transfer processes.

In the monograph, the theoretical substantiation of the mass transfer efficiency between gas and liquid in vortex flows is given. A theoretical description of such a motion is presented using mathematical equations obtained based on the analytical solution of differential equations for a viscous gas flow motion. Equations for calculating a new vortex spraying countercurrent mass transfer apparatus have been substantiated analytically. The developed mathematical models have been proven

experimentally. The impact of technological and geometric parameters on the local velocity and pressure fields is shown. Up-to-date approaches to rational design of vortex spraying countercurrent mass transfer apparatuses are presented. The development of progressive designs of mass transfer equipment using countercurrent vortex motion of liquid droplets and gas along the radius of the vortex chamber is presented. Experiments and practical experience have developed methods for evaluating hydraulic and mass transfer characteristics for vortex spraying countercurrent mass transfer apparatuses.

Ways for the organization of gas-droplet flows in vortex spraying countercurrent mass transfer apparatuses are described in Chapter 1. The theoretical background of mass transfer intensification between droplets and gas at a vortex countercurrent motion is presented in Chapter 2. Based on the theoretical and experimental studies presented in Chapters 3–4, the following new results are recommended:

– fundamentals of organizing the movement of phases in countercurrent vortex flows of liquid droplets and gas have been obtained; the dependence of circulation flows in liquid droplets on the hydrodynamic characteristics of a flow has been established; the impact of internal circulation flows on the efficiency of the mass transfer process has been substantiated;

– the nature of the interaction of vortex flows of liquid droplets and gas has been studied;

– dependencies for calculating local fields of velocity and pressure in a gas vortex flow have been obtained for given geometric and technological parameters of the vortex spraying countercurrent mass transfer apparatus;

– experimental data on the local velocity and pressure fields in a working chamber have been presented; this allows one to deeper understand the essence of the mass transfer processes

in a vortex chamber and determine the mass transfer characteristics in the processes of absorption (desorption) and rectification;

– the fundamental principles of increasing efficiency and productivity of vortex spraying countercurrent mass transfer apparatuses have been formulated based on experiments on improved designs of such devices;

– new designs of vortex sprayers have been developed considering the achievement of the most effective spraying;

– physical and mathematical models of the motion of liquid droplets and gas in a working chamber have been proposed in terms of impact on circulation flows in droplets; the most favorable conditions for movement and interaction of phases have been proposed;

– efficiency of vortex spraying countercurrent mass transfer apparatuses has been compared with other designs of mass transfer equipment;

– conditions are formulated under which using the vortex spraying countercurrent mass transfer apparatus is the most appropriate.

Chapter 5 presents the mass transfer characteristics of the vortex spraying countercurrent mass transfer apparatus. Recommendations for designing vortex spraying mass transfer equipment and their applications are described in Chapter 6.

Described designs of vortex spraying countercurrent mass transfer apparatuses and methods for calculating their hydrodynamic and mass transfer characteristics have been implemented in the technological processes in the industry, mainly as follows:

– distribution of products in the synthesis of butoxybutenine;

– purification of gas emissions from dimethylformamide (dimethylacetamide); purification of gas emissions from ammophos production from fluorine and ammonia;

– natural gas dehydration.

Thus, developing a method for countercurrent mass transfer in vortex flows has allowed us to improve designs of highly efficient mass transfer apparatuses, in which vortex countercurrent motion of phases is carried out in the entire volume of a vortex chamber. As a result, a change in the concentration of phases is achieved, corresponding to several theoretical stages of change in concentration. Such organization of flows allows one to carry out mass transfer processes in smaller volumes, reduce the number of steps and the dimensions of apparatuses, and reduce the consumption of material and reflux in the rectification process. As a result, more significant savings in materials and energy are provided.

In the monograph, mathematical models of two-phase vortex countercurrent flow in the entire volume of a working chamber are given. Along with creating highly efficient designs, much attention is paid to studying various factors restraining the widespread implementation of the considered mass transfer approach. Particular attention is also paid to promising designs of mass transfer equipment to identify possible ways of developing vortex spraying countercurrent mass transfer apparatuses.

It is noteworthy that the authors paid particular attention to the effect occurring due to exposure high-speed gas flow (with the transverse velocity gradient) on internal flows in liquid droplets. Notably, it has been proven for the first time that this effect intensifies internal currents inside droplets and the mass transfer process in the vortex spraying countercurrent mass transfer apparatus.

The results have been achieved within the research project of Sumy State University “Creation of new granular materials for nuclear fuel and catalysts in the active hydrodynamic environment” (State Reg. No. 0120U102036) ordered by the

Ministry of Education and Science of Ukraine due to the close cooperation between the Department of Chemical Engineering, the Department of Computational Mechanics named after Volodymyr Martynkovskyy of Sumy State University (Sumy, Ukraine), and the Faculty of Manufacturing Technologies with a seat in Prešov of Technical University of Košice (Prešov, Slovakia) under the support of the International Association for Technological Development and Innovations.

Authors: *V. Sklabinskyi*
I. Pavlenko
J. Piteľ

Nomenclature

A, B, C – dimensionless parameters;
A_3, A_4 – aspect ratios;
A_d – work on moving a droplet, J;
a, b, c – coefficients of approximating equations;
a_1, a_2 – parameters of the transversal velocity distribution;
a_s – specific interfacial surface, m^2/m^3;
b_1, b_2, b_3, b_4 – boundary values;
C_1, C_2 – integration constants;
d_0 – droplet diameter, m;
d_{e3}, d_{e4} – equivalent diameters of pipes, m;
d_n – diameter of a nozzle, m;
E_{Mx} – Murfrey's desorption efficiency;
F – interfacial surface, m^2;
F_c – the surface of a camera, m^2;
F_{cf} – centrifugal force, N;
F_{cfe} – effective centrifugal force, N;
F_d – hydrodynamic force acting on a droplet, N;
F_{df} – drag force, N;
F_g – gas-dynamic force, N;
F_{in} – inlet tangential nozzle area, m^2;
F_s – interfacial surface, m^2;
G – mass flow rate of a gas, kg/s;
g – acceleration of gravity, m/s^2;
H_c – the height of camera/channel, m;
h – height, m;
h_g – tangential gap, m;
I_1, I_2, I_1 – auxiliary integrals;
I_z – a moment of inertia, $kg \cdot m^2$;
i, j – node numbers;
K, K_g – kinetic moment, $kg \cdot m^2/s^2$;
K_m – dimensionless factor;
K_N – correction factor;
k – mass transfer coefficient;
k_1 – swirl drop coefficient;
k_2, k_3, k_4 – auxiliary coefficients;
k_t – turbulence parameter, m^2/s;

L – mass flow rate of a liquid, kg/s;
L_0 – mass flow rate of inert liquid carrier, kg/s;
L_{in} – flow rate of a supplied liquid, kg/s;
L_{out} – a fluid flow of a discharge liquid, kg/s;
l – mixing path, m;
l_3, l_4 – auxiliary lengths, m;
l_F – arm length, m;
M – mass transfer rate;
M_d – hydrodynamic moment acting on a droplet, N·m;
M_F – a moment of force, N·m;
M_f – friction moment, N·m;
M_g – gas mass, kg;
M_l – liquid mass, kg;
M_z – a moment of a force about the rotation axis, N·m;
m – droplet mass, m;
$\dot{m}$ – mass flow, kg/s;
N, N_x – number of transfer units;
N_0 – solution normality;
N_a – the power of a centrifugal atomizer, W;
N_h – the total number of gaps;
Nu – Nusselt number;
N_v – the power of vane system, W;
n – exponent index;
n_0 – number of droplets;
n_1 – number of blades;
n_n – number of nozzles;
P – hydrodynamic pressure, Pa;
P_1, P_{in} – inlet pressure, Pa;
P_2 – total pressure of the gas flow, Pa;
P_3 – pressure in the annular chamber, Pa;
Pe – Peclet number;
P_{out} – inlet pressure, Pa;
P_{st} – static pressure, Pa;
Q_g – gas flow rate, m^3/s;
Q_l, q – liquid flow rate, m^3/s;
R – droplet radius, m;
R_0 – radius of maximum flow velocity, m;
R_1 – gas inlet radius, m;
R_2 – gas outlet radius, m;
R_3, R_4 – radiuses of annular sections, m;
R_a – radius of atomizer, m;
R_b – radius of the bushing, m;

R_c – vortex chamber radius, m;
Re – Reynolds number;
r – radius, m;
r_{av} – average radius, m;
r_F – radius of the point of force application, m;
r_q – radius of quasi-rigid rotation, m;
S_0 – droplet surface, m^2;
s –cross-sectional area of a droplet, m^2;
T – friction force, N;
t – time, s;
t_l – liquid temperature, °C;
u – velocity potential, m^2/s;
V – gas velocity, m/s;
V_1 – solution volume, ml;
V_2 – sample volume, ml;
V_{av} – average velocity, m/s;
V_c – a volume of a camera, m^3;
V_{in}, V_{in1}, V_{xN} – inlet velocity of a gas, m/s;
V_l – liquid volume, m^3;
V_g – gas volume, m^3;
V_r – radial gas velocity, m/s;
V_{rel} – relative phase velocity, m/s;
V_s – droplet surface velocity, m/s;
V_x, V_y – velocity components in a plane, m/s;
V_{yM} – outlet velocity, m/s;
V_z – axial gas velocity, m/s;
V_{z2} – outlet axial velocity of a gas, m/s;
V_{zav} – average axial velocity, m/s;
V_φ – angular velocity of gas, m/s;
$V_{\varphi1}$, $V_{\varphi2}$ – inlet and outlet angular velocities of a gas, m/s;
$V_{\varphi av}$ – average angular velocity, m/s;
$V_{\varphi e}$ – effective angular velocity, m/s;
W_A – mass flow rate, kg/s;
We – Weber number;
W_{in} – inlet velocity of a liquid, m/s
W_r – radial velocity of a liquid, m/s;
W_φ – angular velocity of a particle, m/s;
x, x_1, x_2 – concentration of a liquid phase;
x, y, z – Cartesian coordinates, m;
x_e – equilibrium concentration;
z_v, z_1, z_2 – vane height, m;

β_x – mass transfer coefficient, kg/(m^2·s);
β_{xV} – volume mass transfer coefficient, s^{-1};
Δ – a driving force of the mass transfer process;
ΔL – flow rate difference, kg/s;
ΔP – pressure difference, Pa;
ΔP_1 – pressure loss, Pa;
ΔP_c – pressure difference in camera, Pa;
ΔP_{in} – inlet pressure difference, Pa;
ΔP_{st} – hydrostatic pressure difference, Pa;
Δx – concentration difference;
Δx_{av} – average concentration difference;
δ – boundary layer thickness, m;
δ_L – relative spray blower;
ε – kinematic viscosity, m^2/s;
ζ, ζ_1, ζ_2, ζ_3, ζ_4 – local loss coefficients;
ζ^* – hydraulic resistance coefficient;
θ – angle in spherical coordinates, rad;
λ_3, λ_4 – length loss factors;
μ_g – dynamic viscosity of a gas, Pa·s;
ν_g – kinematic viscosity of a gas, m^2/s;
ρ – polar radius, m;
ρ_0 – droplet density, kg/m^3;
ρ_g – gas density, kg/m^3;
ρ_l – liquid density, kg/m^3;
σ – surface tension coefficient, N/m;
τ – shear stress, N/m^2;
τ_{xy} – Prandtl's shear stress, N/m^2;
φ – polar angle, rad;
ψ – drag coefficient;
Ω – droplet volume, m^3;
ω – angular velocity, rad/s;
ω_0 – angular velocity at the boundary layer, rad/s;
ω_g – gas angular velocity, rad/s.

1 Organization of Gas-Droplet Flows in Vortex Spraying Countercurrent Mass Transfer Apparatuses

1.1 Liquid spraying and vortex flow. Factors intensifying mass transfer

The designs of mass transfer apparatus allow us to note one of the directions in their development. Mainly, these are spraying devices in which the flow is turbulent. Spraying liquid into small droplets significantly speeds up the mass transfer process [1]. This is due to an increase in the interfacial surface and mass transfer rate [2]:

$$M = kF\Delta, \tag{1.1}$$

where F – interfacial surface depending on the average droplets' size for the sprayed liquid, m^2; Δ – a driving force of the mass transfer process; k – mass transfer coefficient.

The droplet diameter decreases with an increase in the relative velocity of the gas and the sprayed liquid [3]. This dependence is inversely proportional to the square of the relative flow rate.

In this regard, attention is drawn to a number of devices in which the spraying of the liquid phase occurs due to the action of a high-speed gas flow on the liquid jets that are introduced into it. A number of designs implementing this effect for the intensification of mass transfer are presented below.

Many publications are devoted to reviewing various designs that underlie effective high-speed devices and methods for calculating such mass transfer devices [4–12].

The Venturi tube is one of the elements of a commonly used apparatus that allows one to obtain a significant gas velocity, a relatively fine spray of liquid, and turbulize the flow.

In a nozzleless Venturi apparatus (Figure 1.1), the breakup process is characterized by significant droplet polydispersity. Mass transfer processes proceed at different rates throughout the volume of the apparatus due to the unevenness of the velocity field of the two-phase flow.

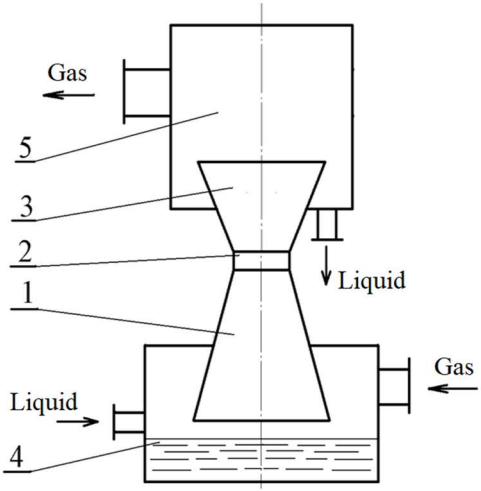

Figure 1.1 – The nozzleless Venturi apparatus: 1 – confuser; 2 – throat; 3 – diffuser; 4, 5 – tanks

In a nozzle Venturi apparatus (Figure 1.2), despite the significant alignment of the two-phase gas-droplet flow in the confuser and throat and positive flow turbulization, in the diffuser, reverse currents and uneven distribution of velocities occur. These phenomena adversely affect the mass transfer process.

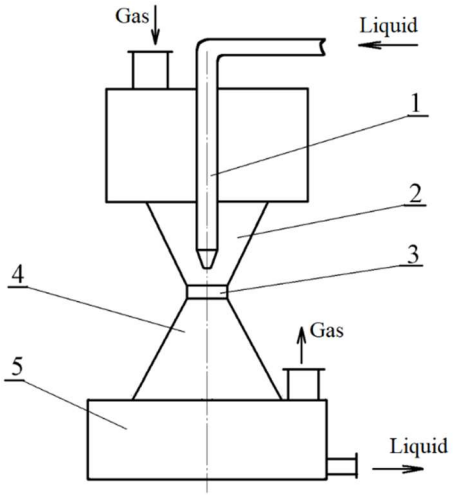

Figure 1.2 – The nozzle Venturi apparatus: 1 – nozzle; 2 – confuser; 3 – throat; 4 – diffuser; 5 – tank

In a film Venturi apparatus (Figure 1.3), film stripping, and breakup of droplets occur under conditions that do not allow the creation of a monodisperse droplet composition of the liquid phase. This is where the above drawbacks in the flow structure follow. They do not ensure the maximum effect of fine atomization of a liquid with a high-speed gas flow and organize a uniform mass transfer process throughout the operating volume.

Representatives of another series of devices in which liquid spraying with a gas stream is used are spray-type devices (Figure 1.4).

The gas flow, passing through the axial swirlers, acquires a rotational motion, sprays, and carries the liquid. After, under the action of centrifugal force occurring in a two-phase flow, the droplets move to the periphery.

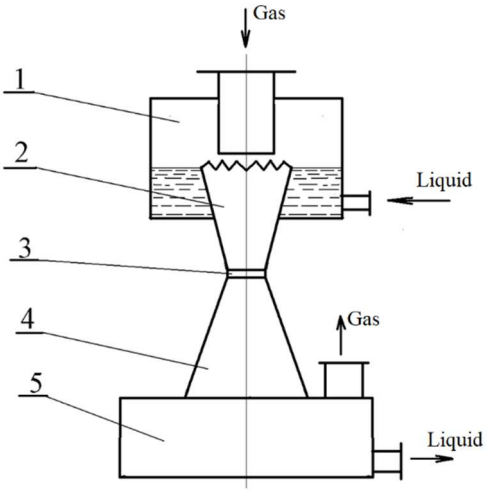

Figure 1.3 – The film Venturi apparatus: 1, 5 – tanks; 2 – confuser; 3 – throat; 4 – diffuser

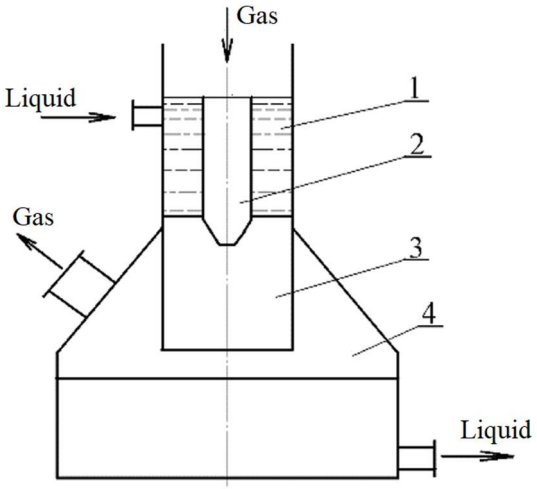

Figure 1.4 – The spray-type apparatus: 1 – annular chamber; 2 – branch pipe; 3 – camera; 4 – tank

The principle of operation of the spray-type apparatus is as follows. The liquid entering the annular chamber is entrained in the gas flow. This gas passes through the branch pipe and forms a gas-droplet mixture in the chamber, separated in a tank. Such a design may be fundamental for a tray element in a column apparatus.

A number of designs based on fine atomization of liquid by swirling gas flows with subsequent separation of droplets are presented. These designs allowed increasing the productivity of the equipment by 2–3 times compared with cap devices [13].

Figure 1.5 presents a design scheme of an apparatus with axial swirlers located along the vessel's perimeter, where the liquid phase enters [14].

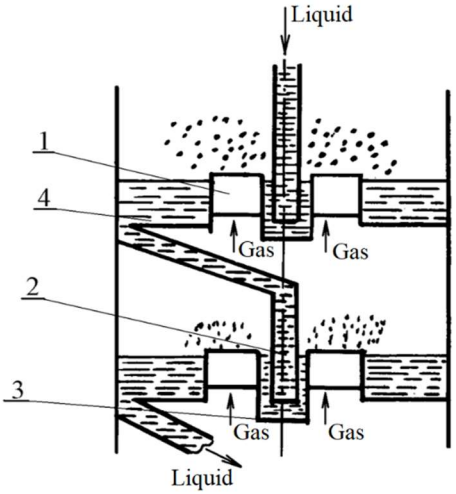

Figure 1.5 – The apparatus with the axial swirlers: 1 – axial swirlers; 2 – overflow pipe; 3 – hydraulic seal cup; 4 – circular pocket

Further, the separated liquid is collected in an annular pocket and fed through the overflow pipe into the liquid gate of the next stage.

In this design, despite direct flow movement occurring at each stage, it is necessary to note the implementation of the principle of countercurrent movement of phases for the apparatus.

It is not possible to create significant peripheral velocity in the gas flow using axial swirlers. Therefore, the use of tangential swirlers is justified. This made it possible to create high velocities in the center of the vortex chamber and obtain a finer spray of the liquid phase. All this is due to the interaction of a high-speed gas flow with a liquid than the use of axial swirlers.

This approach allowed designing an apparatus with tangential swirlers (Figure 1.6) [15].

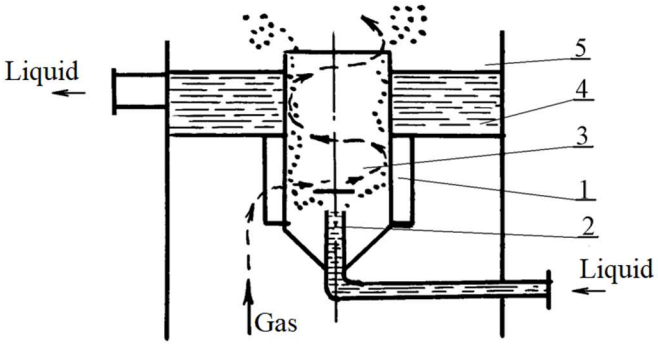

Figure 1.6 – Apparatus with tangential swirlers: 1 – tangential swirlers; 2 – atomizer; 3 – vortex chamber; 4 – annular chamber; 5 – tank

The apparatus works as follows. The gas flow passing through the tangential swirler, acquires a rotational motion. Towards the center of the vortex chamber, the tangential components of the gas velocity reach large values (from 60 to

100 m/s). This fact positively affects the spray dispersion of the liquid phase, which is fed to the bottom through a special device.

Liquid droplets entrained by the gas flow move along helical trajectories to the outlet of the vortex chamber. Simultaneously, a movement of droplets to the periphery under the action of centrifugal forces occurs. When leaving the vortex chamber, the liquid is separated by subsequent removal through the annular chamber.

In a direct-flow vortex contact device [16], the central area of the vortex chamber is used more efficiently. It contains an area of high tangential gas flow velocities (Figure 1.7).

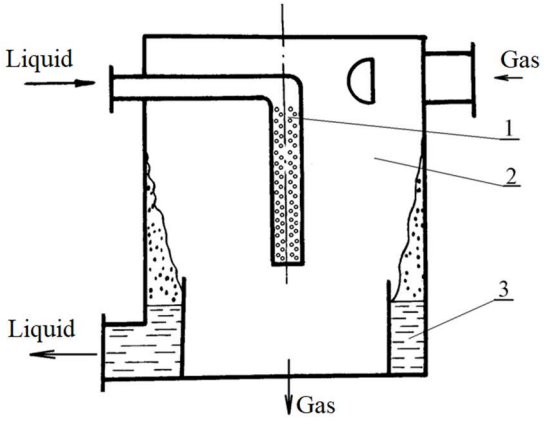

Figure 1.7 – Direct-flow vortex apparatus with a volumetric spray torch: 1 – atomizer; 2 – vortex chamber; 3 – annular outlet channel

The gas draws liquid droplets resulting from spray in the chamber's center into rotational motion by helical expanding trajectories. Under the action of centrifugal forces, they move to the walls, settle, and create a film. This film flows into the

annular channel. Finally, the liquid is removed from the apparatus.

Such a design of the direct-flow vortex contact device is the basis of the operating of a multistage vortex absorption apparatus [17]. Due to the loss of gas flow swirling through the apparatus, axial swirlers are installed before the second and subsequent stages. The design of the first stage is similar to that shown in Figure 1.7.

Studies of this absorption apparatus have shown the greatest efficiency in modes that ensure the breakup of liquid jets into droplets. The considered efficiency of the contact stage and the specific hydraulic resistance of the theoretical contact stage indicate that the studied apparatus is better than many devices for purifying industrial gas emissions.

In a countercurrent phase interaction approach [18], in multistage mass transfer apparatuses, the pressure drop is used during the movement of phases between adjacent stages and between the central region and the periphery. This makes it possible to create conditions for the reverse flow of liquid. After using this method, a direct-flow movement of the phases is carried out in each stage. Therefore, it is impossible to achieve many theoretical concentrations change stages in one liquid spraying stage. This fact is even due to countercurrent movement being organized on the whole device.

Notably, swirling gas flows are used in various mass transfer apparatuses to clean gases from harmful impurities and suspended solids, e.g., dust [19–27]. The principle of operation of these devices essentially converges with those described in the literature. They differ mainly only in design features.

It is impossible to describe all the various design solutions substantiated by applying various processes in specific conditions. Remarkably, swirling flows are also used for efficient

dispersion of liquid, its separation in the field of centrifugal forces, and other technologies.

However, the search for new directions in the use of vortex flows for mass transfer technologies is not limited to the field of direct-flow devices. Particularly, an example of the design of a counterflow vortex apparatus is presented in Figure 1.8.

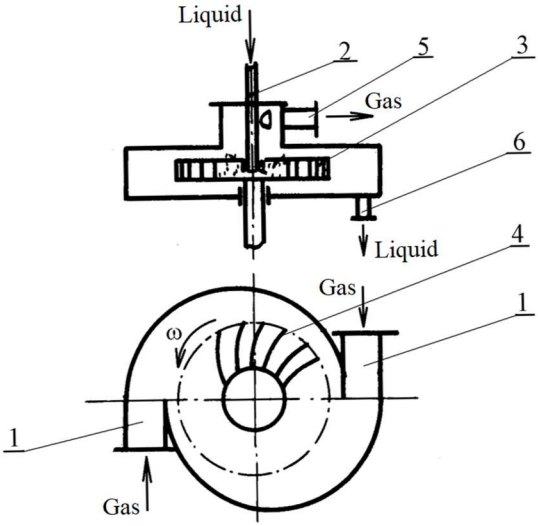

Figure 1.8 – Gas flushing and absorption device: 1, 5 – branch pipes; 2 – atomizer; 3 – rotor; 4 – plates; 6 – liquid outlet

The gas supplied by nozzles moves through a rotor channel system in this device. The liquid supplied by a sprayer is rotating in the same direction as a rotor. The liquid is atomized. Under the centrifugal forces, a thin liquid film moves to the periphery along the rotor channels formed by a number of horizontal plates. A countercurrent vortex motion of gas and liquid film is realized in such a device. This leads to a decrease in the interface area compared with spraying devices.

These examples present many of the most diverse designs of mass transfer apparatus, in which liquid spraying and vortex motion of a gas flow is used. Nevertheless, there is still no design of an apparatus in which the countercurrent vortex motion of droplets in a vortex gas flow along the radius of the mass transfer chamber in one stage would be ensured. Mainly, a direct flow and cross-phase movement have been realized.

For the first time, the idea of the possibility of creating a countercurrent movement of a swirling gas flow and microdroplets of liquid in mass transfer apparatus was proposed by Kholin [28]. Based on the theoretical analysis of conditions necessary for countercurrent movement, the basic principles of creating countercurrent vortex spraying mass transfer apparatuses were formulated. Therefore, prerequisites were expressed to create a method and a vortex apparatus that realizes the countercurrent vortex motion of phases in the contact area.

Finally, the main hydrodynamic processes are highlighted below, analyzing the operation of the vortex and spraying mass transfer apparatus.

The first one is the movement of a vortex gas flow in a vortex chamber. It is necessary to know the law of the change in the gas flow rates along the radius of the vortex mass transfer chamber of the spraying apparatus. For determining the hydraulic resistance of the apparatus, the following parameters should be known: the pressure distribution in the vortex mass transfer chamber; the ratio of hydraulic losses between the mass transfer chamber and various structural elements of the apparatus (e.g., tangential gaps for gas inlet, radial diffuser).

The second one is the influence of a liquid phase on the hydrodynamics of a vortex gas flow. Spraying of liquid jets introduced into the gas flow occurs due to the gas energy. Gas flow draws liquid droplets into a rotary motion. All these factors lead to energy redistribution between the gas flow and liquid

droplets. Simultaneously, a decrease in gas flow rates leads to an increase in the size of sprayed liquid droplets. Peculiarities of the mutual influence of flows are necessary for calculating their hydrodynamic parameters.

The third process is atomizing liquid jets at high relative velocities of phases. The dispersity (i.e., the size of sprayed liquid droplets) depends on the difference in the velocities of the liquid and gas phases in the spray area. Therefore, it is necessary to determine the area of the highest gas flow rates and parameters of the sprayer correctly.

The fourth one is the countercurrent vortex motion of liquid and gas microdroplets. In a counterflow apparatus, it is necessary to ensure the movement of liquid droplets from the center to the periphery of the operating chamber under centrifugal forces. Therefore, the ratio between the mass and aerodynamic forces acting on droplets should be chosen correctly.

The fifth one is the influence of hydrodynamic characteristics of vortex gas flow on the intensity of internal circulation flows in droplets. Remarkably, the intensification of internal circulation flows in droplets leads to an acceleration of the renewal of the interface [4]. This fact positively impacts the mass transfer processes.

Finally, the sixth process is the end effect associated with the movement of a liquid film under the influence of pressure droplets from the periphery to the center, along the end covers of the mass transfer chamber [29]. This effect negatively affects the overall efficiency of mass transfer since it leads to the return of a liquid previously contacted with the gas or steam to the center of the vortex mass transfer chamber.

The comprehensive analysis of these processes makes it possible to increase the efficiency of mass transfer equipment.

1.2 Fundamentals of hydrodynamics in a vortex chamber

The vortex motion of gas has found its application in various technology fields. A number of research work are devoted to studying the gas flow structure in vortex chambers of various designs [30–45].

Depending on the vortex chamber application, the flow structure may differ. However, in general, many common patterns in vortex chambers can be seen.

A typical example of the flow structure is a diagram, which shows the change in the circumferential velocity of the gas flow in the vortex chamber (Figure 1.9).

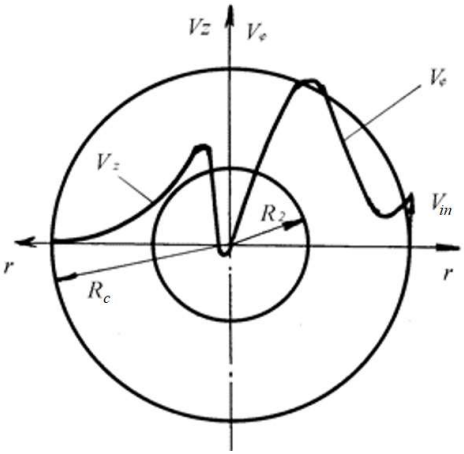

Figure 1.9 – Characteristic charts of circumferential and axial velocities along the radius of the vortex chamber: V_φ, V_r, V_z – circumferential, radial, and axial gas flow velocities, m/s; R_c, R_2 – radiuses of the vortex chamber and gas outlet, m

Four main areas can be distinguished following the change in peripheral velocity along the radius. The flow in each area has different characteristic features.

The first area is the flow area near the wall. There is a slight decrease in velocity due to friction with the chamber walls.

A significant increase in circumferential velocity characterizes the second area. Here, the circumferential velocity reaches its maximum. However, radial and circumferential velocities are uniform along with the height of the vortex chamber.

In the third area, an increase in the axial velocity occurs. Due to a significant pressure drop, reverse flow area sometimes occurs in the central region. Depending on the primary geometric dimensions of the vortex chamber, it is possible to eliminate the reverse flow area.

In the vortex countercurrent spraying mass transfer apparatus, the main working space is in the second area of the potential rotation. A significant flow pinch creates conditions for eliminating the reverse flow area in this area. The essential value of the peripheral velocity reduction does not significantly affect the potential rotation area.

Thus, two main areas will be considered. The first area is characterized by a significant increase in the circumferential velocity of the gas flow as the peripheral or working area. The second one is the area of quasi-rigid rotation (central area). It is characterized by an increase in the axial velocity of the gas flow.

The main factor determining the sizes of these areas is the radius of quasi-rigid rotation r_q, m. At this radius, circumferential velocity reaches the highest value.

A number of research works were devoted to this radius's theoretical and experimental study. Particularly, [46] stated that the maximum circumferential velocity is observed at the edge of the gas outlet. In the studies [47, 48], a number of geometrical

characteristics of vortex chambers were proposed. However, a method for determining r_q based on the minimum kinetic energy in the inlet section, maximum flow rate, and minimum resistance of the vortex chamber should be proposed.

To create a calculation technique for determining the radius of quasi-rigid rotation of vortex chambers used in direct-flow spraying mass transfer apparatus, the study [49] was carried out.

As a result, the following empirical formula is proposed:

$$\frac{r_q}{R_2} = 0.35\sqrt{\frac{\sum F_{in}}{K_m F_c}}, \tag{1.2}$$

where $\sum F_{in}$ – total area of inlet tangential nozzles, m^2; $K_m = R_2/R_c$ – dimensionless factor; R_c – camera radius, m; F_c – chamber area, m^2.

Comparison of the experimental data on changes in relative circumferential velocities along the radius gives fundamentals to suggest that changes in the magnitude of these velocities depend on the geometric features of the vortex chambers.

According to the theoretical description of the flow, the following attention can be paid to the peripheral area. This finds its explanation from the specifics of the vortex chambers applications in various technology fields, mainly for the cases of a small length of the peripheral area. It is proposed to adopt the variation law for the circumferential velocity of a viscous medium similar to the circumferential velocity variation along the radius, m/s:

$$V_\varphi = \frac{V_{in} R_c}{r}, \tag{1.3}$$

where V_{in} – inlet velocity, m/s; r – radius, m.

However, this dependence is reliable for a small area. When moving towards the center, especially in the maximum circumferential velocities, discrepancies with experimental data reach larger values.

The study [50] gave a theoretical description of the flow in the vortex chamber using the Navier–Stokes equations by replacing the kinematic viscosity coefficient with the turbulent kinematic viscosity coefficient. For the peripheral zone, the assumptions were made that the flow is plane, helical, and symmetrical concerning the axis.

Comparison with experimental data made it possible to put forward a proposal on the possibility of assuming in the calculations a constant coefficient of turbulent viscosity along the radius of the vortex chamber. As a result, exponent index n in the equation of the change in peripheral velocity was introduced:

$$\frac{V_\varphi}{V_{\varphi_1}} = \left(\frac{R_c}{r}\right)^n, \tag{1.4}$$

where $V_{\varphi 1}$ – circumferential velocity near chamber radius, m/s; $n = 1.6$ – the value obtained as a result of solving a system of differential equations.

Considering the assumption that it is possible to describe the flow in the peripheral zone by a power law, comparisons were made of the change in the value of n along the radius for various types of chambers.

The value of n is determined by the results of experiments published in various literature sources. The results of published experimental studies were processed based on the following dependence:

$$n = \frac{ln\left(\frac{V_\varphi}{V_{in}}\right)}{ln\left(\frac{R_c}{r}\right)}. \tag{1.5}$$

High gas flow velocities in the vortex chamber raise a critical question about energy losses during the motion of two-phase media. In some cases, energy losses during the movement of a single-phase medium are estimated by the drag coefficient, which is the ratio of the total pressure drop at the inlet and outlet of the vortex mass transfer chamber to the velocity head at the inlet to the mass transfer chamber. This is since the vortex process is most fully reflected, and the coefficient hydraulic resistance is related to the geometry of the swirler:

$$\zeta^* = \frac{2\Delta P}{\rho_g V_{in}^2}. \quad (1.6)$$

where ΔP – pressure difference at the inlet and outlet of the vortex mass transfer chamber, Pa; ρ_g – gas density, kg/m^3.

The following features of the change in the drag coefficient (for the presence of droplets of atomized liquid phase) compared to the drag coefficient of the vortex chamber when a single-phase flow moves should be noted.

Reducing the circumferential velocity of the gas flow reduces the value ζ^* due to a decrease in radial pressure drop. Simultaneously, there are additional losses for the transportation of droplets of the liquid phase. In general, with an increase in the load on the liquid phase, there is a slight decrease ζ^*. However, for loads ratio $L/G > 1$ (L, G – loads for liquid and gas phase, respectively, kg/s), there is a continuous increase in the drag coefficient. The self-similarity of the relative velocity for a two-phase flow was noticed.

An analysis of the change in the coefficient of hydraulic resistance of direct-flow vortex devices made it possible to assume that the operation of a counterflow mass-exchange apparatus in a mode where there are additional energy losses for transporting liquid is unacceptable. This is since there is a direct-flow phase movement. The problem of determining the zone of

stable operation of the apparatus in the counterflow mode should be given great attention. Otherwise, with the appearance of a direct flow, one can expect a decrease in the efficiency of the mass transfer apparatus.

The above review of studies by various authors, which concerns the study of the movement of one- and two-phase flows, showed that the studies were mainly carried out in vortex chambers, in which the dimensions in height are more significant than the diameter of the chamber itself, and to study the movement of phases in direct-flow vortex mass transfer apparatuses extensions were used. As a result, the flow structure is characterized by axial velocity. The influence of the chamber geometry on the flow is also confirmed by the difference in the peripheral velocity profiles along the radius of the vortex chamber. It is not possible to organize the countercurrent movement of liquid droplets in vortex chambers of such structures.

In the vortex chamber of the countercurrent mass transfer apparatus, the peripheral zone is used as the main working zone, where the primary importance for calculating hydrodynamic and mass transfer processes is the patterns of changes in peripheral velocity.

The results previously obtained by the authors for other designs of vortex chambers cannot sufficiently reliably reflect the flow pattern in this region.

An example confirming the limited scope of the techniques that relate to the flow calculation in the vortex chamber can be the discrepancy between the theoretical and experimental values of the radius r_q (1.5).

Therefore, the authors of this monograph tested the effectiveness of the existing calculations and created a technique that makes it possible to describe the flow pattern of a single- and two-phase medium in the working chamber of a countercurrent

vortex apparatus quite accurately both quantitatively and qualitatively.

Information about the motion of two-phase systems is even more limited. On the one hand, this is connected with the complexity of the theoretical description of such motion and, on the other hand, with great difficulties in studying dispersed flows.

The countercurrent vortex motion of a free gas flow and microdroplets in the entire volume of the vortex chamber has not been used before, and therefore there is no information on such flows.

In this regard, this paper presents the results of theoretical and experimental studies to identify the pattern of two-phase countercurrent vortex motion of liquid and gas microdroplets, based on which a calculation method has been created. It allows determining effective modes, a change in concentration in one stage of spraying, and others.

1.3 Spraying liquid with a gas flow

Due to the widespread use of liquid spraying in mass transfer apparatuses, drying processes, in furnace processes, in combustion chambers of air-jet engines, and other areas of technology, the physical meaning for the breakup of liquid jets into droplets and their subsequent crushing into smaller ones, when moving in a turbulent gas flow, was studied entirely.

As noted in works devoted to the problem of spraying [51–54], the theoretical solution of the breakup of a turbulent jet, considering the aerodynamic influence of the gas flow, is associated with great difficulties. The more straightforward problem of the breakup of a cylindrical jet of an inviscid fluid was solved by Rayleigh in 1878 [55]. In this case, the influence of the gas flow was not considered.

If the breakup of the jet into droplets at a low exhaust velocity occurs under the action of disturbances caused by the flow before entering the nozzle (e.g., the shape of the channels and their roughness), then with an increase in the exhaust velocity, the aerodynamic influence from the gas flow becomes the main reason. In this case, the jet bends, various complex symmetric and asymmetric perturbations arise, and the spraying mode starts.

The accumulation of experimental material made it possible to create empirical formulas, which led to reasonably good results for practical calculations. For example, when a jet flows out from the nozzle 0.34–1.20 mm at a velocity of up to 16 m/s, it is recommend the following empirical equation:

$$d_0 = \frac{6d_n}{Re^{0.15}}, \tag{1.7}$$

where d_0, d_n – droplet and jet diameters, respectively, m; Re – Reynolds number.

The formula proposed by Nukiyama and Tanasawa is widely used in practical calculations [56]. The validity of this empirical formula for subsonic velocities is shown in the work by Lewis et al. [57], and for subsonic and supersonic velocities of the spraying gas flow – in the work by Bitron [58].

With further movement, the droplets are crushed in the flow, which positively affects the process of mass transfer. After considering the motion of an individual droplet in a gas flow, the criterion for droplet breakup was experimentally established:

$$We = \frac{\rho_g V_{rel}^2 d_0}{\sigma}, \tag{1.8}$$

where ρ_g – gas density, kg/m^3; σ – surface tension coefficient, N/m; V_{rel} – relative phase velocity, m/s.

This Weber number *We* characterizes the ratio of aerodynamic forces that affect the droplet from the side of the gas flow and surface tension forces, under which the droplet breaks up.

Upon reaching *We* = 14, almost all droplets of a dispersed flow are subject to crushing. The physical meaning of droplet decay is as follows. During the movement of a droplet in a gas flow, the latter is exposed to aerodynamic forces, resulting in its shape changes. The shape of the liquid surface becomes unstable from the energy point of view, and the droplet is separated into smaller ones. There are various models of mechanical destruction of droplets, which are based on identifying individual processes, such as destruction due to breaking of waves from a disturbed surface, breaking of a boundary layer on the windy side of a droplet, and droplet deformation.

Studies have confirmed the destruction of droplets in a turbulent flow and the dependence of the droplet size on the residence time in it [59–61].

A number of theoretical studies were devoted to the disintegration of liquid droplets. Thus, in [62], using the method of small perturbations, the change in the shape of a droplet and its subsequent destruction under the influence of perturbations that are symmetric with respect to the axis were studied. Numerical integration of the obtained equations makes it possible to trace the thinning of the droplet in the longitudinal direction and the formation of an irregular shape.

Considering the works describing the disintegration of liquid jets into droplets and their further movement in a gas flow, we can draw the following conclusions. A droplet of liquid moving in a gas flow is subject to the body, drag, and surface tension forces. The shape of droplets larger than 1 mm in diameter is not given but is formed in moving. This shape is determined by the balance of pressure forces or resistance forces acting on the surface from the side of the continuous medium, which deforms droplets in this direction, and the surface tension force, which prevents deformation. In addition to deformation, the influence of the resistance force on the droplet can lead to its secondary crushing. The resistance forces and surface tension depend on the following parameters: the velocity of the droplet relative to the gas flow, the density and viscosity of the gaseous medium, the viscosity of the liquid phase, the surface tension, and the characteristic radius of the droplet.

Some of these parameters are included in the Weber number, which can be used to determine the conditions for the disintegration of a liquid jet into droplets. At a particular critical value of the Reynolds criterion, a sharp change in the behavior of moving droplets occurs. The drag coefficient increases rapidly with increasing Reynolds number, and the movement velocity decreases with increasing liquid droplet size.

Almost all researchers who have studied the motion of droplets noted that a sharp increase in the drag coefficient is associated with the onset of a noticeable deformation of droplets.

The use of a vortex chamber makes it possible to achieve circumferential velocities of the gas flow of the order of 100 m/s. Therefore, it is possible to create conditions for dispersing liquid jets into droplets of 50–100 μm in size. The information given in [59] on the study of the effect of gas velocities on the crushing of liquid droplets shows that droplets of such a small size are less amenable to deformation and secondary crushing due to the large magnitude of the surface tension forces. Therefore, for purposes of mass transfer intensification, it is necessary to consider the effect of a high-velocity gas flow in the vortex chamber on internal circulation flows in droplets.

Due to the above physical meaning for the breakup of liquid droplets, it is interesting to study the movement of droplets in a gas flow, where there is a gas velocity gradient directed along the normal to the direction of droplet movement. Such a movement takes place in the working chamber of a countercurrent vortex spraying apparatus during the movement of liquid droplets from the center to the periphery. In this case, there is a gradient of the circumferential velocity of the gas, increasing from the periphery to the center. The difference in velocities on the droplet' surface on its opposite sides along the radius of the mass transfer chamber leads to the appearance of internal circulation flows. The angular velocity:

$$\omega = \frac{15\psi}{32\pi}\frac{\rho_g}{\rho_0}\left(\frac{dV}{dr}\right)^2 t, \qquad (1.9)$$

where ψ – drag coefficient; ρ_0 – droplet density, kg/m^3; t – time, s.

The process of spraying the liquid phase in a vortex countercurrent mass transfer apparatus is carried out due to the high relative velocities of gas and liquid in the central region.

Atomizing mass transfer apparatuses have a low material consumption since the process takes place in a volume of a nozzle. Widespread use of spraying mass-exchange apparatuses makes it possible to achieve significant metal savings. These devices also have low labor intensity of manufacture. They are easy to maintain reliable in operation. However, the efficiency of atomizing absorption and distillation apparatuses is low, which is explained by the absence of fine liquid atomization into droplets with a diameter of 20–100 μm. Centrifugal atomizers, centrifugal atomizers, pneumatic atomizers, and other atomizing devices are widely used for fine liquid atomization.

In vortex atomizing countercurrent mass transfer apparatuses, some conditions make it possible to achieve fine atomization of the liquid.

At the moment of its entry into the gas flow in the radial direction, the jet of the liquid has a zero circumferential velocity. The magnitude of the relative velocities is entirely determined by the magnitude of the circumferential velocity of the gas flow at the site of liquid-phase decomposition.

As the formulas described above and the results of visual observations show, such a spray is highly effective. Due to their small size, the micro-droplets of the liquid formed in this process are very quickly entrained in a rotational motion. Simultaneously, in the process of moving to the periphery under the action of centrifugal forces, further deformation of the drop-lets occurs, the internal circulation flows in their increase. These effects significantly impact the development of the interfacial surface and contribute to the intensification of the mass transfer process.

1.4 Describing the movement of two-phase flows

At present, the gas dynamics of multiphase flow are developing in several directions, each of which is based on models, where a number of simplifying assumptions are at the forefront, which allow the use of modern mathematical tools for a qualitative description of the flow pattern. This approach is associated with the complexity of the structure of a two-phase medium, the presence of heat and mass transfer processes, and phase transitions.

Various physical models were used to describe the flow pattern, such as motion in a porous medium, averaged equations of motion with allowance for phase transitions, and averaged equations without phase transitions.

The most well-suited to mathematical description are flow models in which the dispersed phase is uniformly distributed over the entire volume since, in this case, it is possible to use a well-developed apparatus of differential calculus.

Usually, in chemical technology apparatuses, the ratio of loads by phases and, accordingly, the volume fraction of the dispersed phase can vary within relatively wide limits. For the mathematical description of flows, which is used to describe the motion of two-phase flows, models of the separate motion of phases are also widely used. This two-fluid model considers two-phase flow as interpenetrating and interacting, filling the same volume. For such a model, the condition is assumed that the dispersed phase is distributed over the entire volume occupied by the two-phase flow, and the parameters that describe the state of the two-phase flow are taken as the holding capacity or volume fraction of the continuous phase, average velocity, temperature, pressure, and other parameters. It is possible to apply the methods of continuum mechanics to such a medium because the average velocity of the phase is defined

as the volume average, and its movement occurs not over the entire cross-section of the considered flow but over the part that is proportional to the volumetric part of this phase in a two-phase flow. It is assumed that the size of the dispersed parts of the linear scale of hydrodynamic processes is significantly less than the linear size characteristic of the geometry of the flow part of the apparatus in which these processes occur. The equations that describe the laws of conservation of mass and momentum of the dispersed phase include components that consider the corresponding exchange between the phases within the selected volume of the two-phase flow.

There are various methods of averaging. This is statistical averaging, time-averaging, or volume averaging. The resulting equations have almost the same form, which allows applying existing mathematical methods for their solution.

The considered approach to solving the problem of the movement of two-phase dispersed flows in the elements of the flow part of chemical equipment is based on a number of the above assumptions, which affects the reliability of the obtained quantitative solutions. But, on the other hand, the assumption of the homogeneity of the medium allows using the apparatus for the mathematical description of its movement differential calculus.

However, the resulting differential equations require simplifications for their numerical solution. In [63], an example of the numerical solution of equations describing a two-phase flow is given.

Regarding the considered countercurrent motion of liquid and gas microdroplets, it is interesting to describe the motion of a separate liquid droplet, which can be argued as follows. Firstly, the high relative velocities of gas and liquid make it possible to obtain a droplet spectrum close to monodisperse. The average droplet size, in this case, is determined quite accurately.

Secondly, the same forces act on droplets of the same size, and the droplets move along the same trajectories. As a result, an ordered movement of the discrete droplets and a gas flow occurs in the mass-exchange chamber. Thirdly, when droplets move one after another at a distance of $L > 10d_0$ and close at a distance of $L > 3d_0$, the hydrodynamic influence of droplets among themselves can be neglected. Finally, regarding the determination of the mass transfer coefficient, the validity of such calculations for a single droplet was substantiated by Gal-or et al. [64].

In the case of the laminar motion of a droplet at $Re \leq 1$, the drag coefficient is taken equal to $\psi = 24/Re$. Then, we can obtain a solution in elementary functions when substituting into the differential equation of droplet motion.

An analysis of the experimental data shows that the drag coefficient of a droplet is close to the drag coefficient for solid spherical bodies if

$$Re \leq 4.55 g \frac{\sigma^2 \rho_g^2}{\mu_g^4 (\rho_0 - \rho_g)}, \qquad (1.10)$$

where $g = 9.81$ m/s^2 – acceleration of gravity; μ_g – dynamic viscosity of a gas, Pa·s.

When determining the parameters of the droplet flow, the use of the above drag coefficient makes it possible to simplify the calculations and, in some cases, also obtain quantitative characteristics with acceptable calculation accuracy.

As the Reynolds number increases further, the drag coefficient of the droplet significantly differs from the drag coefficient for solid spherical particles. In practice, this is due to a change in the droplet's shape. Thus, many factors impact the motion of particles in a free flow not compressed by the channel walls. When moving in a compressed flow, a simple formula for spherical particles is used [65].

There are a number of solutions to differential equations using a similar expression for the drag coefficient of a droplet. Particularly, the following general formula can be proposed:

$$\psi = A + \frac{B}{Re^C}, \tag{1.11}$$

where A, B, C – dimensionless parameters depending on the used theory.

Therefore, there is no consensus in the literature about the drag coefficient value of a liquid droplet that moves in a gas flow. The experimental data given in their work allow formulating the following conclusions.

Firstly, the deformation of droplets with a diameter greater than 1–2 mm leads to significant deviations of the drag coefficient of the droplet from the drag coefficient for solid spherical particles.

Secondly, as the droplet diameter decreases, the Laplacian pressure begins to play an increasingly important role, the value of which is inversely proportional to the droplet radius. As a result, the droplet's shape approaches a spherical one. The drag coefficient for a droplet approaches the drag coefficient for a solid sphere.

There are a number of other experimental works on the determination of the drag coefficient of a droplet. For a developed turbulent flow, the drag coefficient can be taken constantly.

In addition to solving the equation of motion of a single droplet in a stationary mode, some works present the results of theoretical and experimental studies in the cases of nonstationary motion [66, 67] and the motion of an evaporating droplet of variable mass [68, 69].

The motion of a solid particle in a rotating gas flow can be considered using the equation of motion in cylindrical coordinates:

$$\begin{cases} \frac{dW_r}{dt} = \frac{V_\varphi^2}{r} + \psi \frac{\pi \mu_g d_0}{8m}(V_r - W_r); \\ \frac{dW_\varphi}{dt} = -\frac{W_r W_\varphi}{r} + \psi \frac{\pi \mu_g d_0}{8m}\left(V_\varphi - W_\varphi\right), \end{cases} \quad (1.12)$$

where W_r, V_r – radial velocities of a particle and a flow, respectively, m/s; W_φ, V_φ – angular velocity of a particle and a flow, respectively, m/s; m – droplet mass, m.

The equations are solved for the case of stationary rotation, when $dW_r/dt = 0$, $W_r = 0$, and $W_\varphi = V_\varphi$. The motion of a solid particle from the periphery to the central region was considered.

In the existing designs of vortex apparatuses, three central cases of liquid and gas droplet motion are described: direct-flow, crossflow, and equilibrium.

With direct flow, microdroplets of atomized liquid are carried away by the gas flow from the apparatus. In the case of a cross-current, liquid droplets and gas participate both in rotational motion and in motion along the radius and along the mass transfer chamber axis. In the equilibrium mode of motion. At a certain radius of the mass-exchange chamber, the values of the centrifugal force acting on the droplet and the resistance forces can equalize. Then, the movement of the droplet to the periphery will stop, and the droplet rotates in a circle with a constant radius.

Before designing vortex counterflow mass transfer apparatuses, theoretical and experimental studies of the countercurrent vortex motion of liquid and gas microdroplets were not previously carried out. This is explained by the complexity of solving such a problem analytically.

1.5 The motion of liquid films and the end effect in a vortex chamber

When moving from the center to the periphery of the vortex mass transfer chamber, under centrifugal forces, the liquid is a droplet medium distributed over the volume of the vortex chamber. After reaching the cylindrical walls of the working chamber, the liquid settles on them in the form of a film. The gas flow, which is introduced into the mass transfer chamber tangentially at the periphery of this vortex chamber, moves in the circumferential direction along the chamber wall, taking the liquid film with it and involving it in rotational motion. Since the circumferential velocity of the gas near the cylindrical wall is small in magnitude, the forces acting on the film from the side of the gas flow will be commensurate with the gravity forces that drag the film to the lower end cap. Thus, the liquid film on the inner cylindrical surface of the wall of the mass transfer chamber takes part in two movements. Under the action of the gas flow, the liquid moves in the circumferential direction and, simultaneously, flows down to the lower end cap (Figure 1.10).

From the point of view of evaluating the effect of film flow in a vortex countercurrent mass transfer apparatus on the efficiency of mass transfer processes that occur in it, it can be noted that the presence of such a film flow worsens its characteristics. This happens due to the direct-flow movement of liquid films with gas (steam), both along the cylindrical surface and along the end caps.

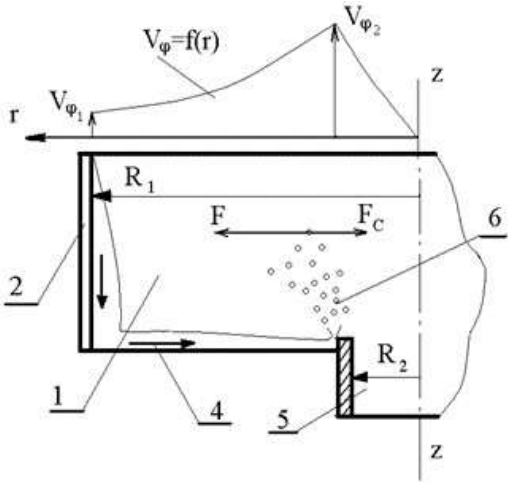

Figure 1.10 – Movement of liquid films in a vortex chamber:
1 – vortex chamber; 2 – tangential slots; 4 – end cap;
5 – gas outlet pipe; 6 – liquid film shear zone

Along with positive factors, such as improving the conditions for dispersed liquid into droplets increasing the degree of flow turbulence, flows arise that adversely affect the efficiency of the countercurrent spraying mass transfer apparatus. One of them is the flow of a liquid film over the end caps of the mass transfer chamber.

The reason that causes the phenomena of the end motion of the liquid film is as follows. As the end cap is approached, the velocities in the vortex gas flow decrease due to the presence of viscosity and friction of the gas against the end caps. In this case, in the core of the flow, as the velocity increases, the pressure decreases. Moreover, for an ideal gas, the circumferential velocity tends to infinity towards the center of the vortex chamber, and the pressure decreases to zero.

In an actual flow, due to the presence of viscosity and the removal of the gas flow from the vortex chamber in one of the

end caps, the flow pattern differs significantly from the flow of an ideal gas, but the tendency for a drop in static pressure is clearly stated (Figure 1.11).

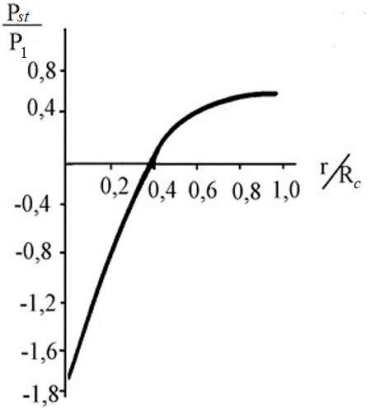

Figure 1.11 – Change in static pressure along the radius of the mass transfer chamber

Thus, in the layer close to the end cap, the pressure field becomes dominant over the field of centrifugal forces. In this case, under the action of a pressure droplet, the thin liquid film is involved in a movement on the periphery of the end cap. This movement is directed to the center of the vortex chamber, where the film can be torn off at the exit from the chamber and further direct-flow movement of liquid and gas droplets. Such a phenomenon in a countercurrent apparatus is undesirable.

A theoretical study of a vortex flow and its friction against a plane normal to the axis of the vortex confirmed the possibility of the appearance of radial and axial flows on the end cap.

Ways to eliminate end currents in vortex mass transfer chambers can be determined based on an analysis of the hydrodynamic situation in which these flows arise. A decrease

in the pressure drop along the end cap can be achieved by reducing the gas velocity in the central region, which is unacceptable since it entails an increase in the size of the sprayed liquid droplets. The most expedient is the timely removal of liquid from the cylindrical walls of the mass transfer chamber and the reduction of the replenishment of the end flow with liquid that flows down from the walls of the working chamber.

Based on the limited information in the literature on the end effect in a vortex apparatus, it can be concluded that these problems have not been sufficiently studied. An urgent need to study end currents arose with the development of devices that use the vortex motion of flows. The end effect requires further study to consider radial end fluid flows and develop methods to eliminate this phenomenon.

1.6 Differences between direct vortex flow, crossflow, and counterflow of gas and droplet flows

The schemes of flow movement in the vortex chambers of direct-flow vortex devices and devices with cross-phase movements considered in the previous sections make it possible to analyze the movement of droplets to determine the cause of the appearance direct-flow or crossflow. In Figure 1.12, a diagram of the flow of flows in a direct-flow vortex contact device is shown.

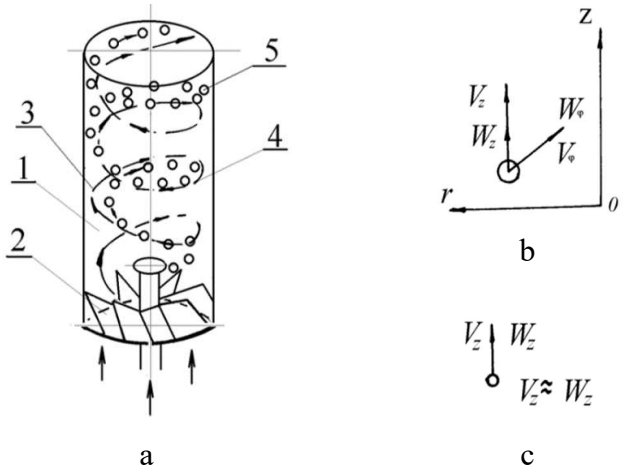

Figure 1.12 – Flow movement in a cocurrent vortex contact device (a), and flow velocity in absolute (b) and relative (c) movements: 1 – mass transfer chamber; 2 – axial swirler; 3 – atomizer; 4 – direction of gas flow; 5 – droplet direction

The interaction of the phases and the spraying of the liquid occurs in the lower part. For clarity, the figure shows a diagram with an axial gas swirler. In the case of a tangential swirler located in the lower part, the flow pattern would change somewhat only near the swirler itself. The main part of the contact device is occupied by a vortex chamber, in which there is a helical joint movement of liquid in the form of droplets and gas. The diagram of the direction of phase velocities is shown in Figure 1.12 b. The flows move along the axis of the apparatus, simultaneously, participating in the rotational movement. If the coordinate system is rotated together with the gas flow, i.e., we consider the movement of the liquid phase relative to the gas (Figure 1.12 c), then due to the small difference in the circumferential velocities of the gas and liquid, their joint movement along the apparatus axis is apparent.

In Figure 1.13, a flow diagram explains the crossflow of phases. The gas introduced in the upper part of the chamber through the swirler moves along a helical expanding trajectory to the lower part of the apparatus, sprays the liquid in the upper part, and captures it in a rotational motion.

In Figure 1.13 b, the direction of the phase velocities is shown, from which it can be seen that a droplet of liquid, like a gas, participates in three movements. If we consider the movement of liquid relative to gas, that is, in a coordinate system that rotates together with the gas, then we can see that the movement of gas and liquid flows (Figure 1.13 c) occurs at an angle to each other, which characterizes the cross movement.

Figure 1.13 c shows that the phases' cross-motion can be considered the sum of countercurrent (along the chamber radius) and cocurrent (along the chamber axis) movements.

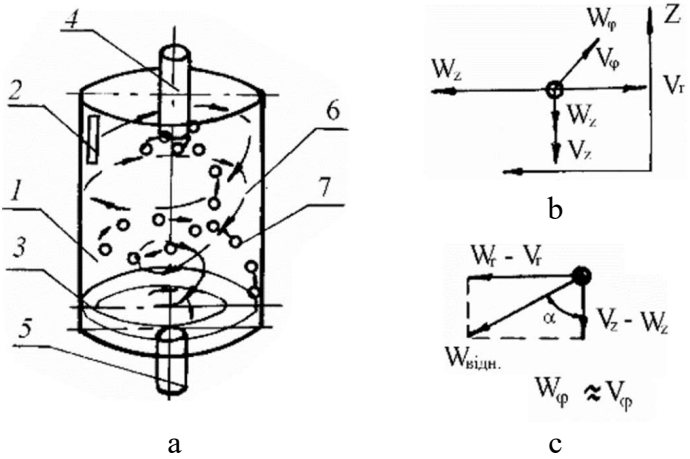

Figure 1.13 – The movement of flows in the device with cross current (a), and the velocity of flows in absolute (b) and relative (c) movement: 1 – mass transfer chamber; 2 – tangential gas inlet; 3 – liquid outlet; 4 – atomizer; 5 – gas outlet; 6 – gas movement; 7 – the movement of droplets

The presence of direct-flow phase movement in the two schemes of flow organization considered leads to the fact that in devices that implement such flows, about one theoretical stage of changing the concentration in one spraying step is achieved. Analysis of the reasons for direct-flow phase movement's appearance and elimination leads to the following flow diagram, shown in Figure 1.14.

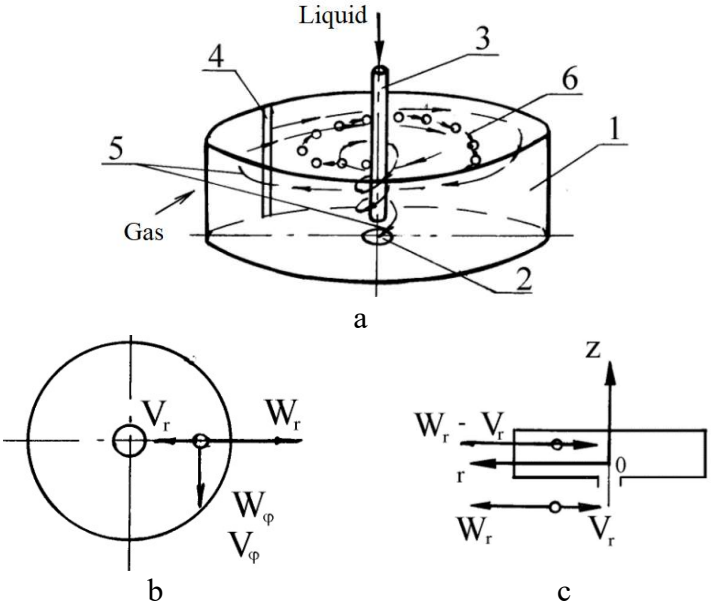

Figure 1.14 – Flow movement in a vortex apparatus with phase counterflow in the contact zone (a), and flow velocity in absolute (b) and relative (c) motions: 1 – mass transfer chamber; 2 – gas outlet; 3 – atomizer; 4 – tangential gas inlet; 5 – direction of gas movement; 6 – direction of droplet movement

Here, the gas is introduced at the periphery through tangential inlets and moves towards the center along a flat spiral trajectory. Only directly at the axis of the apparatus is the restructuring of the gas flow, an axial flow appears, and the gas is removed in the axial direction through one of the end caps.

Figure 1.14 b shows the direction of flow velocities in absolute motion. The gas flow entrains liquid droplets in rotational motion. As the peripheral velocities increase, centri-

fugal forces begin to act on the liquid droplets, entraining the droplets from the center to the periphery.

Figure 1.14 c shows the case of the small difference between the circumferential velocities of gas and liquid and considering the movement of droplets relative to the gas flow, the possibility of countercurrent movement of a continuous phase (gas) and a dispersed phase (liquid droplets) along the radius of the mass transfer chamber in the phase contact zone.

After analyzing the design of the mass transfer chamber, from the point of view of creating a flat spiral gas flow, it can be assumed that with a low apparatus height and sufficiently large radial dimensions, such flow organization becomes possible. In this case, two more factors arise that positively affect the process of mass transfer intensification. Due to the increase in the radial dimensions of the mass transfer chamber, one should also expect a significant increase in the circumferential velocity of the gas near the central region, which is confirmed by the formulas given earlier, for example, (1.3) and (1.4). The liquid introduced into the spray zone will be affected by a high-speed gas flow, which leads to a significant decrease in the size of liquid droplets (1.9), the development of an interfacial surface, and an increase in the mass transfer rate (1.1).

In addition, as the droplet moves along the radius of the mass transfer chamber, it is affected by the field of circumferential gas velocities. The presence of a sizeable peripheral velocity field gradient (Figure 1.15) shows that a drop moving along the radius is affected by gas with different peripheral velocities on both sides of the droplet along the radius of the mass transfer chamber. The surface of the droplet is deformed. The internal circulation currents increase. The process of renewal of the interfacial surface is significantly accelerated, which also leads to an increase in the mass transfer rate.

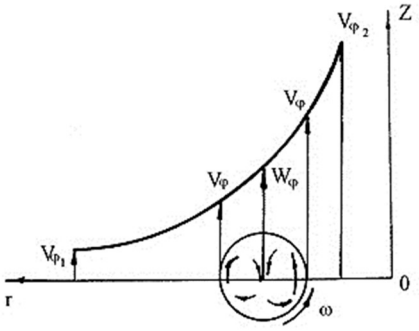

Figure 1.15 – Scheme of influence on a droplet in a gas flow in a countercurrent apparatus

Thus, all these physical processes, such as the development of the interfacial surface, turbulence of flows, and an increase in internal circulation flows in droplets, together with the possibility of organizing countercurrent movement of phases in such a flow, made it possible to obtain several theoretical stages of concentration change in one spray stage.

Based on the analysis carried out, the following basic requirements for the organization of flows can be distinguished to create countercurrent vortex motion of gas (steam for the rectification process) and liquid, in the form of droplets, phases.

Firstly, the movement of the gas flow must be flat spiral in the predominant part of the mass transfer chamber.

Secondly, the liquid droplets obtained from spraying must be very small. In this case, the droplets are practically immediately involved in rotational motion with a circumferential velocity close to the gas velocity.

Finally, the velocity field of the gas flow must be uniform along with the height of the chamber in the contact zone, which makes it possible to organize (in relative motion) the movement of droplets along flat spiral trajectories countercurrent to the gas.

2 Theoretical Background of Mass Transfer Intensification between Droplets and a Gas at a Vortex Countercurrent Motion

2.1 Features of a flow around droplets in vortex gas flows

During the movement of the gas-droplet mixture in mass-exchange apparatuses of the atomizing type, the Venturi apparatus, in the vortex apparatuses of the atomizing type with a cross-flow or direct-flow movement of the phases, the liquid droplets move in the gas flow, which changes velocity in the course of its movement. If we consider the movement of liquid droplets in these apparatuses in a plane that coincides with the direction of gas flow, we can see that the gas flow flows around it on both sides of the droplet with velocities equal in magnitude or slightly different from each other. Another picture is observed during the movement of liquid droplets in the working chamber of the vortex spraying countercurrent mass transfer apparatus.

As already shown in Chapter 1, along the radius of the vortex mass transfer chamber with a counterflow of droplets and gas along the radius of the vortex mass transfer chamber, there is a gradient of circumferential gas velocities. The experimental data of various researchers presented in the following chapters show that, when the diameter of the vortex mass transfer chamber is 1.5 m, the tangential velocity of the gas flow when moving from the periphery to the center changes from 30 m/s to 100 m/s. In these devices, the liquid is introduced into the vortex mass-transfer chamber in the zone of highest velocities. Such a high-speed gas flow breaks liquid jets into liquid droplets, which

have a small diameter of about 50 μm and participate together with the gas flow in rotational motion around the axis of the mass transfer chamber with velocities close in magnitude to the gas velocities. The movement of droplets in the radial direction relative to the gas flow has the opposite direction.

Thus, moving from the center to the periphery of the vortex mass-transfer chamber, the droplets cross the gas flow, directed both circumferentially and countercurrent to the droplets from the periphery to the center along the radius of the vortex chamber.

In this case, in the circumferential direction of the liquid droplet, a gas flow flows around. The velocities differ significantly from each other on both sides on the surface of the droplet.

Such an influence of gas on droplets, in the direction transverse to the radial motion, affects the hydrodynamics of the liquid in the droplet and, in general, the process of mass transfer. The results of theoretical studies of the hydrodynamics of one- and two-phase vortex flows presented below allow us to conclude that it is possible to create conditions for finely dispersed liquid spraying into droplets 50–100 μm in size. This makes it possible to obtain a developed interfacial surface and, as a result, intensify mass transfer processes.

However, on the other hand, droplets of such a diameter are less susceptible to deformation and secondary breakup, reducing the mass transfer rate and further searching for an effective mechanism for intensifying heat and mass transfer processes.

The interaction of a vortex gas flow, which moves with a significant change in the circumferential velocity, has not been solved with droplets. Existing works on circulating currents in a droplet [70, 71] mainly consider an equal-velocity gas flow. Therefore, it is relevant to analyze the hydrodynamics of a liquid

droplet that moves in a vortex gas flow from the center to the periphery of the mass transfer chamber to determine the force effect of the gas on the droplet, its rotation velocity, the intensification of internal circulation currents and their effect on the efficiency of mass transfer processes. The solution to such problems is given in this monograph.

Such a theoretical analysis of the interaction of droplets with a vortex gas or vapor flow is based on the following substantiated, both theoretically and experimentally, assumptions:

– a liquid droplet has a small size, as a result of which its shape approaches a spherical one, and there will be no conditions for its secondary breakup;

– the value of the drag coefficient approaches the value of the drag coefficient for a solid sphere;

– when droplets move along the radius from the center to the periphery, the distance between them increases, making it possible to neglect their mutual influence. The ratio of loads in the gas and liquid phases is less than one;

– the droplet's movement is carried out along a flat spiral trajectory. The circumferential velocities of the gas increase from the periphery to the center.

2.2 Force impact on a liquid droplet in a gas flow with a transverse velocity gradient

Let us consider a liquid droplet involved in rotational motion around the A-A axis and moving in the vortex chamber from the center to the periphery at a distance r from the chamber axis (Figure 2.1).

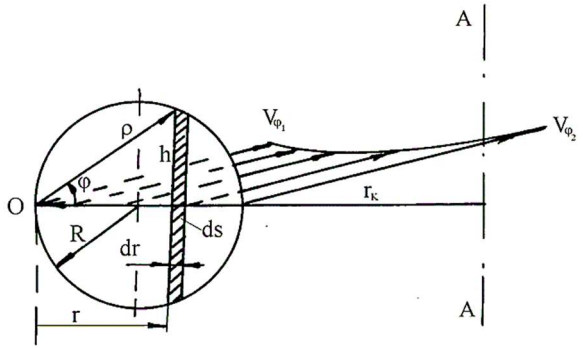

Figure 2.1 – Scheme of the gas effect on a drop

The gas flow fed in the tangential direction into the vortex chamber with a velocity $V = \sqrt{V_\varphi^2 + V_r^2}$ (V_φ and V_r – circumferential and radial velocities, respectively). Gas moves from the periphery to the center of the mass transfer chamber.

In the general case, the change in the circumferential velocity of the gas is described by a non-linear law, but based on the small size of the droplets, which is usually sought in spray-type apparatus to increase the interfacial surface, in a zone of 2R (R – droplet radius), a linear law can be considered:

$$V_\varphi = a_1 r + a_2;\ a_1 = \frac{V_{\varphi_2} - V_{\varphi_1}}{2R};\ a_2 = V_{\varphi_2}, \qquad (2.1)$$

where R – droplet radius, m; a_1 – transversal velocity gradient, s^{-1}; $V_{\varphi 1}$, $a_2 = V_{\varphi 2}$ – angular velocities on both sides of a droplet, m/s.

The force acting on the droplet from the side of the gas stream, N:

$$F_d = \int_s dF_d, \qquad (2.2)$$

where s – droplet's cross-sectional area, m^2; ψ – drag coefficient; ρ_g – gas density, kg/m^3; ds – infinitesimal area normal to the circumferential direction, m^2.

Under the predominance of centrifugal forces over the forces involving droplets to the center, V_φ will significantly exceed the value of V_r. Therefore:

$$dF_d = \psi \frac{\rho_g V_\varphi^2}{2} ds. \quad (2.3)$$

Value of ds is determined as follows:

$$ds = 2hdr, \quad (2.4)$$

where dr – infinitesimal increment of droplet radius, m; h – the height of the elementary part of the droplet cross-section, m.

Introducing polar coordinates with angle φ, rad, and radius ρ, m:

$$\begin{gathered} \rho = 2Rcos\varphi; r = \rho cos\varphi; \\ dr = 4Rcos\varphi sin\varphi d\varphi; h = \rho sin\varphi, \end{gathered} \quad (2.5)$$

it can be obtained:

$$ds = -16R^2\, cos^2\, \varphi\, sin^2\, \varphi\, d\varphi. \quad (2.6)$$

Thus, equation (2.3) takes the form:

$$dF_d = 8\psi\rho_g V_\varphi^2 R^2\, cos^2\, \varphi\, sin^2\, \varphi\, d\varphi, \quad (2.7)$$

and considering equation (2.1) –

$$dF_d = 8\psi\rho_g V_\varphi^2 R^2 (a_1 r + a_2)^2\, cos^2\, \varphi\, sin^2\, \varphi\, d\varphi. \quad (2.8)$$

The total force F_d can be determined by integrating this equation over the angle range φ from $\pi/2$ to 0. Considering

$$r = \rho \cos\varphi = 2R\cos^2\varphi, \tag{2.9}$$

it can be obtained:

$$F_d = 8\psi\rho_g R^2(I_1 + I_2 + I_3), \tag{2.10}$$

where the following auxiliary integrals have been introduced:

$$\begin{gathered} I_1 = 4R^2a_1^2\int_0^{\pi/2}\cos^6\varphi\sin^2\varphi\,d\varphi = \frac{5}{8}\pi R^2a_1^2; \\ I_2 = 4Ra_1a_2\int_0^{\pi/2}\cos^4\varphi\sin^2\varphi\,d\varphi = \frac{\pi}{8}Ra_1a_2; \\ I_3 = a_2^2\int_0^{\pi/2}\cos^2\varphi\sin^2\varphi\,d\varphi = \frac{\pi}{16}a_2^2. \end{gathered} \tag{2.11}$$

Then the final expression for determining the force takes the form:

$$F_d = 8\pi\psi\rho_g R^2\left(\frac{5}{8}R^2a_1^2 + \frac{R}{8}a_1a_2 + \frac{a_2^2}{16}\right). \tag{2.12}$$

If transversal velocity gradient in the gas flow will be absent, i.e., $V_{\varphi 1} = V_{\varphi 2} = a_2$, then $a_1 = 0$, and equation (2.12) takes the following form:

$$F_d^* = 8\pi\psi\rho_g R^2\frac{V_{\varphi_1}^2}{16} = \psi\frac{\rho_g V_{\varphi_1}^2}{2}\pi R^2 = \psi\frac{\rho_g V_{\varphi_1}^2}{2}S. \tag{2.13}$$

Of particular interest is the problem of finding the point of application of the resultant force F_d. This is because moment M_d, N·m, leads to the droplet rotation. This moment can be obtained

considering action of elementary moments of forces *dF* about the origin 0 (Figure 2.1):

$$M_d = \int_s dM_d, \tag{2.14}$$

where

$$dM_d = rdF_d = 16\psi\rho_g R^3(2Ra_1\cos^2\varphi + a_2)^2 \times \\ \times \cos^4\varphi \sin^2\varphi\, d\varphi, \tag{2.15}$$

where *r* – radius, m.

After identical transformations, the value of *M* is as follows:

$$M_d = 16\psi\rho_g R^3(I_1^* + I_2^* + I_3^*), \tag{2.16}$$

where the following integrals have been introduced:

$$I_1^* = 4R^2a_1^2\int_0^{\pi/2}\cos^8\varphi \sin^2\varphi\, d\varphi = \frac{7}{128}\pi R^2a_1^2; \\ I_2^* = 4Ra_1a_2\int_0^{\pi/2}\cos^6\varphi \sin^2\varphi\, d\varphi = \frac{5}{8}\pi Ra_1a_2; \\ I_3^* = a_2\int_0^{\pi/2}\cos^4\varphi \sin^2\varphi\, d\varphi = \frac{\pi}{32}a_2^2. \tag{2.17}$$

After considering the integration results, the dependence (2.14) takes the form:

$$M_d = 16\pi\psi\rho_g R^3\left(\frac{7}{128}R^2a_1^2 + \frac{5}{8}Ra_1a_2 + \frac{a_2^2}{32}\right). \tag{2.18}$$

Quantities M_d and F_d allow determining the distance r_F from the origin 0 to points of application of force, m:

$$r_F = \frac{M_d}{F_d} = 2R\,\frac{\frac{7}{128}R^2a_1^2+\frac{5}{8}Ra_1a_2+\frac{a_2^2}{32}}{\frac{5}{8}R^2a_1^2+\frac{1}{8}Ra_1a_2+\frac{a_2^2}{16}}. \qquad (2.19)$$

For a uniform gas flow ($V_{\varphi 1} = V_{\varphi 2}$), values M_d^* and r^* are

$$M_d^* = \pi\psi\rho_g R^3\,\frac{a_2^2}{32} = \frac{\psi}{2}\rho_g V_\varphi^2 sR; \qquad (2.20)$$

$$r_F^* = \frac{M_d^*}{F_d^*} = R. \qquad (2.21)$$

Thus, the point of application of the resultant is at the center of the symmetry of the droplet. Therefore, rotation of a droplet does not occur.

Overall, the transverse velocity gradient in the gas flow leads to the droplet rotation and additional shear stresses on its surface due to the friction of the gas flow over the droplet surface. This, in turn, affects the turbulence of internal flows in the droplet and the intensification of mass transfer processes.

2.3 Intensification of internal currents in a droplet under the impact of a gas flow with a transverse velocity gradient

As shown in Chapter 1, the difference in velocities in the gas flow on the droplet's surface leads to a shift in the application point of the resultant aerodynamic forces acting on the droplet and leading to its rotation. On the other hand, the movement of the outer layers leads to internal circulation currents and acceleration of the mass transfer inside the droplet. In other words, such processes lead to an acceleration of mass transfer. From this point of view, it is of considerable interest to reveal the relationship between the parameter a_1, which characterizes the intensity of the increase in the peripheral gas velocity gradient along the radius of the mass transfer chamber, and the increase in the intensity of internal circulations.

Let us consider the influence of a gas flow on a droplet of a viscous liquid in a spherical coordinate system, the center of which coincides with the center of the droplet (Figure 2.2), which leads to the occurrence of a moment determined by the mathematical expression (2.18).

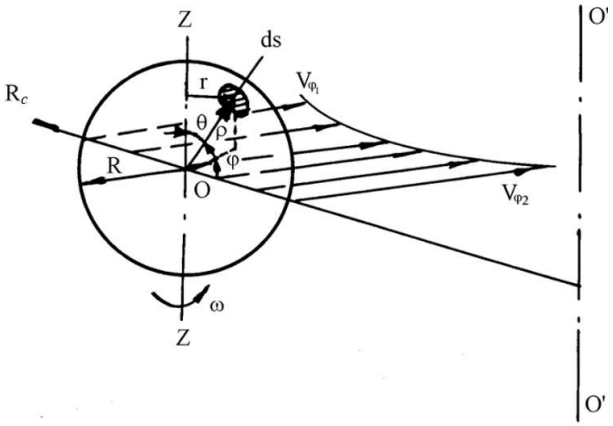

Figure 2.2 – Scheme of the motion of a droplet in a vortex gas flow: O/-O/ – vortex chamber axis; ρ – radius, m; θ, φ – angles, rad; ω – angular velocity, rad/s; R – droplet radius; r – radius of rotation for elementary area ds

As a result of rotation, shear stress appears on the droplet surface, N/m^2:

$$\tau = \mu_g \frac{dV_s}{d\rho}, \tag{2.22}$$

where μ_g – gas dynamic viscosity coefficient, Pa·s.
The linear velocity on the droplet surface, m/s:

$$V_s = \omega r. \tag{2.23}$$

where ω – angular velocity of the selected element, rad/s.
Therefore, infinitesimal velocity increment dV_s, m/s:

$$dV_s = \omega dr + r d\omega. \tag{2.24}$$

where $d\omega$ – infinitesimal increment of angular velocity, rad/s.

After considering $r = \rho \sin\theta$ (where θ – angle, rad), and

$$dr = \sin\theta\, d\rho + \rho \cos\theta\, d\theta, \quad (2.25)$$

equation (2.24) takes the following form:

$$dV_s = \omega \sin\theta\, d\rho + \omega\rho \cos\theta\, d\theta + \rho \sin\theta\, d\omega, \quad (2.26)$$

where $d\rho$ – infinitesimal increment of radial coordinate, m.

Therefore, the expression for the normal velocity gradient takes the form:

$$\frac{dV_s}{d\rho} = \omega \sin\theta + \omega\rho \frac{d\theta}{d\rho} + \rho \sin\theta \frac{d\omega}{d\rho}, \quad (2.27)$$

and the magnitude of shear stress is equal to

$$\tau = \mu_g \left(\omega \sin\theta + \omega\rho \cos\theta \frac{d\theta}{d\rho} + \rho \sin\theta \frac{d\omega}{d\rho}\right). \quad (2.28)$$

After considering the boundary layer of gas on the surface of a droplet with a thickness δ, m, under the assumption that $d\rho \approx \delta$, and $d\omega \approx \omega_0 - \omega_g$ (where ω_0 and ω_g – the angular velocities of the droplet and gas, respectively, rad/s), after simplification $\omega_g \approx 0$, the last equation converted as follows:

$$\tau = \mu_g \left(\omega_0 \sin\theta + \frac{\omega_0}{\delta} R \cos\theta\, d\theta + R \sin\theta \frac{\omega_g}{\delta}\right). \quad (2.29)$$

The friction force acting on the elementary area of the droplet surface, N:

$$dT = \tau ds = \mu_g \omega_0 \left(\sin\theta + \frac{R}{\delta} \cos\theta\, d\theta + \frac{\rho}{\delta} \sin\theta\right) ds. \quad (2.30)$$

where $ds = R^2 \sin\theta d\theta d\varphi$ in the spherical coordinate system, and $r = R sin\theta$ – on the droplet surface.

Equation (2.27) can be simplified, assuming that the term containing the factor $d\theta$ is small concerning other terms. In this case,

$$dT = \mu_g \omega \left(1 + \frac{R}{\delta}\right) sin\,\theta\, ds. \tag{2.31}$$

Then the value of the friction force of the gas on the surface of the rotating droplet is equal to:

$$T = 2\mu_g \omega_0 R^2 \left(\int_0^\pi \int_0^\pi sin^2\,\theta\, d\theta d\varphi + \frac{R^3}{\delta} \int_0^\pi \int_0^\pi sin^2\,\varphi\, d\varphi\right), \tag{2.32}$$

or after integration:

$$T = \pi^2 \mu_g \omega_0 R^2 \left(1 + \frac{R}{\delta}\right). \tag{2.33}$$

If we assume that the droplet's rotation axis passes through its center 0 (Figure 2.2), an elementary moment of friction force, N·m:

$$dM_f = rdT = \mu_g \omega_0 \left(1 + \frac{R}{\delta}\right) R^3\, sin^3\,\theta\, d\theta d\varphi. \tag{2.34}$$

After integration over the entire surface of the droplet, the moment of friction forces is equal to:

$$\begin{aligned} M_f &= 2\mu_g \omega_0 \left(1 + \frac{R}{\delta}\right) R^3 \int_0^\pi \int_0^\pi sin^3\,\theta\, d\theta d\varphi = \\ &= \frac{8}{3} \pi \mu_g \omega_0 \left(1 + \frac{R}{\delta}\right) R^3. \end{aligned} \tag{2.35}$$

The following motion equation describes the droplet's rotational motion dynamics:

$$\frac{d(I_z\omega)}{dt} = \sum M_z, \tag{2.36}$$

where I_z – the moment of inertia of the droplet about the axis of rotation, kg·m^2; ΣM_z – the sum of the moments about the rotation, N·m.

The droplet is not a rigid body, and its moment of inertia is as follows:

$$I_z = \int_\Omega r^2 \rho_0 d\Omega, \tag{2.37}$$

where $d\Omega$ – infinitesimal volume, m^3; r – distance from this volume to the rotation axis, m.

In a spherical coordinate system $d\Omega = \rho^2 \sin\theta dr d\theta d\varphi$, the last equation can be rewritten as follows:

$$I_z = \rho_0 \int_\Omega \rho^4 \, cos^2\,\theta \, sin^3\,\theta \, d\rho d\theta d\varphi, \tag{2.38}$$

and $d(I_z\omega)$ – as a sum:

$$d(I_z\omega) = \omega dI_z + I_z d\omega, \tag{2.39}$$

where $dI_z = \rho_0\rho^4\cos^2\theta\sin\theta d\rho d\theta d\varphi$, and $I_z = (2/5)mR^2$ for a droplet as a solid sphere with the mass of $m = \rho_0\Omega = \rho_0(4/3)\pi R^3$, kg. Therefore, $I_z = (8/15)\rho_0\pi R^5$.

After, equation (2.36) takes the form:

$$\omega\rho_g\rho^4 \, cos^2\,\theta \, sin\,\theta \frac{d\rho}{dt} d\theta d\varphi + \frac{8}{15}\rho_g \pi R^5 \frac{d\omega}{dt} = \sum M_z. \tag{2.40}$$

Due to the shear stresses on the droplet, the value of ΣM_z can be defined as the difference between the moments of velocity gradient and resistance force:

$$\sum M_z = M_d - M_f = 16\pi\varphi\rho_g R^3 \left(\frac{7}{128}R^2 a_1^2 + \frac{5}{8}Ra_1a_2 + \frac{a_2^2}{32}\right) - \\ -\frac{8}{3}\pi\mu_g\omega_0\left(1+\frac{R}{\delta}\right)R^3. \tag{2.41}$$

In turn, the derivative $d\rho/dt$ is the radial component of the fluid velocity W_r, m/s. It characterizes the mass transfer rate inside the droplet.

The value of $\rho^2 \sin\theta d\theta d\varphi$ is an expression for defining an element of a spherical surface ds. Thus, the elementary fluid flow rate dq, m^3/s, through the surface ds:

$$dq = \omega r ds = \frac{d\rho}{dt}\rho^2 \sin\theta \, d\theta d\varphi. \tag{2.42}$$

After considering expressions (2.40)–(2.42), equation (2.36) takes the following form:

$$\omega\rho_g\rho^2 \cos^2\theta \, dq = 16\pi\psi\rho_g R^3 \left(\frac{7}{128}R^2 a_1^2 + \frac{5}{8}Ra_1a_2 + \frac{a_2^2}{32}\right) - \\ -\frac{8}{3}\pi\mu_g\omega_0\left(1+\frac{R}{\delta}\right)R^3 - \frac{\delta}{15}\rho_g\pi R^5\frac{d\omega}{dt}. \tag{2.43}$$

After analyzing this equation, it is possible to reveal the dependence between dq (characterizes the magnitude of radial currents in the droplet) and a_1 (characterizes the peripheral velocity gradient), which is non-linear:

$$dq = \left[16\pi\psi\rho_g R^3 \left(\frac{7}{128}R^2 a_1^2 + \frac{5}{8}Ra_1a_2 + \frac{a_2^2}{32}\right) - \right. \\ \left. -\frac{8}{3}\pi\mu_g\omega_0\left(1+\frac{R}{\delta}\right)R^3 - \frac{\delta}{15}\rho_g\pi R^5\frac{d\omega}{dt}\right] / \left(\omega\rho_g\rho^2 \cos^2\theta\right). \tag{2.44}$$

Thus, the resulting equation confirms the relationship between the transverse gas velocity gradient, radial currents in the droplet, and the intensity of mass transfer processes.

2.4 Intensification of mass transfer in a droplet under a vortex countercurrent gas-liquid flow

Before, it was shown how the transverse gradient of gas flow velocities affects the increase in the internal circulation of the liquid in droplets, the rotation of the droplet in the gas flow, that is, the movement of the upper layers of the liquid in the droplet occurs, which makes it possible to base the theoretical conclusion on the relationship between the circulation currents in the droplet and the intensification of mass transfer processes the following model.

The droplet has a spherical surface. Therefore, the surface layers of the liquid move in the gas flow direction. The last one flows around the droplet in the circumferential direction relative to the axis of the vortex mass transfer chamber. A change in the movement of the liquid towards the center occurs. On the front side of the droplet, there is a radial liquid flow directed from the center to the periphery. It gradually changes the movement direction, growing into a flow along the droplet circumference on both sides.

For each infinitesimal time interval dt, the droplet passes a certain distance together with the gas in the circumferential direction, moving along with the radius of the chamber. This generally determines the spiral trajectory.

Considering the above model of flow movement, for the surface element ds of the droplet, we can write the material balance equation in the differential form:

$$dW_A = -L_0 dx;\ dW_A = \beta_x (x_e - x) ds, \qquad (2.45)$$

where W_A – mass flow rate; β_x – mass transfer coefficient in the liquid phase, kg/(m^2·s); x, x_e – actual and equilibrium

concentrations of the component in the liquid phase, respectively; L_0 – mass flow rate of inert liquid carrier, kg/s:

$$L_0 = \rho_0 dq. \tag{2.46}$$

Then the number of transfer units in the liquid phase:

$$N = \int_{x_1}^{x_2} \frac{dx}{\beta_x(x_p - x)} = -2 \int_0^{\pi} \int_0^{\pi} \frac{ds}{\rho_0 dq}. \tag{2.47}$$

In the spherical coordinate system, values of *ds* and *dq* have been defined above.

After integration over the surface and applying mathematical transformations, it can be obtained:

$$N = \frac{R\omega}{6\left[\frac{\mu_g \omega_0}{3}\left(1+\frac{5}{8}\right)+\frac{\rho}{15}R^2\frac{d\omega}{dt}-2\psi\rho_g\left(\frac{7}{128}R^2a_1^2+\frac{5}{8}Ra_1a_2+\frac{a_2^2}{32}\right)\right]}. \tag{2.48}$$

Let us consider the case when the transverse velocity gradient is absent in the gas flow ($V_{\varphi 1} = V_{\varphi 2}$, and $a_1 = 0$). Then the number of transfer units is determined by the following expression:

$$N^* = \frac{R\omega}{6\left[\frac{\mu_g \omega_0}{3}\left(1+\frac{5}{8}\right)+\frac{\rho}{15}R^2\frac{d\omega}{dt}-2\psi\rho_g\frac{a_2^2}{32}\right]}. \tag{2.49}$$

When comparing the obtained formulas, it becomes evident that $N > N^*$ because the denominators are not equal.

From the expressions mentioned above, it can be concluded that the transverse gas velocity gradient leads to the intensification of internal circulation currents. This fact, in turn, increases the intensity of mass transfer and the number of theoretical units:

$$\frac{N}{N^*}=\frac{\frac{\mu_g\omega_0}{3}\left(1+\frac{5}{8}\right)+\frac{\rho}{15}R^2\frac{d\omega}{dt}-2\psi\rho_g\frac{a_2^2}{32}}{\frac{\mu_g\omega_0}{3}\left(1+\frac{5}{8}\right)+\frac{\rho}{15}R^2\frac{d\omega}{dt}-2\psi\rho_g\left(\frac{7}{128}R^2a_1^2+\frac{5}{8}Ra_1a_2+\frac{a_2^2}{32}\right)}>1. \quad (2.50)$$

The quantitative solution of equation (2.48) is complicated due to the uncertainty of the constituent containing ω_0, $d\omega/dt$, and δ. This complexity is predetermined by the non-stationary nature of the hydrodynamic interaction of flows.

The identification of mass transfer characteristics and their relationship with the hydrodynamics of flows in the vortex chamber can be studied theoretically and experimentally, as presented below.

3 Monitoring of Hydrodynamics of a Two-Phase Vortex Gas-Droplet Flow

3.1 Hydrodynamic features of vortex spraying countercurrent mass transfer apparatuses

The study of hydrodynamic processes in various designs of mass transfer equipment, including in vortex mass transfer chambers, is the subject of many works, both foreign and leading scientists from Europe. However, as the analysis of literary sources shows, the hydrodynamics of the vortex mass transfer chamber depends on its design features, which in turn affects the dispersion of the droplet flow, the time the droplets stay in the contact zone, the turbulence of the liquid in the droplets, the spray entrainment and other factors that determine the operation of the apparatus.

Thus, the main task of the vortex mass transfer apparatus researchers with phase counterflow in the contact zone was to study the essence of the processes occurring in the vortex working chamber to determine the scope and expediency of using the considered apparatuses in various industries. This monograph presents the results of both theoretical and experimental studies confirming the high efficiency of vortex apparatuses and the adequacy of the mathematical models underlying the description of the physical processes occurring in the working vortex chamber.

Theoretical studies of the hydrodynamics in a vortex countercurrent mass transfer apparatus identify the most favorable form of a gas flow in the area where liquid droplets move. The most rational way to spray liquid in such a gas flow is creating conditions for regular countercurrent movement of vortex gas-droplet flows throughout the entire volume of the

working chamber with the same intensity of mass transfer processes.

Such studies make it possible to identify the main patterns of changes in the hydrodynamic situation depending on the determining geometric dimensions of the working chamber, their ratio, changes in the shape of flows, and, consequently, factors that can affect the intensity of mass transfer under various technological modes of operation of the apparatus.

On the other hand, the theoretical study of hydrodynamics is highly complicated due to the three-dimensional two-phase turbulent flow. This fact leads to the need to solve high-order partial differential equations with variable coefficients, which, despite the significant development in recent years of various methods of numerical solutions, complicates obtaining results that are sufficiently accurate for engineering practice. In particular, the pattern of motion becomes more complicated in the presence of a liquid phase in the flow, both in the form of films and droplets, which in the most general case have a polydisperse composition.

Thus, to obtain solutions that would be effective for describing hydrodynamic processes in a working vortex mass transfer chamber, an approach based on various simplifying proposals and semi-empirical theories is of interest.

After considering all the above remarks, this study presents the results of the following research algorithm. First of all, the results of studies of the vortex motion for a single-phase gas flow are presented. The results of studies allow determining parameters of countercurrent movement of the gas flow with liquid droplets, the effect of phase loads on the dispersion of the spray, the effect of the location of the atomizer in the working chamber on the quality of the spray, and the regular countercurrent movement of droplets and gas. In this case, some assumptions and simplifications were used, which made it

possible to obtain a solution in the form of elementary functions, which makes it possible to carry out a multifaceted analysis of the qualitative influence of both the geometric dimensions of the apparatus and the flow regimes on the countercurrent movement of phases in the working mass transfer chamber.

The information obtained made it possible to create semi-empirical calculation methods suitable, with sufficient accuracy for engineering calculations, determine the geometry of the working chamber of a vortex countercurrent mass transfer apparatus, and select the optimal mode of its operation.

3.2 Movement of a single-phase vortex gas flow in a working chamber

After sequent considering all the stages in liquid's movement in the mass transfer chamber of a vortex spraying countercurrent mass-exchange apparatus, it is possible to identify the main features of the movement of a single-phase gas flow in the working chamber.

For creating a fine spray of a liquid into microdroplets with a size of about 50 μm, it is necessary to achieve gas flow velocities of up to 100 m/s in the spray zone.

It is necessary to create a counterflow gas (in relative motion) of liquid droplets to provide appropriate conditions along the radius of the mass transfer chamber. The value of circumferential gas velocities must be sufficient to create a field of centrifugal forces that involve liquid droplets in motion from the center to the periphery of the vortex chamber (countercurrent gas along the radius). The same condition follows the requirement for the axial composite velocity of the gas flow, which should not impede the movement of liquid droplets along flat

spiral trajectories in the plane perpendicular to the axis of the vortex mass transfer chamber.

The movement of the vortex gas flow is decisive in the hydrodynamics of the mass transfer chamber in terms of high-quality atomization due to the difference in phase velocities and the formation of a droplet vortex flow by involving droplets in rotational motion. Under centrifugal forces, droplets move from the center to the periphery of the chamber.

The requirements listed above for the organization of gas movement and the need to create a uniform and intense mass transfer throughout the volume of the chamber with minimal spray entrainment make it possible to highlight some features of the gas flow in the vortex chamber.

Fristly, the movement of the vortex gas flow in the predominant part of the mass transfer chamber should occur in a plane normal to the axis of the chamber. In the predominant region of the volume of the vortex chamber, there should be no axial components of the total gas velocity. In this case, the gas flow will not affect the droplets along the chamber axis, due to which the liquid may be entrained towards one of the end caps to the gas outlet from the chamber. In this case, the conditions favorable for spray entrainment (entrainment of droplets together with the gas flow from the vortex mass transfer chamber) will disappear.

Secondly, in the area of plane spiral motion of the gas, there should be a maximum of circumferential gas velocities, which should be used to atomize the liquid into small droplets, which immediately after atomization fall into the zone of a flat gas flow. These droplets are entrained by the gas in a rotational motion and will move along flat spiral trajectories to the periphery of the mass transfer chamber, which is an essential condition for the efficient operation of the apparatus.

In the ideal case, the organization of the movement of the gas flow is as follows. The gas is introduced in the tangential direction evenly over the entire height of the mass transfer chamber at its periphery. Gas removal is carried out directly at the axis of the chamber evenly over the entire height.

However, the gas outlet is made as a round hole in the end cap's center in practice. The presence of such a branch leads to the appearance of axial flows, the non-uniformity of the gas velocity field, and the chamber's height, which bends the vortex gas-droplet flow and adversely affects the efficiency of mass transfer.

In its movement from the inlet to the outlet of the mass transfer chamber, the gas takes part in two movements. One of them is the rotation of the gas flow around the axis of the chamber. According to the law of conservation of kinetic moment for an ideal gas:

$$\mathrm{m_i}\frac{\mathrm{d}}{\mathrm{dt}}\left(\mathrm{rV_\varphi}\right) = 0, \tag{3.1}$$

where m_i – the mass of i-th gas volume, kg.

Therefore, the law of change of peripheral gas velocity is as follows:

$$V_\varphi = V_\varphi^{max}\frac{R_0}{r}, \tag{3.2}$$

where R_0 – radius of maximum flow velocity, m.

In actual conditions, due to viscosity and gas removal in the axial direction, the law of variation of the circumferential velocity differs significantly from the law of variation for an ideal gas.

The second component of the gas flow is the flow from the inlet to the outlet of the mass transfer chamber, and for its analysis, it is best to consider the gas flow in a plane that passes

through the axis of the mass transfer chamber. This movement is characterized by the absence of an axial component of the total velocity in the peripheral zone, the appearance, and the increase of this velocity near the central region, where it reaches its maximum value.

As mentioned above, the absence or minimum value of the axial velocity in the zone of countercurrent phase motion is a prerequisite that promotes the creation of a regular counterflow, prevents the curvature of flat spiral trajectories, and the involvement of droplets in the helical motion.

When an axial velocity occurs, the value of which is sufficient to entrain droplets with a gas flow, conditions appear for the occurrence of spray entrainment, the uniform saturation of the chamber with liquid by volume is disturbed, zones with different intensities of mass transfer processes appear, which generally leads to a significant deterioration in the operation of the apparatus.

3.3 Impact of vortex chamber's geometric parameters on flow unevenity

When analyzing the rotational motion of a gas flow, we select a region that is bounded by two cylindrical surfaces (Figure 3.1).

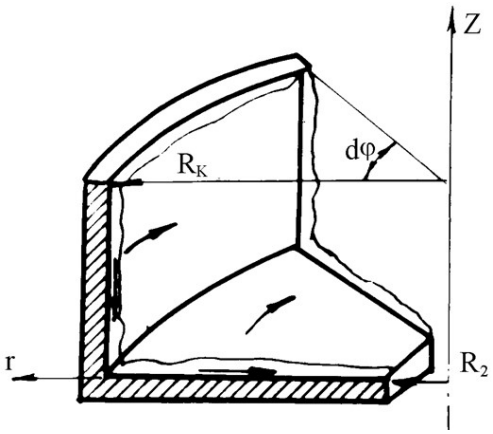

Figure 3.1 – Area marked by an infinitesimal angle $d\varphi$

The inner surface has a radius equal in magnitude to the radius of the surface on which the circumferential gas velocity has a maximum value. The area inside this surface is not considered since it is of no interest for the formation of counter-current phase motion due to the presence of high axial and low circumferential velocities.

The gas motion in the confuser area bounded by two cylindrical surfaces with radiuses R_1 and R_2 (Figure 3.2).

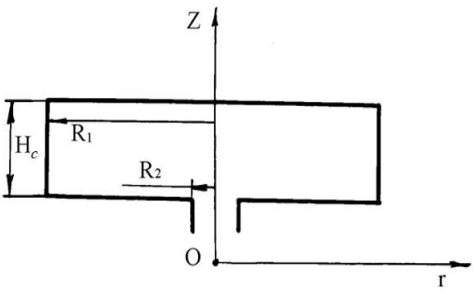

Figure 3.2 – Scheme of the chamber section in a plane

According to the continuity of the medium, the radial velocity from radius R_1 to radius R_2 increases due to a decrease in the cylindrical section's area. Calculations of such three-dimensional confuser flows can be reduced to a two-dimensional problem of gas motion in a layer of variable thickness using a description of the motion of a gaseous medium using potential flows by solving the Laplace equation:

$$\frac{\partial^2 u}{\partial r^2} + \frac{\partial^2 u}{\partial z^2} + \frac{1}{r}\frac{\partial u}{\partial r} = 0, \qquad (3.3)$$

where u – velocity potential, m^2/s; $V_r = \frac{\partial u}{\partial r}$, and $V_z = \frac{\partial u}{\partial z}$ – radial and axial velocity components, respectively, m/s.

However, by analyzing the possible direction of changing the ratio of geometric dimensions to create a flat gas flow, one can be convinced that to achieve this goal, a particular geometry of the vortex chamber with a small (relative to the radius of the vortex chamber) height is required H_c, m.

If the height of the chamber is relatively large, then the unevenness in its height occurs mainly due to the asymmetrical removal of gas, which is usually located in one of the two end caps. It follows that the non-uniformity of the gas flow can be reduced by making two holes symmetrically in both covers or by other design measures, which are described below.

It is possible to qualitatively substantiate the possibility of smoothing the non-uniformity of the flow before it turns, normal to the direction of its initial movement, for example, by solving the problem of the motion of a plane potential gas flow of an ideal liquid in an L-shaped region.

Drawing a simplified analogy between the main geometric dimensions of the mass transfer chamber in the plane that passes through the axis and the main dimensions that characterize the gamma-type turn along which the idealized potential gas flow moves, by using the Laplace equation for a plane flow:

$$\frac{\partial^2 u}{\partial x^2} + \frac{\partial^2 u}{\partial y^2} = 0, \qquad (3.4)$$

where $V_x = \frac{\partial u}{\partial x}$, and $V_y = \frac{\partial u}{\partial y}$ – velocity components in a plane, m/s.

This equation is solved numerically using difference equations:

$$u_{i,j} = \frac{u_{i+1,j} + u_{i-1,j} + u_{i,j+1} + u_{i,j-1}}{4}, \qquad (3.5)$$

which allows analyzing the change in the non-uniformity of the gas velocity field in the cross-section $y = R_2$ (Figure 3.3).

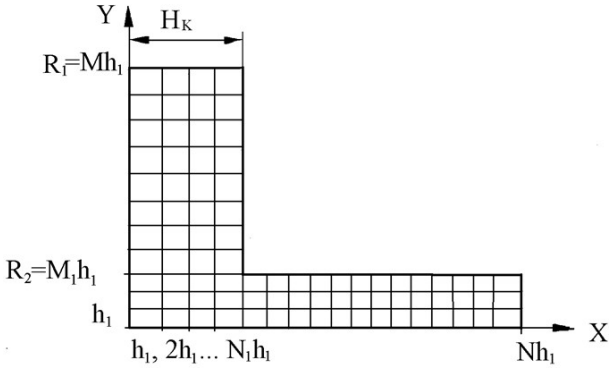

Figure 3.3 – Mesh design for numerical calculations

Based on the features of the movement of the gas flow in the vortex mass-transfer chamber of the countercurrent spray apparatus, it is possible to determine the scheme of movement of a single-phase gas flow, which is as follows.

The gas flow enters the periphery of the vortex mass transfer chamber through tangential slots or a tangential swirl of another design uniformly along with the height. Further, as

mentioned earlier, the gas flow takes part in two movements. The gas flow moves in the radial direction, increasing its velocity and gradually acquiring an axial direction near the center of the vortex chamber.

After setting the boundary conditions about the change in the flow area for the gas flow along with the radius and the gas outlet pipe, it is possible to consider the spatial nature of these flows. Also, the gas flow at the inlet and a considerable distance from the outlet is distributed evenly over cylindrical sections should be considered.

The main assumptions that are used in solving the problem are as follows:

– the gas velocity at the inlet to the mass transfer chamber is the same along with its height;

– at a sufficiently large distance from the section $x = h_1N_1$, the gas velocity equalizes, and in section $x = h_1N$, the gas moves with the same velocity along the x-axis;

– the boundary conditions on the impermeable walls of the region are determined from the condition that no gas flows through these walls;

– the equality in the height of the working chamber at the inlet and outlet, based on the continuity condition:

$$V_{x_N} = \frac{2R_1H_c}{R_2^2}V_{y_M}, \tag{3.6}$$

where R_1 – the radius, at which the inlet tangential slots for gas supply to the vortex chamber are located, m; R_2 – the radius, at which the inlet edge of the branch pipe for the removal of the gas flow is located in one of the end caps, m; V_{y_M}, V_{x_N} – inlet and outlet velocities, respectively, m/s.

The solution of equation (3.5) with boundary conditions in the form of first derivatives is the Neumann problem. It has a unique solution in this area.

If we divide the segments along with the axis *OX* and *OY* into intervals of the same size h_1 and designate *i* and *j* as the numbers of points along these axes, respectively, we can obtain the following expressions for the boundary conditions:

1) for $j = M$, $1 \le i \le N_1 - 1$:

$$\begin{cases} \frac{u_{i,M-1} - u_{i,M}}{h_1} = V_{y_M}; \\ u_{i,M-1} = \frac{V_{i=1,j-1} + V_{i+1,j-1} + V_{i,M} + V_{i,J-2}}{4}, \end{cases} \tag{3.7}$$

or

$$\begin{cases} u_{i,j-1} = V_{y_M} h_1 + u_{i,M}; \\ u_{i,M} = \frac{u_{i-1,j-1} + u_{i+1,j-1} + u_{i,j-2}}{3} - \frac{4h_1 V_{y_M}}{3}; \end{cases} \tag{3.8}$$

2) for $i = 0$, $1 \le j \le M - 1$:

$$\begin{cases} u_{1,j} = \frac{u_{0,j} + u_{2,j} + u_{1,j+1} + u_{1,j-1}}{4}; \\ u_{i,j} - u_{0,j} = 0, \end{cases} \tag{3.9}$$

from where we can get:

$$u_{0,j} = \frac{u_{2,j} + u_{1,j+1} + u_{1,j-1}}{3}; \tag{3.10}$$

3) for $i = N$, $1 \le j \le M_1 - 1$:

$$\begin{cases} u_{N-1,j} = \frac{u_{N,j} + u_{N-2,j} + u_{N-2,j+1} + u_{N-2,j-1}}{4}; \\ \frac{u_{N,j} - u_{N-1,j}}{h_1} = V_{x_N}, \end{cases} \tag{3.11}$$

or

$$\begin{cases} u_{N-1,j} = u_{N,j} - hV_{x_N}; \\ u_{N,j} = \frac{u_{N-2,j}+u_{N-1,j+2}+u_{N-3,j-1}}{3} + \frac{4hV_{x_N}}{3}; \end{cases} \quad (3.12)$$

4) for $i = N_1$, $M_1 \le j \le M - 1$:

$$\begin{cases} u_{N-2,j} = \frac{u_{N-3,j}+u_{N-1,j}+u_{N-2,j+1}u_{N-2,j-1}}{4}; \\ u_{N-2,j} = u_{N-1,j}, \end{cases} \quad (3.13)$$

from where we can get:

$$u_{N-1,j} = \frac{u_{N-3,j}+u_{N-2,j+1}+u_{N-2,j-1}}{3}; \quad (3.14)$$

5) for $j = M_1$, $N_1 + 1 \le i \le N - 1$:

$$\begin{cases} u_{i,M-1} = \frac{u_{i+1M-1}+u_{i-1,M_1-1}+u_{i,M_1}+u_{i,M_1-2}}{4}; \\ u_{i,M_1-1} = u_{i,M_1}; \\ u_{i,M_1} = \frac{u_{i+1,M_1-1}+u_{i-1,M_1-1}+u_{i,M_1-2}}{3}; \end{cases} \quad (3.15)$$

6) for $j = 0$, $1 \le i \le N - 1$:

$$\begin{cases} u_{i,M-1} = \frac{u_{i+1M-1}+u_{i-1,M_1-1}+u_{i,M_1}+u_{i,M_1-2}}{4}; \\ u_{i,M_1-1} = u_{i,M_1}; \\ u_{i,M_1} = \frac{u_{i+1,M_1-1}+u_{i-1,M_1-1}+u_{i,M_1-2}}{3}. \end{cases} \quad (3.16)$$

The solution of the system of differential equations for a large number of nodes by the method of successive approximations requires a significant investment of time. Therefore, here we present the results of calculations using the Gauss–Seidel method, which, when applied to equations, is called the method of successive displacements.

As a result of the solutions obtained, it is possible to consider how the ratio of the three main geometric dimensions affects the non-uniformity of the velocity field in the working chamber. The determining dimensions are the height of the working chamber H_c, the chamber radius R_1, and the radius of the gas outlet R2.

Accordingly, it is convenient to choose their ratios in the form Hc/R_1 and R_1/R_2, which makes it possible to consider the unevenness of the velocity from two variables R_1 and H_c.

A flowchart for solving differential equations is shown in Figure 3.4.

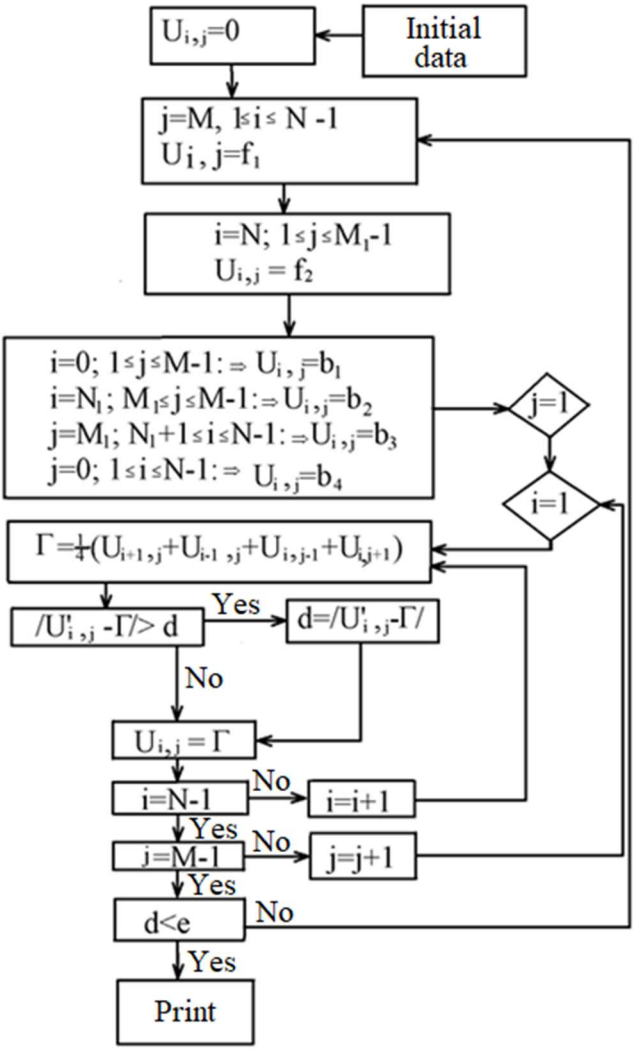

Figure 3.4 – Block diagram for solving difference equations: f_1, f_2 – boundary conditions at the inlet and outlet of the mass transfer chamber; b_1, b_2, b_3, b_4 – boundary conditions on impermeable walls

An example of calculating the change in velocities in the designated section for various values of H_c/R_2 is given in Figure 3.5.

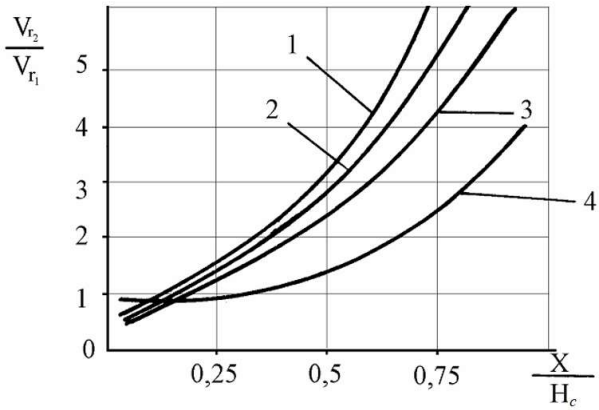

Figure 3.5 – Change of the velocity in relative height of the gamma-type area under $R_1/R_3 = 3.0$ for different values of H_c/R_1: 1 – 1.2; 2 – 1.0; 3 – 0.8; 4 – 0.6.

In Figure 3.6, graphs are shown reflecting the unevenness of the velocity field, which is characterized by the difference between the maximum and minimum velocities in the section $y = R_2$:

$$\left(\frac{V_{r_2}}{V_{r_1}}\right)_{max} - \left(\frac{V_{r_2}}{V_{r_1}}\right)_{min} = \Delta\bar{V}_{r_2}^{rel}. \qquad (3.17)$$

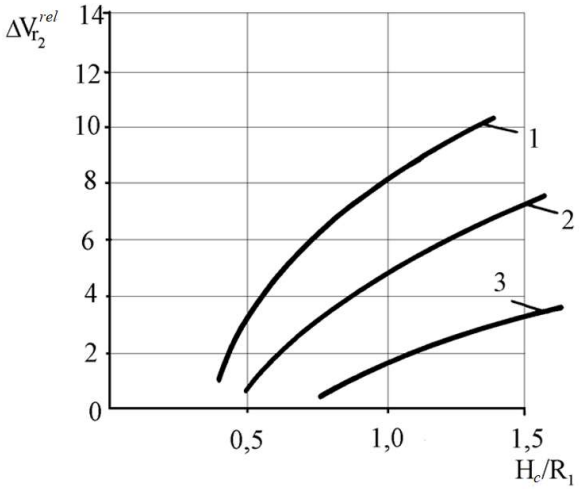

Figure 3.6 – Dependence for dimensionless velocity difference on the relative height of gamma-type area for the different ratio of R_1/R_2: 1 – 4.0; 2 – 3.0; 3 – 2.0

An analysis of the dependence of the non-uniformity of the gas velocity over the width of the gamma-shaped region (before the flow turns from the radial direction to the axial one depends on the value of H_c/R_1) shows that the choice of this ratio (as well as the value of H_c) is ambiguous. It also depends on the ratio of the sizes R_1/R_2. The analysis of graphic dependencies showed that it is possible to determine the ratio H_c/R_1. This value must be less than 0.6.

Given the need to reduce the values of $\Delta\bar{V}_{r_2}^{rel}$ to zero, the analysis of the calculated graphs allows determining the relative size of the gamma-type area. The following formula can be used:

$$\frac{H_c}{R_1} = 1.66 - 0.615\frac{R_1}{R_2} + 0.075\left(\frac{R_1}{R_2}\right)^2. \qquad (3.18)$$

This makes it possible (under the selected dimensions R_1 and R_2) to determine the width of the area under consideration from the condition of achieving the minimum non-uniformity of the flow in the section $y = R_2$ for $R_1/R_2 < 4$.

Examples of the design of gas removal and the possibility of achieving a small non-uniformity of gas velocities during a sharp turn of the flow allow assuming that the gas flow structure between two cylindrical surfaces with radiuses R_1 and R_2 is uniform under the appropriate choice of the ratio of the main geometric dimensions of the working chamber.

3.4 Vortex motion of a viscous gas flow

The study of the vortex gas flow as it rotates around the chamber axis is of the most significant interest. This is because the peripheral velocities of the gas flow created along the radius form a field of centrifugal forces involving liquid droplets in motion from the center to the periphery of the vortex mass transfer chamber along the radius of this chamber in the opposite direction to the movement of gas, which moves along the radius from the periphery to the center. The centrifugal forces acting on the liquid droplets must be greater than the resistance forces, the predominant action of which can lead to the entrainment of the liquid droplets together with the gas flow to the center of the vortex mass transfer chamber and lead to the disruption of the apparatus.

Another critical factor affecting the intensity of mass transfer processes is the relative velocity of phases in the spray zone, which affects the diameter of liquid droplets and the size of the interfacial surface. As the droplet size decreases, the total interfacial surface of all droplets located in the mass transfer zone increases. Conversely, a decrease in the relative velocity of

the liquid-gas jet leads to an increase in the diameter of the sprayed liquid droplets and a decrease in the interfacial surface.

In the considered scheme of the vortex motion of gas in the mass transfer chamber, it is assumed that the spraying of the liquid into droplets occurs due to the action of the gas on the jets introduced in the central zone. It is possible to express the dependence of the diameter of the obtained droplets on the relative flow velocity by the following formula:

$$d_0 = \frac{12}{\rho_g V_{rel}^2}, \tag{3.19}$$

where V_{rel} – relative velocity, m/s.

With an increase in the relative velocity of the gas flow, the size of the droplets of the sprayed liquid decreases. Also, the size of the interfacial surface increases. These facts contribute to the intensification of mass transfer in the working chamber of the apparatus. After spraying into droplets, the liquid is involved in rotational motion around the chamber axis due to the energy of the gas flow. Further organization of the movement of the droplets to the periphery of the mass transfer chamber depends on the effect of the gas flow on the droplets. As mentioned earlier in the previous section, in the area bounded by two cylindrical surfaces (with radiuses R_1 and R_2), it is possible to create a plane vortex motion of the gas, or close to a plain one, with small axial velocities, which are much less than circumferential ones and their effect on liquid droplets can be neglected.

Let us use semi-empirical theories of turbulence, which are based on the Prandtl hypothesis of shear stresses in a turbulent flow, N/m^2:

$$\tau_{xy} = \rho \varepsilon \frac{dV}{dy}, \tag{3.20}$$

where ε – coefficient of kinematic viscosity of turbulent flow, m^2/s, which depends on the mixing path l, m:

$$\varepsilon = l^2 \frac{dV}{dy}, \tag{3.21}$$

or considering the dependence on angular velocity:

$$\varepsilon = l^2 \frac{\partial}{\partial r}\left(\frac{V_\varphi}{r}\right), \tag{3.22}$$

where l is changed by the radius r.

The considered movement of a viscous gas flow is symmetrical about the axis, limited by cylindrical surfaces therefore it is most expedient to carry out theoretical studies and obtain a mathematical description of such a flow in a cylindrical coordinate system. After substituting the turbulent viscosity coefficient to Navier–Stokes equations instead of the kinematic viscosity coefficient, the following system can be considered:

$$\begin{cases} V_r \frac{\partial V_r}{\partial r} + \frac{V_\varphi}{r}\frac{\partial V_r}{\partial \varphi} + V_z \frac{\partial V_z}{\partial z} - \frac{V_\varphi^2}{r} = -\frac{1}{\rho}\frac{\partial P}{\partial r} + \\ +\varepsilon\left(\frac{\partial^2 V_r}{\partial r^2} + \frac{1}{r^2}\frac{\partial^2 V_r}{\partial \varphi^2} + \frac{\partial^2 V_r}{\partial z^2} + \frac{1}{r}\frac{\partial V_r}{\partial r} - \frac{2}{r^2}\frac{\partial V_\varphi}{\partial \varphi} - \frac{V_r}{r^2}\right); \\ V_r \frac{\partial V_\varphi}{\partial r} + \frac{V_\varphi}{r}\frac{\partial V_\varphi}{\partial \varphi} + V_z \frac{\partial V_z}{\partial z} + \frac{V_r V_\varphi}{r} = -\frac{1}{\rho r}\frac{\partial P}{\partial \varphi} + \\ +\varepsilon\left(\frac{\partial^2 V_\varphi}{\partial r^2} + \frac{1}{r^2}\frac{\partial^2 V_\varphi}{\partial \varphi^2} + \frac{\partial^2 V_\varphi}{\partial z} + \frac{1}{r}\frac{\partial V_\varphi}{\partial r} + \frac{2}{r^2}\frac{\partial V_r}{\partial \varphi} - \frac{V_\varphi}{r^2}\right); \\ V_r \frac{\partial V_z}{\partial r} + \frac{V_\varphi}{r}\frac{\partial V_z}{\partial \varphi} + V_z \frac{\partial V_z}{\partial z} = -\frac{1}{\rho}\frac{\partial P}{\partial r} + \\ +\varepsilon\left(\frac{\partial^2 V_z}{\partial r^2} + \frac{1}{r^2}\frac{\partial^2 V_z}{\partial \varphi^2} + \frac{\partial^2 V_z}{\partial z^2} + \frac{1}{r}\frac{\partial V_z}{\partial r}\right); \\ \frac{\partial V_r}{\partial r} + \frac{1}{r}\frac{\partial V_\varphi}{\partial \varphi} + \frac{\partial V_z}{\partial z} + \frac{V_r}{r} = 0, \end{cases} \tag{3.23}$$

where P – hydrodynamic pressure, Pa.

The last equation of this system is the continuity equation.

Under the assumption about the axisymmetricity of the vortex gas flow and the absence of axial velocity in the region along with the height of the chamber ($\frac{\partial}{\partial\varphi} = 0$, $\frac{\partial}{\partial z} = 0$, and $V_z = 0$), after considering the dependence on one variable r in the 1st and 3rd equations, this system of equations can be written as:

$$\begin{cases} V_r \frac{\partial V_r}{\partial r} - \frac{V_\varphi^2}{r} = -\frac{1}{\rho}\frac{\partial P}{\partial r}; \\ V_r \frac{\partial V_\varphi}{\partial r} + \frac{V_r V_\varphi}{r} = \varepsilon \frac{\partial}{\partial r}\left(\frac{\partial V_\varphi}{\partial r} + \frac{V_\varphi}{r}\right); \\ \frac{\partial V_r}{\partial r} + \frac{V_r}{r} = 0. \end{cases} \quad (3.24)$$

From the 3rd equation of this system, under boundary conditions $r = R_1$, and $V_r = V_{r2}$, it can be found:

$$V_r = V_{r_1}\frac{R_1}{r}. \quad (3.25)$$

There are two ways to solve the resulting system of equations. One of them replaces the coefficient of turbulent viscosity with an empirical constant and makes it possible to reduce the problem to the already known solution of the viscous fluid flow between two rotating cylinders. This makes it possible to obtain a solution in elementary functions. However, such an approach requires using experimental data to close the system of equations when determining the boundary conditions and the constant ε^*, m^2/s.

The second way is to use dependence (3.22), where an approximating function changes the mixing path based on the data of experimental blowdowns and the study of vortex gas flows.

After replacing ε by the empirical constant ε^*, then considering (3.25), the 2nd equation of the system (3.24) can be rewritten as followings:

$$\frac{d^2V_\varphi}{dr^2}r^2 + \left(1 - \frac{V_{r_1}R_1}{\varepsilon^*}\right)\frac{dV_\varphi}{dr}r - \left(1 + \frac{V_{r_1}R_1}{\varepsilon^*}\right)V_\varphi = 0. \quad (3.26)$$

Solution of this differential equation:

$$V_\varphi = C_1 r^{Re+1} + C_2 r^{-1}, \quad (3.27)$$

where $Re = V_{r1}R_1/\varepsilon^*$ – Reynolds number for radial flow; C_1, C_2 – unknown constants.

The integration constants can be found based on the boundary conditions: $V_\varphi(R_1) = V_{\varphi 1}$; $V_\varphi(R_2) = V_{\varphi 2}$, where R_1 and R_2 – radiuses of cylindrical surfaces, between which a plane vortex motion of the gas occurs. These radiuses coincide in size with the radiuses of the vortex chamber and gas outlet, respectively.

Therefore:

$$C_1 = \frac{V_{\varphi_1}R_1 - V_{\varphi_2}R_2}{R_1^{Re+2} - R_2^{Re+2}};\ C_2 = \frac{V_{\varphi_2}R_2R_1^{Re+2} - V_{\varphi_1}R_1R_2^{Re+}}{R_1^{Re+2} - R_2^{Re+2}}. \quad (3.28)$$

Considering these constants, the solution (3.27) takes the following form:

$$V_\varphi = \frac{V_{\varphi_1}R_1 - V_{\varphi_2}R_2}{R_1^{Re+2} - R_2^{Re+2}}r^{Re+1} + \frac{V_{\varphi_2}R_2R_1^{Re+2} - V_{\varphi_1}R_1R_2^{Re+2}}{R_1^{Re+2} - R_2^{Re+2}}r^{-1}. \quad (3.29)$$

For determining V_φ by this equation, the values of $V_{\varphi 1}$ and $V_{\varphi 2}$ should be known. Since the gas is introduced to the swirl chamber in the tangential direction, the value of $V_{\varphi 1}$ can be determined as

$$V_{\varphi_1} = \frac{Q_g}{S}, \tag{3.30}$$

where Q_g – flow rate of the gas, m^3/s; S – the total area of tangential slots, m^2.

It is necessary to carry out experimental studies or use additional requirements for the gas flow in the center of the apparatus to find the value of $V_{\varphi 2}$.

Solving the 1st equation of system (3.24) and considering (3.25) and (3.29), we obtain:

$$P = -\frac{\rho_g k^2}{2r^2} + \rho_\Gamma \left(\frac{C_1^2 r^{2\,Re+}}{2\,Re+2} + \frac{2C_1C_2 r^{Re+1}}{Re+1} - \frac{C_2^2}{2}\right) + C_3, \tag{3.31}$$

where $K = V_{r1}R_1$ – the momentum of radial velocity, m^2/s.

Integration constant C_3 is determined from the condition $P(R_1) = P_1$. Therefore:

$$\begin{aligned} P = {} & \frac{\rho_g K^2}{2}\left(\frac{1}{R_1^2} - \frac{1}{r^2}\right) + \\ & + \rho_g \left[\left(\frac{C_1^2 r^{2\,Re+2}}{2\,Re+2} + \frac{2C_1C_2 r^{Re+1}}{Re+1} - \frac{C_2^2}{2r^2}\right) - \right. \\ & \left. - \left(\frac{C_1^2 R_1^{2\,Re+2}}{2\,Re+2} + \frac{2C_1C_2 R_1^{Re+1}}{Re+1} - \frac{C_2^2}{2R_1^2}\right)\right] + P_1 \end{aligned} \tag{3.32}$$

Let us consider what caused the difference and change in the exponent in the expression (1.4) and (3.27). From their equality, we can get:

$$n = \frac{ln\left(\frac{R_1 - V_{\varphi_2} R_2}{R_1^{Re+2} - R_2^{Re+2}} r^{Re+1} + \frac{\frac{V_{\varphi_2}}{V_{\varphi_1}} R_2 R_1^{Re+2} - R_1 R_2^{Re+2}}{R_1^{Re+2} - R_2^{Re+}} r^{-1}\right)}{ln\left(\frac{R_1}{r}\right)}. \tag{3.33}$$

Therefore, in addition to depending on the geometric and hydrodynamic parameters, parameter n is changed towards the chamber's center, which is expressed by the coordinate r.

Under accepting the law of change in the turbulent viscosity coefficient from experimental data, the 2nd equation of the system (3.24) takes the form:

$$\frac{d^2V_\varphi}{dr^2} = \frac{1}{r^2}\left(1 + \frac{k_t}{\varepsilon}\right)V_\varphi - \frac{1}{r}\left(1 - \frac{k_t}{\varepsilon}\right)\frac{dV_\varphi}{dr}, \qquad (3.34)$$

where the turbulence parameter k_t is introduced, m^2/s, and the viscosity coefficient depends on the radius r.

The data presented in the following chapters on the solution of equations (3.32) and (3.27), where the coefficient of turbulent viscosity is constant along the radius of the mass transfer chamber, and their comparison with the experimentally obtained values of velocities and pressure indicate the possibility of using these formulas for engineering applications.

3.5 Hydrodynamics of a vortex gas-droplet

3.5.1 Conditions of countercurrent motion of vortex gas-droplet flows in a mass transfer chamber

To identify the characteristic features of the movement of the liquid phase in the mass-exchange chamber of a vortex countercurrent spray apparatus, we consider the entire movement from the moment the liquid is introduced in the central region to its separation on the cylindrical walls of the vortex chamber.

The scheme of motion of vortex gas and droplet flow in the mass transfer apparatus is shown in Figure 3.7.

The liquid is introduced in thin jets in the radial direction in the central region of the vortex mass transfer chamber. In this case, the direction of movement of the liquid at the initial moment of the outflow of the jet from the atomizer may differ from purely radial. In addition to the radial, the liquid may have a circumferential component of the total velocity. Its value primarily affects the regular and countercurrent movement as a whole.

After introducing thin liquid jets into the mass-exchange apparatus, they begin to be affected by a high-speed gas flow due to the energy of which the liquid is sprayed into droplets.

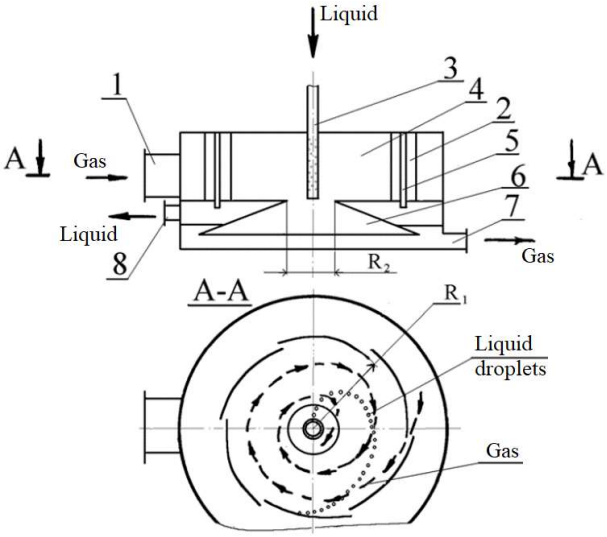

Figure 3.7 – Vortex spraying countercurrent mass transfer apparatus: 1 – gas inlet pipe; 2 – tangential swirler; 3 – atomizer; 4 – mass transfer chamber; 5 – slots for liquid drainage; 6 – radial diffuser; 7 – gas outlet pipe; 8 – liquid outlet pipe

When the liquid is injected strictly in the radial direction, the liquid is sprayed into droplets, the size of which will be inversely proportional to the square of the circumferential velocity of the gas flow (3.19). In spraying, an important place or a cylindrical section in the vortex mass transfer chamber where the liquid enters the gas stream. If liquid jets are fed into a region where they are affected by a gas flow at low velocities, then their trajectories will bend under the action of this gas flow, and the liquid will acquire rotational motion. As a result, upon reaching a cross-section with high circumferential gas velocities, the liquid and gas will have lower relative velocities, and the liquid will be sprayed into large droplets, the interfacial surface will decrease, and the intensity of the mass transfer processes that occur in the apparatus will decrease.

Almost simultaneously with the spraying of liquid jets, the process of involving liquid droplets in rotational motion occurs. To implement a regular countercurrent along the radius of the vortex mass transfer chamber, the movement of droplets and gas, the liquid must be involved in rotational motion and achieve such a value of the circumferential velocities of the droplets, at which the latter, under the action of centrifugal forces, must move to the periphery of the vortex mass transfer chamber.

In addition to the impact in the circumferential direction, the gas acts on the liquid in the radial direction when moving towards the chamber's center. Thus, two forces act on the droplets of liquid, the direction of which is opposite.

Centrifugal force:

$$F_{cf} = \frac{\pi d_K^3}{6} \rho_g \frac{V_\phi^2}{r}, \tag{3.35}$$

and resistance force:

$$F_{df} = \frac{\pi}{8} \psi V_r^2 d_0^2 \rho_g. \tag{3.36}$$

One of the problems of ensuring countercurrent motion in the mass-exchange chamber is the fastest achievement of circumferential velocities sufficient to fulfill the condition $F_{cf} > F_{df}$. For this purpose, it is necessary to involve the droplets in rotational motion with the following velocity:

$$V_\varphi > \sqrt{\frac{3\psi\rho_g r}{4\rho_g d_0}} V_r. \tag{3.37}$$

After expressing this dependence in terms of the geometrical parameters of the vortex chamber and its gas capacity, it can be obtained:

$$V_\varphi > \sqrt{\frac{3\psi\rho_g r}{4\rho_g d_0}} \frac{Q_g}{2\pi r H_c}. \tag{3.38}$$

Regular countercurrent phase movement will occur if this condition is met along the entire radius in the working chamber. Otherwise, if the resistance force and centrifugal force are equal at a certain radius, the movement to the periphery will stop. In this case, possible "hanging" of liquid droplets can occur.

At a low circumferential velocity, liquid droplets will be captured by the gas flow and drawn to the exit from the vortex mass transfer chamber, leading to an increase in spray entrainment and a sharp decrease in efficiency, and even to disruption of the vortex mass transfer apparatus.

At the entrance to the vortex mass transfer chamber, the velocity of the gas flow, to ensure the movement of droplets to the periphery, near the walls of the mass transfer chamber must be greater than:

$$V_\varphi > \sqrt{\frac{3\psi\rho_g}{4\rho_g d_0}} \frac{Q_g/\sqrt{R_1}}{2\pi H_c}. \tag{3.39}$$

The above analysis of the ratio of forces acting on a liquid droplet along the radius of the vortex mass transfer chamber shows that when calculating the total circumferential and radial velocities, to ensure regular countercurrent movement of the gas and liquid phases, condition (3.19) should be checked over the entire area from the center to the periphery working chamber.

The presence of a liquid phase in a vortex gas flow and the imposed condition, which consists of the countercurrent movement of the phases along the radius of the working chamber, affects the magnitude of the hydraulic resistance of the mass transfer chamber.

Droplets of liquid are entrained in rotational motion due to the energy of the gas flow. The gas flow rates decrease, which leads to a decrease in the pressure droplet between the center and periphery of the vortex mass transfer chamber and a decrease in the hydraulic resistance of the working chamber. The solution to these problems is given in the following sections, which outline the theoretical justification for reducing hydraulic resistance due to a decrease in the circumferential velocities of the gas flow.

3.5.2 Impact of droplet flow on the hydrodynamics of a gas

The hydrodynamics of the gas-droplet flow will largely depend on how, at what velocities, and in what direction the liquid jets will be introduced in the central region of the vortex chamber.

If we proceed from relation (3.19), then it is expedient to introduce liquid in the circumferential direction, opposite to gas flow. However, the positive effect of increasing the interfacial surface due to a decrease in the diameter of the droplets of the sprayed liquid may not be achieved. This is because of decreasing circumferential velocity of the gas flow due to non-

compliance with condition (3.39). Overall, this effect leads to a breakdown in the apparatus operation.

The introduction of liquid in the circumferential direction and in the same direction as the circumferential velocities of the gas flow provides the condition for the countercurrent movement of the phases, which consists of the predominant effect of centrifugal forces on the liquid droplets. However, in this case, poor-quality atomization of liquid jets into droplets of large diameter is possible, too little time for the liquid to stay in the contact zone, which in turn can adversely affect the operation of the vortex spraying countercurrent mass transfer apparatus.

It should be noted here that the quality of a finely dispersed and uniform atomization of a liquid into droplets can be achieved using special mechanical or pneumatic atomizers. However, in this case, it is still necessary to analyze the further movement of the droplets, their influence on the hydrodynamics of the gas flow, on such essential parameters as, for example, the hydraulic resistance of the mass transfer apparatus.

The problem's solution is also necessary from the influence of the ratio of loads in the liquid and gas phases on the stable operation of the vortex spraying countercurrent mass transfer apparatus.

Let us consider how the gas flow pattern changes in the presence of a liquid phase. Let us allocate an elementary volume between two cylindrical sections I-I and II-II, lying between surfaces with radiuses R_1 and R_2 (Figure 3.8), the value of which is equal to:

$$dV = 2\pi r dr dz. \tag{3.40}$$

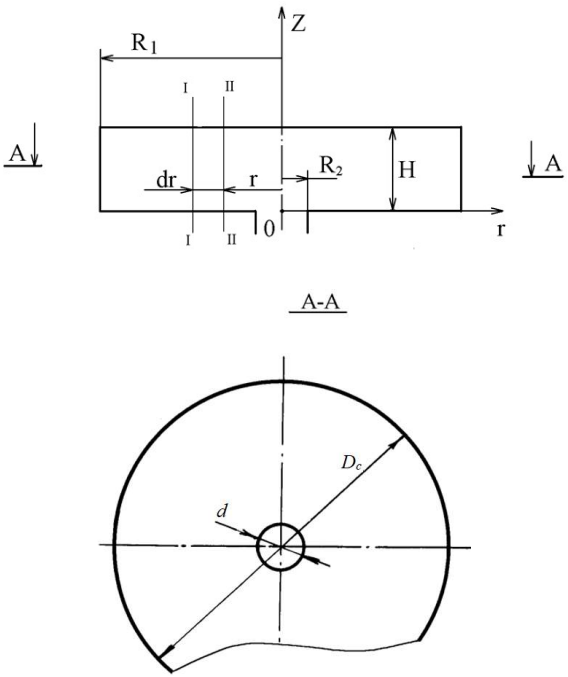

Figure 3.8 – Design scheme of the vortex chamber

The kinetic moment of the gas enclosed in this volume, in the absence of a liquid phase, is equal to:

$$dK_g = 2\pi\rho_g V_\varphi r^2 dr dz. \quad (3.41)$$

Since there will be no impact from external forces, when a liquid phase appears in the volume under consideration, the latter is involved in rotational motion due to the energy of the gas flow. In this case, the angular momentum of the gas volume will decrease accordingly and will be equal to:

$$dK_g^* = 2\pi\rho_g V_\varphi^* r^2 dr dz. \quad (3.42)$$

Кинетический момент жидкой фазы, приобретенный в результате взаимодействия с газовым потоком, имеющим окружную скорость, kg·m^2/s^2:

$$dK_g = M_g W_\varphi r. \tag{3.43}$$

Liquid phase volume V_l, m^3, in the considered area of the mass transfer chamber is determined by the relation:

$$V_l = V_g \frac{Q_l}{Q_g}, \tag{3.44}$$

where V_g – gas volume, m^3.

Therefore, equation (3.43) is rewritten in the form:

$$dK_g = 2\pi\rho_L \frac{Q_l}{Q_g} W_\varphi r^2 dr dz. \tag{3.45}$$

In the explanations of the interaction between gas flows and liquid droplets, the assumption was introduced (since the volumes of a unit mass of gas and liquid differ by several orders of magnitude) that the volume of gas in the region under consideration remained practically unchanged before and after the liquid phase was supplied.

Since liquid droplets are involved in rotational motion due to the energy of the gas flow, the kinetic moment of the gas before the introduction of liquid should be equal to the sum of the kinetic moments of the gas and the liquid phases:

$$K = K_g^* + K_g. \tag{3.46}$$

After considering equations (3.41)–(3.43), this equality becomes:

$$\rho_g V_\varphi = \rho_g V_\varphi^* + \rho_l \frac{Q_l}{Q_g}, \tag{3.47}$$

from which the circumferential velocity of the gas flow is determined after interaction with liquid droplets:

$$V_\varphi^* = V_\varphi - \frac{\rho_l}{\rho_g}\frac{Q_l}{Q_g} W_\varphi. \tag{3.48}$$

If we consider the movement of liquid droplets in a mass-exchange chamber in two planes normal to its axis, which are separated from each other at a small distance, and assume that the amount of liquid that takes part in the plane countercurrent vortex motion in these planes is different, then the following picture is possible.

Due to a large amount of liquid in one of the considered layers, the gas flow velocities decrease, and the pressure increases.

Thus, a pressure droplet arises between the layers under consideration, associated with different gas flow velocities. Under the action of this pressure droplet, the movement of liquid droplets from a layer with a lower velocity to a layer with a higher velocity should begin. This process will take place until the energy parameters are equalized between the nearest layers and, in general, along with the height of the entire mass transfer chamber.

The above reasoning follows the assumption of uniform saturation in any cylindrical section of the chamber and its height with liquid in the form of moving droplets. For the entire droplet vortex flow, the characteristic features of its motion will accurately determine the motion of a single droplet. As mentioned above, considering the mutual influence of droplets on each other during their general motion is a challenging problem requiring special theoretical and practical studies. But in this

case, due to the sufficiently large distance between the droplets, this mutual influence will be negligible and neglected.

Determination of the circumferential velocity of the gas flow is a problem of solving (3.48) if the values of the circumferential velocities of gas before interaction with the liquid and liquid phase are known. The liquid phase is a droplet evenly distributed over the area of any cylindrical section in the working chamber. The law of variation of circumferential velocities in the gas flow of a "dry" apparatus (3.29) and the velocity of liquid droplets allows correcting circumferential velocity of the gas under the load on the liquid phase.

After assuming that for all liquid droplets in the working chamber, a certain diameter is characteristic, from equations (1.12), we obtain:

$$\begin{cases} \frac{dW_r}{dt} = \frac{W_\varphi^2}{r} + \frac{3\psi\mu_g}{4\rho_0 d_0}(V_r - W_r); \\ \frac{dW_\varphi}{dt} = -\frac{W_r W_\varphi}{r} + \frac{3\psi\mu_g}{4\rho_0 d_0}\left(V_\varphi - W_\varphi\right). \end{cases} \tag{3.49}$$

The most appropriate is the solution of this system numerically. The analytical solution's complexity is due to the dependence of the drag coefficient of the droplet on the flow parameters. The process of compiling programs is greatly simplified when determining the drag coefficient of a droplet, according to the three-term formula widely used in practical calculations:

$$\psi = \frac{24}{Re} + \frac{4.565}{\sqrt[3]{Re}} + \frac{0.491}{\sqrt{Re}}, \tag{3.50}$$

where $Re = V_{rel}d_0/v_g$ – Reynolds number for relative motion; $v_g = \mu_g/\rho_g$ – kinematic viscosity of a gas, m^2/s.

Let us consider a scheme for calculating and changing the picture of the movement of a gas and liquid flow along the radius

of the mass transfer chamber. The calculation scheme is as follows.

Firstly, according to the known geometric dimensions of the vortex chamber (radius, height of the vortex chamber, radius of the hole for gas removal, dimensions of the inlet tangential slots) using the formula (3.29), we calculate the values V_φ along with the camera radius.

Secondly, assuming that liquid spraying occurs at radius R_2 in the region of maximum circumferential gas velocities, we determine the diameter of the resulting droplets (3.19). Solving equation (3.49), we find the values of the circumferential and radial velocities of the droplets along the radius of the mass transfer chamber. This makes it possible to determine the residence time of the liquid in the mass transfer chamber.

Thirdly, a decrease in peripheral gas velocities at radius R_2 (3.39) leads to an increase in the size of droplets (3.19) and to some rearrangement of the liquid and gas velocity fields, which is determined by equations (3.49) and (3.48), respectively.

The calculation process lasts until the stabilization of the gas-droplet flow pattern in the working chamber of the apparatus.

The calculation data of the hydrodynamics of the vortex mass transfer chamber of the countercurrent apparatus, which are given in the following sections, show that the apparatus is best operated at a ratio of loads in the liquid and gas phases less than one. In this case, the volume of the liquid phase in the working chamber of the apparatus is much less than the volume of gas. The distances between the droplets meet the conditions set out in Chapter 1.4, which allows equation (3.49) to be used to calculate fluid velocities.

3.5.3 Hydraulic resistance of a vortex chamber

The theoretical studies of the hydrodynamics of the vortex mass-transfer chamber of a spraying countercurrent apparatus presented in the previous sections make it possible to determine the main design features of the apparatus.

The requirement for a uniform gas flow supply over the entire height of the mass transfer chamber can be met by placing tangential swirlers or tangential slots in the cylindrical wall of the vortex chamber. Moreover, it is desirable to supply the gas flow through several tangential swirlers located evenly around the circumference. This achieves the uniformity of the gas supply along the perimeter of the mass transfer chamber and the axisymmetry of the vortex gas flow in the vortex chamber itself. In addition, in front of the tangential swirlers, installing an annular or spiral supply for uniform distribution of gas around the circumference is necessary.

The vortex mass transfer chamber itself is a cylindrical cavity whose height is more than two times less than its diameter. In one of the end caps (for a more uniform removal of gas from the vortex chamber, it is possible to perform gas removal in both end caps), the gas is removed in the form of a round hole. In the case of gas venting in one of the end caps, to create a flat spiral gas flow in the phase contact zone in the mass transfer chamber and uniform gas venting in the central region, gas venting can be made in the form of many concentric annular nozzles of various heights (Figure 3.9).

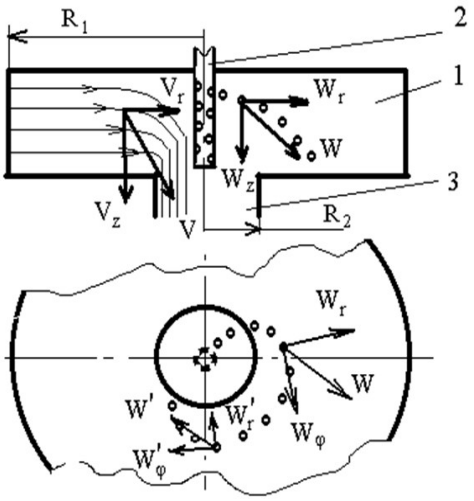

Figure 3.9 – Scheme of the movement of gas and liquid in the area of the gas outlet pipe: 1 – vortex chamber; 2 – liquid atomizer located in the center; 3 – gas outlet pipe

As shown earlier (3.19), to achieve fine atomization of liquid jets into droplets with a diameter close to 50 μm, near the exit from the vortex mass transfer chamber, the circumferential velocities of the gas flow should reach values of up to 100 m/s. If the gas is removed from the mass transfer chamber at such high circumferential velocities, this can lead to considerable energy losses. Therefore, for the economic conversion of the high kinetic energy of the gas flow, it is advisable to install a radial diffuser behind the gas outlet from the vortex mass transfer chamber.

The initial data for calculating a radial diffuser are the gas flow parameters at its inlet. Thus, both for calculating the hydraulic resistance of the entire vortex spraying countercurrent mass transfer apparatus and for calculating the radial diffuser, it is necessary to know the balance (distribution) of energy losses

over the apparatus elements. In particular, it is necessary to determine the hydraulic resistance of the vortex mass transfer chamber under various operating modes.

At the diffuser inlet, the energy state of the gas flow is characterized by static pressure and velocity in a cylindrical section of size $r = R_2$. These parameters are decisive for further movement along with the radial diffuser since the absence of radial currents is assumed during the spiral movement of gas from the mass transfer chamber into the diffuser. The velocity and pressure in the cylindrical section $r = R_2$ of the diffuser will be somewhat different than in the same section in the vortex chamber due to the loss of flow twist when passing through the gas outlet (Figures 3.5, 3.6), but the values of the energy parameters will be close to the values of the gas parameters in a section of the same size in a mass transfer chamber. Thus, after making changes in the pressure and velocity of the gas in the cylindrical section of the chamber with $r = R_2$ (as the determining change in the energy of the flow that leaves the chamber), it is possible to reveal the characteristic change in the drag coefficient of the vortex chamber with increasing load in the liquid phase determined by (1.6).

Let us rewrite equation (1.6) in a slightly different form:

$$\zeta^* = \frac{2\Delta P^*}{\rho_g V_{\varphi_1}^2}. \tag{3.51}$$

The resistance coefficient of the working chamber of a "dry" apparatus, i.e., in the absence of a liquid phase, is equal to:

$$\zeta = \frac{2\Delta P}{\rho_g V_{\varphi_1}^2}. \tag{3.52}$$

Since the parameters of the gas flow at the inlet to the mass transfer chamber do not change with increasing loads in the

liquid phase, the change in the ratio of the resistance coefficients depends on the change in the total pressure at the outlet of the mass transfer chamber:

$$\frac{\zeta^*}{\zeta} = \frac{\Delta P^*}{\Delta P}. \tag{3.53}$$

As shown earlier, introducing a liquid phase causes a rearrangement of the gas flow, which is expressed in a decrease in the circumferential velocities (3.48).

Then we can find out what the effect of changing the circumferential gas velocities on the energy loss in the vortex chamber of the countercurrent apparatus looks like:

$$\Delta P = \Delta P_{st} - \frac{\rho_g V_{\varphi_1}^2}{2} - \left(\frac{\rho_g V_{\varphi_2}^2}{2} + \frac{\rho_g V_{z_2}^2}{2}\right), \tag{3.54}$$

where ΔP_{st} – hydrostatic pressure difference, Pa.

Assuming quantity $V_{\varphi 1}$ and axial velocity at the exit V_{z2} close in magnitude, we can get:

$$\Delta P = \Delta P_{st} - \frac{\rho_g V_{\varphi_2}^2}{2}. \tag{3.55}$$

The value of ΔP_{st} is determined from the equation (3.32):

$$\begin{gathered}\Delta P_{st} = \frac{\rho_g K^2}{2}\left(\frac{1}{R_1^2} - \frac{1}{R_2^2}\right) + \\ +\rho_g\left[\left(\frac{C_1^2 R_2^{2\,Re+2}}{2\,Re+2} + \frac{2C_1C_2R_1{}^{Re+1}}{Re+1} - \frac{C_2}{2R_2^2}\right) - \right. \\ \left. -\left(\frac{C_1^2 R_1^{2\,Re+2}}{2\,Re+2} + \frac{2C_1C_2R_1^{Re+1}}{Re+1} - \frac{C_2}{2R_1^2}\right)\right]\end{gathered} \tag{3.56}$$

With an increase in the ratio of L/G in the section $r = R_2$, the value of $V_{\varphi 2}$ from the last equation is expressed by (3.28).

Figure 3.9 shows that with a change in loads by phases, a general view of the pattern for $V_\varphi(r)$ is not changed. Assuming that with a change in values $V_{\varphi 2}$, equation (3.56) remains valid, we rewrite this expression by defining the variable $V_{\varphi 2}$:

$$\Delta P_{st} = b_1 V_{\varphi_2}^2 + b_2 V_{\varphi_2} + b_3, \tag{3.57}$$

where the following coefficients have been introduced:

$$b_1 = \rho_g \left[\frac{(R_2^{2\,Re+2} - R_1^{2\,Re+2}) R_2^2}{(2\,Re+2)\left(R_1^{Re+2} - R_2^{Re+2}\right)^2} + \frac{2R_2^2 R_1^{Re+2}(R_1^{Re+1} - R_2^{Re+1})}{(R_1^{Re+2} - R_2^{Re+2})(Re+1)} + \right.$$
$$\left. + \left(\frac{1}{2R_1^2} - \frac{1}{2R_2^2}\right)\left(\frac{R_2 R_1^{Re+2}}{R_1^{Re+2} - R_2^{Re+2}}\right) \right];$$

$$b_2 = \rho_g \frac{2R_2^{Re+} - 2R_1^{Re+}}{Re+1} \left[\frac{V_{\varphi_1} R_2 R_1^{Re+3}}{\left(R_1^{Re+2} - R_2^{Re+2}\right)^2} + \right. \tag{3.58}$$
$$\left. + \frac{V_{\varphi_1} R_1 R_2^{Re+3}}{\left(R_1^{Re+2} - R_2^{Re+2}\right)^2} \right];$$

$$b_3 = \rho_g \left[\frac{V_{r_1}^2 R_1^2}{2}\left(\frac{1}{2R_1^2} - \frac{1}{2R_2^2}\right) + \frac{(R_2^{2\,Re+2} - R_1^{2\,Re+2}) V_{\varphi_2}^2 R_1^2}{(2\,Re+2)(R_1^{Re+} - R_2^{Re+2})} + \right.$$
$$+ \frac{2V_{\varphi_1}^2 R_1^2 R_2^{Re+2}(R_1^{Re+1} - R_2^{Re+1})}{(R_1^{Re+2} - R_2^{Re+2})^2 (Re+1)} +$$
$$\left. + \left(\frac{1}{2R_1^2} - \frac{1}{2R_2^2}\right) \frac{V_{\varphi_1} R_1^2 R_2^{2\,Re+4}}{(R_1^{Re+2} - R_2^{Re+2})^2} \right].$$

After introducing

$$b_4 = b_1 - \frac{\rho_g}{2}, \tag{3.59}$$

the following approximation can be obtained:

$$\Delta P = b_4 V_{\varphi_2}^2 + b_2 V_{\varphi_2} + b_3. \quad (3.60)$$

Equation (3.60) clearly shows the quadratic dependence of the total head loss along with a flat vortex gas flow, which corresponds to a generally accepted knowledge of hydraulic resistance.

A similar relationship can be written for any cylindrical section between sections with radiuses R_1 and R_2. The energy loss after liquid supply to the mass transfer chamber is defined as:

$$\Delta P^* = b_4 V_{\varphi_2}^{*2} + b_2 V_{\varphi_2}^* + b_3. \quad (3.61)$$

Substituting (3.60) and (3.61) into (3.53), we get:

$$\frac{\zeta^*}{\zeta} = \frac{b_4 V_{\varphi_2}^{*2} + b_2 V_{\varphi_2}^* + b_3}{b_4 V_{\varphi_2}^2 + b_2 V_{\varphi_2} + b_3}. \quad (3.62)$$

In most cases, to achieve fine liquid atomization in the central region, it is necessary to obtain a circumferential gas velocity, which can reach 100 m/s. Simplified, when evaluating the effect of changing the load in the liquid phase on the nature of the change in the coefficient of hydraulic resistance of the mass transfer chamber, you can use the ratio:

$$\frac{\zeta^*}{\zeta} = \left(\frac{V_{\varphi 2}^*}{V_{\varphi 2}}\right)^2. \quad (3.63)$$

It should be noted that due to high circumferential velocities, the hydraulic resistance of the vortex spraying countercurrent apparatus must be higher than the resistance of such contact devices as plates of various designs or direct-flow vortex elements.

Therefore, when analyzing the hydraulic resistance of the studied countercurrent apparatuses, one should consider (when compared with other types of devices) the specific hydraulic resistance, which falls on a single theoretical stage of changing the concentration in one stage of spraying, since in the countercurrent vortex apparatus several theoretical stages of changing the concentration in one spray are achieved.

3.6 Impact of flow hydrodynamics on the design of spray nozzles and gas outlet pipes

The previously given theoretical studies of vortex flow in the working chamber of the apparatus make it possible to use the obtained results for choosing: the design of the atomizer, gas removal, the region of injection of jets into the gas flow and determining the energy characteristics of the atomizer.

The gas flow first moves along flat spiral trajectories and then moves to axial in the central region. This affects the occurrence of axial velocities in liquid droplets, leading to spray entrainment.

After considering the main features of liquid spraying in the working chamber of a countercurrent vortex mass transfer apparatus, it is necessary to be guided by specific requirements to create the most favorable conditions for highly efficient mass transfer.

Firstly, for the most rational use of the entire volume of the working chamber, the liquid must be sprayed so that the gas flow is saturated with liquid droplets evenly over the volume of the mass transfer chamber.

Secondly, at the moment the liquid is injected, two main forces begin to act on the droplets that form as a result of atomization from the side of the gas flow. Centrifugal forces involve the droplets in the movement towards the periphery, and

the aerodynamic force, due to the presence of axial and radial velocities in the gas, involves the droplets in direct-flow movement with the gas.

The choice of the spray zone should be aimed at finding an area with low axial but high circumferential gas velocities. It is necessary to achieve the involvement of droplets of the injected liquid immediately after spraying into an intense rotational movement sufficient to create a field of centrifugal forces. This prevents the liquid from being carried away together with the gas flow.

There are various possible schemes for introducing liquid into the central region of the working chamber. It is possible to make the atomizer in the form of a branch pipe located in the center of the mass transfer chamber on the same axis as the apparatus.

One of the variants of the atomizer is in the form of a central pipe. In this case, centrifugal nozzles are located over the entire surface of the atomizer (both in circumference and in height), which are vortex chambers with a radial size of up to 10 mm. A conical hole is located on the axis of this vortex chamber. The liquid is fed into such a nozzle in a tangential direction, and the outflowing jet of liquid is a fan-like torch, which makes it possible to distribute the liquid more evenly over the volume of the mass transfer chamber and spray the jet into small droplets due to the additional action of a high-speed gas flow.

The radius of a bushing for the atomizer is R_b. We assume that between two cylindrical surfaces, R_1 and R_2, the change in the circumferential velocity of the gas flow obeys the law, which is described by equation (3.29). Between two cylindrical surfaces with radiuses R_2 and Rb, the peripheral gas velocity decreases according to a linear law:

$$V_\varphi = \frac{r-R_b}{R_2-R_b} V_{\varphi_2}. \quad (3.64)$$

But in this region, the axial velocities are already significant and have a significant effect on the liquid jets. But as mentioned earlier, in the considered scheme of gas flow movement, the cylindrical section with radius R2 is the most preferable for liquid spraying.

If liquid spraying occurs near a cylindrical section with a radius close to R_2, we get the following picture. When introduced into a gas, liquid jets immediately fall under the action of a high-velocity gas flow. The relative velocities in the circumferential direction, with radial inlet, are entirely determined by the maximum circumferential velocity of the gas flow.

Such conditions are most favorable for obtaining small droplets (3.19). In addition, the absence or low value of axial velocities in the gas flow in the area of droplet acceleration makes it possible to involve the latter in a plane spiral movement, which is opposite to the gas movement along the radius of the vortex chamber.

Another possible design in a cross-section with a radius close to radius R_2 is a liquid atomizer in the form of annular tubes, on the outer surface of which a number of nozzles are placed (Figure 3.10), which makes it possible to create a constructive scheme that also facilitates the regulation of the velocity field in the gas flow according to the height of the mass transfer chamber.

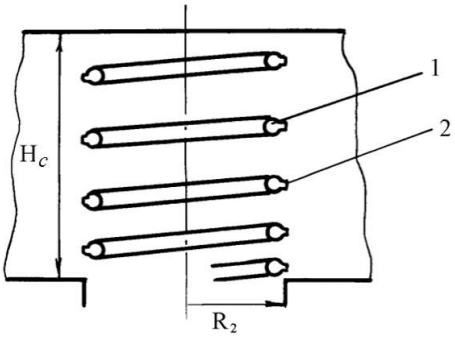

Figure 3.10 – One of the options for the location of the sprayer in the form of annular tubes: 1 – tubes; 2 – nozzles

This regulation can be done in the following way. Let the annular tubes (or one tube in the form of a coil) form annular channels with the same cross-sections between themselves. The geometric dimensions of the vortex chamber R_1, R_2, H_c, and their ratio are such that when gas passes through the mass transfer chamber in a cylindrical section with a radius R_2, the fields are uneven of radial and axial velocities along with the height of the chamber. That is, in the lower part, near the end cover with gas removal, the velocities are high, and, consequently, the amount of gas that passes through the annular channels is increased compared to the amount of gas that passes through the annular channels of the atomizer in the upper part of the chamber. By increasing the density of the atomizer tubes near the lower end cap, it is possible to increase the hydraulic resistance of the lower part of the atomizer and achieve a redistribution of the gas flow.

Another direction that allows you to equalize the gas flow along the height of the mass transfer chamber is the creation of a gas outlet in the form of several concentric nozzles (Figure 3.11).

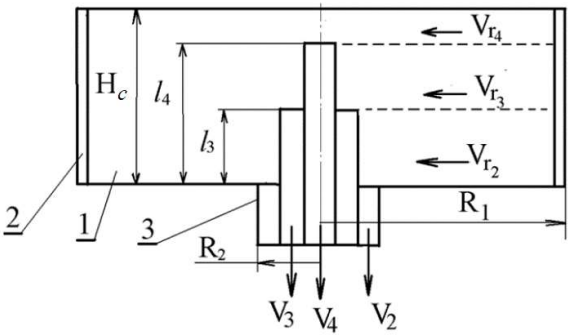

Figure 3.11 – Flow distribution scheme: 1 – mass transfer chamber; 2 – tangential gas inlet; 3 – gas outlet pipe

It is also possible to perform a combined outlet, in which the gas flow is equalized, by changing the density of the annular tubes of the atomizer and the area of the annular channels of the concentric nozzles for the removal of the gas flow (Figure 3.12).

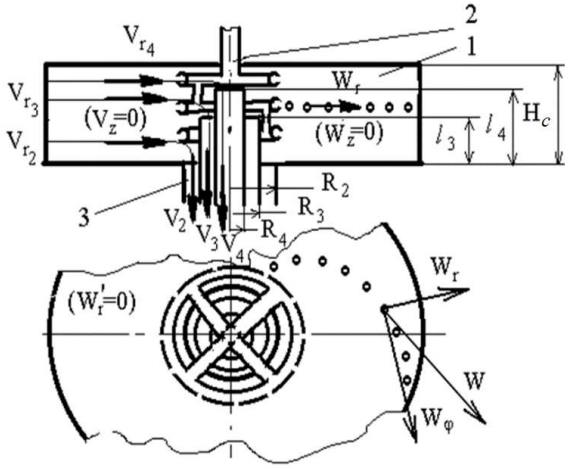

Figure 3.12 – The scheme of the combined gas outlet with annular nozzles and tubes

It is not advisable to install a large number of concentric pipes in the gas outlet since this complicates the design and will increase the resistance of the mass transfer apparatus.

Therefore, considering the relatively low height of the working chamber, it is sufficient to make a tap in the form of three cylindrical elements (Figure 3.11).

The main problem in calculating such an outlet is determining the radial and axial dimensions of the gas outlet nozzles to create a uniform velocity field in the spray zone, usually located near the radius R_2.

Asking for values of auxiliary lengths

$$l_3 = H_c/3;\ l_4 = 2H_c/3. \tag{3.65}$$

from the condition of equality of gas flow through cylindrical and annular sections, we can write the following relationships:

$$\begin{gathered}\pi(R_2^2 - R_3^2)V_2 = 2\pi R_2 l_3 V_{r_2};\\ \pi(R_3^2 - R_4^2)V_3 = 2\pi R_3(l_4 - l_3)V_{r_3};\\ \pi R_4^2 V_4 = 2\pi R_4(H_c - l_4)V_{r_4},\end{gathered} \tag{3.66}$$

where R_3, R_4 – radiuses of annular sections, m.

A uniform field of radial velocities is achieved if $V_{r_4} = V_{r_3} = V_{r_2} = V_r$, where $V_r = \frac{Q_g}{2\pi R_2 H_c}$.

On the other hand, the magnitude of the gas velocities depends on the energy losses when the gas passes through the annular and cylindrical channels in the outlet:

$$\Delta P_2 = \zeta_2 \frac{\rho_g V_2^2}{2};\ \Delta P_3 = \left(\zeta_3 + \lambda_3 \frac{l_3}{d_{e_3}}\right)\frac{\rho_g V_3^2}{2};$$
$$\Delta P_4 = \left(\zeta_4 + \lambda_4 \frac{l_4}{d_{e_4}}\right)\frac{\rho_g V_4^2}{2}, \quad (3.67)$$

where ζ_2, ζ_3, ζ_4 – local loss factors; λ_3, λ_4 – length loss factors; d_{e3}, d_{e4} – equivalent nozzle diameters, m.

The exhaust system of three channels is a parallel branch of pipelines, where the gas flow rates are redistributed from the condition of $\Delta P_2 = \Delta P_3 = \Delta P_4$.

Assuming that the coefficients of local energy losses at the nozzle inlet are equal, we can obtain relations that relate the axial gas velocities in the outlet channels:

$$V_3 = \mathrm{A}_3 V_2;\ V_4 = \mathrm{A}_4 V_r;$$
$$A_3 = \sqrt{\frac{\zeta}{\zeta + \lambda_3 \frac{l_3}{d_{e_3}}}};\ A_4 = \sqrt{\frac{\zeta}{\zeta + \lambda_4 \frac{l_4}{d_{e_4}}}}, \quad (3.68)$$

where A_3, A_4 – coefficients of proportionality.

After considering (3.66), it can be found:

$$\frac{R_3(l_4 - l_3)}{(R_3^2 - R_4^2)A_3} = \frac{R_2 l_3}{R_2^2 - R_3^2};\ \frac{R_2 l_3}{R_2^2 - R_3^2} = \frac{(H_K - l_4)}{R_4 A_3}, \quad (3.69)$$

or, leading to a form convenient for calculations:

$$R_3^3 + aR_3^2 + bR_3 + c = 0;\ R_4 = \frac{(H_K - l_4)(R_2^2 - R_3^2)}{A_4 R_2 l_3};$$
$$a = \frac{R_2 l_3 A_3}{l_4 - l_3};\ b = \frac{R_2^2 l_3 - R_2^2 l_4}{l_4 - l_3};\ c = \frac{R_2 l_3 R_4^2 A_3}{l_4 - l_3}, \quad (3.70)$$

where a, b, c – coefficients of the cubic equation.

The atomizer design, presented in Figure 3.10, makes it possible to redistribute the gas flow by changing the density of

the annular tubes along with the height of the mass transfer chamber. By increasing the density of the atomizer tubes at the end cap with the gas outlet, we decrease the free area through which the gas moves. Additional resistance to gas flow is created in the lower part of the chamber. The amount of gas that passes through the annular slots in the upper part of the chamber increases. The free section here also increases, the resistance decreases, and the reverse occurs in the lower part.

Thus, by varying the density of the annular tubes of the atomizer, it is possible to obtain a uniform gas flow along with the height of the mass transfer chamber at a relatively large height with respect to the radius of the working chamber.

From the condition for obtaining maximum circumferential velocities in a cylindrical section and a given value of the average droplet diameter, we determine the boundary conditions for equation (3.27) at $r = R_2$.

After considering (3.19):

$$V_{\varphi_2} = \sqrt{\frac{12\sigma}{\rho_g d_0}}. \tag{3.71}$$

Then the constants of integration, which are determined by equations (3.28) considering condition (3.66), are equal to:

$$C_1 = \frac{V_{\varphi_1} R_1 - \sqrt{\frac{12\sigma}{\rho_g d_0}} R_2}{R_1^{Re+2} - R_2^{Re+2}};\ C_2 = \frac{\sqrt{\frac{12\sigma}{\rho_g d_0}} R_2 R_1^{Re+2} - V_{\varphi_1} R_1 R_2^{Re+2}}{R_1^{Re+2} - R_2^{Re+2}}. \tag{3.72}$$

If we simplify the scheme of the movement of the gas flow at the outlet of the mass transfer chamber, assuming an average axial velocity, for example, from considerations of optimizing losses in the gas outlet pipe within V_{z2} = 20–30 m/s, the radius R_2 is determined from the equation:

$$R_2 = \sqrt{\frac{Q_g}{\pi V_{z_2}}}. \quad (3.73)$$

After optimizing energy losses in tangential slots, $V_{\varphi 1} = V_{in}$ (for V_{in} = 30–40 m/s), the radius of the mass transfer chamber can be determined:

$$R_1 = \frac{(V_{\varphi_1} R_1 - V_{\varphi_2} R_2)}{V_{\varphi_1}(R_1^{Re+2} - R_2^{Re+2})} R_1^{Re+2} + \frac{V_{\varphi_2} R_2 R_1^{Re+2} - V_{\varphi_1} R_1 R_2^{Re+2}}{V_{\varphi_1}(R_1^{Re+} - R_2^{Re+2})}. \quad (3.74)$$

where $V_{\varphi 2}$ and R_2 are determined from the conditions (3.71) and (3.73), respectively.

Equation (3.74) is written in a form convenient for solving using the method of successive approximations.

There are, in addition to the transfer of the spray surface in the direction along the radius of the vortex mass transfer chamber, two more ways to change the liquid spray conditions to influence the overall pattern of the vortex flow:

– change in the amount of liquid that is supplied through the atomizer along with the height of the vortex mass transfer chamber (uneven atomization);

– and the introduction of liquid into the spray zone with a circumferential velocity having a different direction with respect to the circumferential velocity of the vortex gas flow.

Uneven liquid atomization has many features that lead to significant difficulties in solving the problem in the theoretical description of this process, together with the effect on the vortex gas flow, which leads to the creation of designs of vortex spraying countercurrent mass transfer apparatuses that differ from those considered in this work.

The apparatus considers a vortex gas-droplet flow uniform along with the height of the working chamber. This movement is strongly influenced by the initial conditions of the movement of droplets of the sprayed liquid.

We use equation (3.48), rewritten in a slightly different form:

$$V_{\varphi}^{*} = V_{\varphi} - \frac{L}{G} W_{\varphi}, \qquad (3.75)$$

where L, G – liquid and gas phase loads, respectively, kg/s; W_{φ} – circumferential fluid velocity, m/s.

Suppose a liquid is introduced at a circumferential velocity, the value of which is close in magnitude to the circumferential velocity of the gas. In that case, we obtain an increase in the interfacial surface due to an increase in the relative velocity of the phases and a decrease in the droplet diameter (3.19).

When the phase load ratio approaches unity ($L/G = 1$), the circumferential velocities of the vortex gas flow decrease or become equal to zero, the positive effect obtained by finely dispersed spraying of liquid into small-diameter droplets does not justify itself.

In this case, after spraying, the liquid droplets enter the vortex gas flow, which has low circumferential velocities. Liquid droplets are not involved in rotational motion. The own rotational motion of liquid droplets quickly decays. Under the action of aerodynamic forces from the side of the gas moving towards the center, the droplets are captured and carried along with the gas to the exit from the vortex mass transfer chamber. There is a breakdown in the operation of the vortex spraying countercurrent mass transfer apparatus.

The introduction of liquid with peripheral velocity, which has the same direction as the peripheral velocity of the gas flow, leads to a significant improvement in the hydrodynamic situation in the vortex chamber.

First, the energy losses of the gas flow associated with the involvement of liquid droplets in rotational motion are reduced.

Secondly, the conditions for introducing fluid are improved. Droplets already at the initial moment of their stay in the vortex mass transfer chamber move in a circumferential direction. Centrifugal forces immediately begin to act on them, which entrain the liquid to the periphery of the vortex mass transfer chamber.

The presence of a significant circumferential velocity field in the vortex mass-transfer chamber leads to complete involvement in the countercurrent movement of droplets of a polydisperse composition. The flight path of droplets along flat spiral trajectories to the cylindrical wall of the vortex mass transfer chamber is lengthened.

Thirdly, it becomes possible to use the kinetic energy of the gas flow that has left the vortex chamber to atomize the liquid and impart rotational motion.

The design of a vortex countercurrent atomizing mass transfer apparatus with a rotating atomizer that rotates and uses the gas flow energy is shown in Figure 3.13.

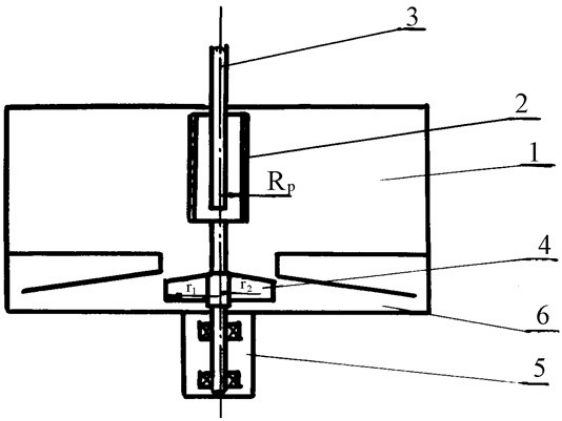

Figure 3.13 – Design scheme of the rotating atomizer: 1 – mass transfer chamber; 2 – permeable shell; 3 – fluid supply pipe;
4 – bladed system; 5 – bearing assembly; 6 – radial diffuser

Let us determine the rotation velocity of the atomizer, which works as follows. A liquid medium is fed into the semi-permeable shell through a branch pipe in the upper cover of the vortex mass transfer chamber. The atomizer is driven into rotation by the vortex gas flow on the vane system, which is located in the radial diffuser behind the vortex mass transfer chamber. In the hollow shell of the atomizer, the liquid, under the action of centrifugal forces, is distributed over the cylindrical walls and, flowing through them into the gaseous medium, has the same circumferential velocity, in the direction with the circumferential velocity of the gas flow.

Considering that the circumferential velocity is not equal to zero at $r = R_{in}$, equation (3.64) can be rewritten in the form:

$$V_\varphi = k_1 r, \tag{3.76}$$

where k_1 – coefficient of flow swirl droplet when passing through the gas outlet pipe ($k_1 < V_{\varphi 2}/R_2$).

Spraying power of a centrifugal atomizer, W:

$$N_a = GR_a^2\omega^2, \tag{3.77}$$

where R_a – radius of the atomizer.

The power of a vane system is as follows:

$$N_v = n_1 \int_{N_v} dN_v, \tag{3.78}$$

where n_1 – number of blades; dN – elementary power under the influence of a gas flow on an elementary blade area:

$$dN_v = \zeta \frac{\rho_g (V_\varphi - \omega r)^2}{2} \omega r z dz, \tag{3.79}$$

where r – radius, m; z_v – vane height, m.

If the blade height changes linearly ($z_v = z_1$ for $r = r_1$, and $z_v = z_2$ for $r = r_2$):

$$z = k_2 r + k_3; k_2 = \frac{z_2 - z_1}{r_2 - r_1}; z_3 = z_1 - \frac{z_2 - z_1}{r_2 - r_1} r_1, \tag{3.80}$$

equation (3.78) is rewritten in the form:

$$\begin{aligned} N_v = \frac{n_1 \zeta \rho_g \omega}{2} k_1^2 \Big[& \int_{r_1}^{r_2} r^3 (k_2 r + k_3) dr - \\ & - 2\omega k_1 \int_{r_1}^{r_2} r^3 (k_2 r + k_3) dr + \\ & + \omega^2 \int_{r_1}^{r_2} r^3 (k_2 r + k_3) dr \Big]. \end{aligned} \tag{3.81}$$

Calculating the integrals, finally, it can be obtained:

$$N_v = \frac{n_1 \zeta \rho_g}{2}\left[\frac{k_2}{5}(r_2^5 - r_1^5) + \frac{k_3}{4}(r_2^4 - r_1^4)\right] \times \\ \times (k_1^2 - 2\omega k_1 + \omega^2). \quad (3.82)$$

From the condition of the consumption of all energy for liquid spraying ($N_a = N_v$), and after considering the dependence (3.77):

$$GR_a^2\omega = \frac{n_1 \zeta \rho_g}{2}\left[\frac{k_2}{5}(r_2^5 - r_1^5) + \frac{k_3}{4}(r_2^4 - r_1^4)\right] \times \\ \times (k_1^2 - 2\omega k_1 + \omega^2). \quad (3.83)$$

Having marked

$$k_4 = \frac{n_1 \zeta \rho_g}{2}\left[\frac{k_2}{5}(r_2^5 - r_1^5) + \frac{k_3}{4}(r_2^4 - r_1^4)\right], \quad (3.84)$$

from equation (3.83) we get:

$$\omega^2 - \left(2k_1 + \frac{GR_a^2}{k_4}\right)\omega + k_1^2 = 0. \quad (3.85)$$

Therefore, the atomizer's angular velocity is:

$$\omega = \frac{1}{2}\left(2k_1 + \frac{GR_a^2}{k_4}\right) \pm \sqrt{\frac{1}{4}\left(2k_1 + \frac{GR_a^2}{k_4}\right)^2 - k_1^2}. \quad (3.86)$$

A significant improvement in the hydrodynamic situation in the mass-exchange chamber of a vortex apparatus can be achieved by using a variety of atomizers, in particular, vibrating ones, to obtain a monodisperse composition of sprayed liquid droplets.

In this case, one should expect a sharp decrease in spray entrainment, improvement, and adjustment of the movement of the vortex droplet flow, which generally leads to the

intensification of mass transfer processes in the vortex spray mass transfer apparatus.

Thus, the organization of liquid spraying in the vortex chamber is a significant design and technological reserve in increasing the efficiency of the apparatus because on the dispersion of liquid droplets.

3.7 Separation of droplet liquid in a working chamber

When using vortex apparatuses in some processes (e.g., drying natural gas before its transportation through pipelines), the use of hollow vortex chambers for preliminary separation of condensed moisture to reduce the consumption of absorbent in the mass transfer chamber is of considerable interest.

If the gas flow enters the vortex chamber with liquid droplets, then the circumferential velocities of the gas flow at the periphery of the vortex chamber are not sufficient in magnitude to create a centrifugal force field for separating settling the liquid on the cylindrical walls. With further movement of the droplets and the gas flow to the center of the vortex chamber, as the circumferential velocity of the gas increases, the droplets are deformed and further crushed. Droplets of small diameter will be involved in rotational motion at velocities sufficient to create a field of centrifugal forces, under the influence of which the droplets can begin to move towards the periphery and settle on the cylindrical wall.

Implementing the separator in the form of a vortex chamber with the exact radial dimensions as the vortex chamber of the countercurrent mass transfer apparatus makes it easy, from the point of view of design, to link it with the main mass transfer apparatus. The hydrodynamic parameters of the separator can be controlled by changing the height, number, and

width of tangential slots for gas injection. This affects the value of the peripheral velocities at the entrance to the vortex chamber and the value of the peripheral velocities along the radius to the center of the vortex chamber. The calculation of separation characteristics is based on considering the relationship between centrifugal forces and resistance forces and the magnitude of these forces and, accordingly, their ratio varies significantly along the radius.

According to (3.35), the resultant force under which a liquid droplet moves to the periphery of the vortex chamber is determined by the following relationship:

$$F_d = \frac{\pi}{6} d_0^3 \rho_0 \frac{V_\varphi^2}{r} - \frac{\pi}{8} \psi V_r^2 d_0 \rho_0. \tag{3.87}$$

Elementary work that is performed by this force on the radial displacement of the droplet, J:

$$\delta A_d = F_d dr = \frac{\pi}{2} d_0^2 \left[\frac{d_0}{3} \rho_0 \frac{V_{\varphi 1}^2 \left(\frac{R_1}{r}\right)^{2n}}{r} - \frac{\psi \rho_g Q_g^2}{16 \pi H_c^2 r^2} \right] dr. \tag{3.88}$$

After integration within the boundaries from R_2 to R_1:

$$A_d = \frac{\pi}{2} d_0 \left[\frac{d_0 \rho_0 V_{\varphi 1}^2 R_1^{2n}}{3(3n+1)} (R_1^{3n+1} - R_2^{3n+1}) - \right. \\ \left. - \frac{\psi \rho_g Q_g^2}{16 \pi H_c^2} \left(\frac{1}{R_1} - \frac{1}{R_2} \right) \right]. \tag{3.89}$$

On the other hand, the movement of a droplet from radius R_2 to R_1 can be considered as the result of an effective centrifugal force:

$$F_{cf_e} = \frac{\pi d_0^3 \rho_0}{6} \frac{V_{\varphi e}^2}{R_2} (R_1 - R_2), \tag{3.90}$$

where $V_{\varphi e}$ – effective angular velocity, m/s.

Its work to move the droplet from the central region to the periphery is equal to:

$$A_d = F_{cf_e}(R_1 - R_2). \tag{3.91}$$

Having determined from equations (3.89) and (3.90) the effective circumferential velocity of the gas:

$$V_{\varphi_e} = \left\{ \frac{3R_2}{d_0 \rho_0 (R_1 - R_2)} \left[\frac{d_0 \rho_0 V_{\varphi 1}^2 R_1^{2n}}{3(3n+1)} (R_1^{3n+1} - R_2^{3n+1}) - \right. \right. \\ \left. \left. - \frac{\psi \rho_g Q_g^2}{16\pi^2 H_c^2} \left(\frac{1}{R_1} - \frac{1}{R_2} \right) \right] \right\}^{\frac{1}{2}}, \tag{3.92}$$

it is possible to analyze the operation of the working chamber as a preliminary separator.

For subsequent refinement of the calculation of the geometrical parameters of the vortex chamber of the separator, it is necessary to perform a complete calculation of the peripheral gas velocity field along the radius.

An example of the layout of a separator in the form of a vortex chamber with the exact radial dimensions as that of the vortex chamber of a countercurrent mass transfer apparatus can be a diagram of a multistage vortex spray countercurrent mass transfer apparatus.

The height of the vortex chamber of the separator may differ from the height of the vortex mass transfer chamber. The working chamber of the separator must also contain all the structural elements for intensive and timely removal of the liquid being separated from the cylindrical walls so that the liquid film that forms on them does not fall into the tangential swirler and

is not subjected to separation by the gas flow and repeated crushing.

The removal of the liquid film along the cylindrical walls can be carried out through slots along with the entire height of these walls. Behind such slots for draining the liquid, there should be voids for collecting it, and in the lower part of each of these voids, it is necessary to organize the liquid drainage through the holes in the bottom end cover outside the swirl chamber.

If the hole for the gas outlet from the vortex chamber is located in the upper-end cover, then the liquid outlet design can be simplified and made in the form of slots at the base of the cylindrical wall since the end flow on the lower end cover does not significantly affect the increase in spray removal.

3.8 Hydrodynamic factors affecting the movement of a droplet flow

Suppose we use the method described in the previous sections to calculate a gas-droplet flow characteristic. In that case, it is possible to determine the effect of geometric and hydrodynamic parameters on the motion of a two-phase flow in the mass-exchange chamber of a vortex spray countercurrent apparatus. Calculations are performed under the block diagram given in Figure 3.14.

Figure 3.15 shows characteristic curves that reflect the change in the circumferential velocity of the gas along the radius of the vortex chamber depending on the phase loads.

Based on the tendency to decrease the relative velocities of gas and liquid in the spray zone, which is located in the section with the maximum circumferential velocities of the gas flow at the radius R_2 (Figure 3.16), we obtain an increase in the diameter of the sprayed liquid droplets (Figure 3.17).

Load fluctuations in phases may occur during the operation of the equipment. Let us consider that the interfacial surface, equal in size to the surface of the droplets of the sprayed liquid, is quadratic depending on the diameter of the liquid droplets. An increase in the load on the liquid phase leads to a significant decrease in the rate of mass transfer processes in the working chamber of the vortex spraying countercurrent mass transfer apparatus in the case of an increase in the diameter of the droplets.

An increase in the gas velocity in the spray area during the operation of the apparatus can be achieved by increasing the gas flow velocity in the inlet tangential slots, which can be done constructively by changing the area of these slots.

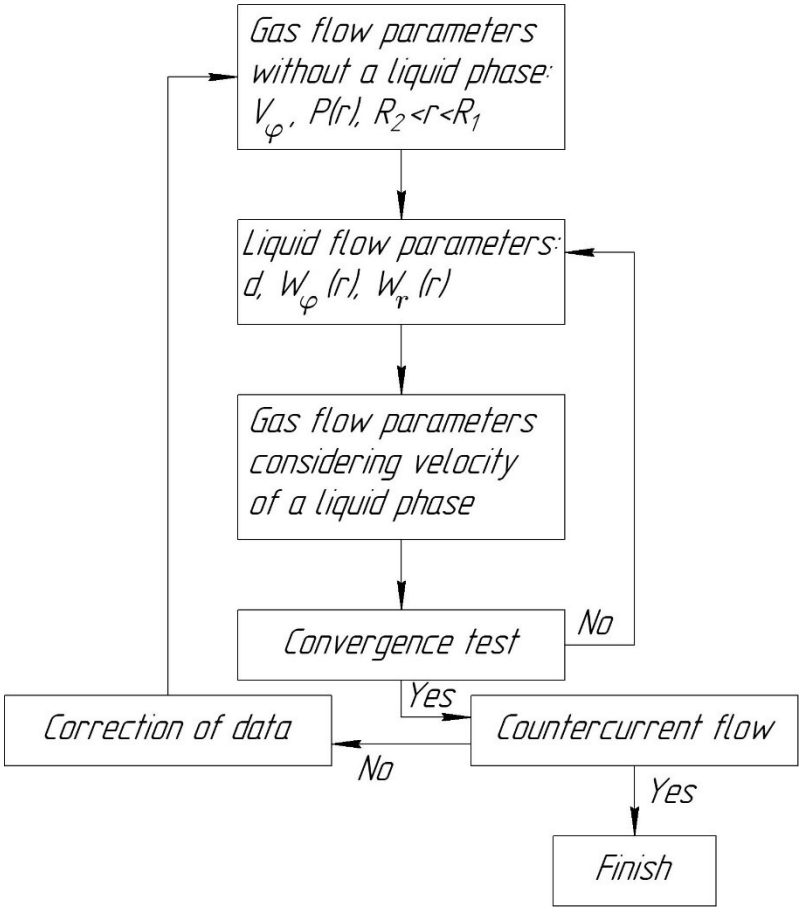

Figure 3.14 – Block diagram for calculating the hydrodynamic parameters of a two-phase vortex gas-droplet flow

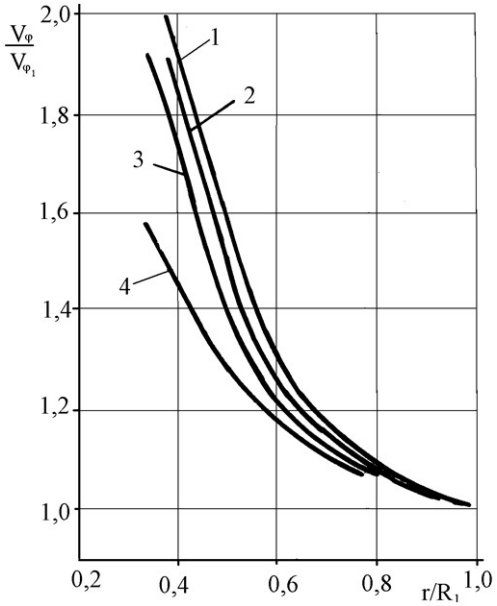

Figure 3.15 – Variation of the circumferential velocity of the gas flow depending on the ratio of loads by phases *L*/*G*: 1 – 0.2; 2 – 0.5; 3 – 1.0; 4 – 1.5

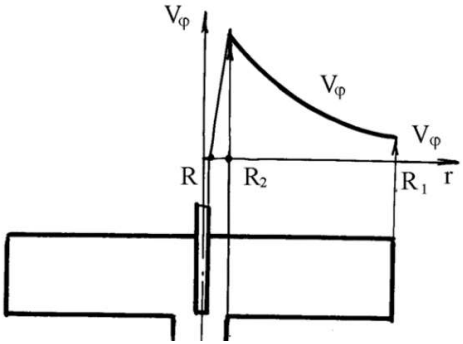

Figure 3.16 – Variation in peripheral gas velocities in the working chamber of the apparatus

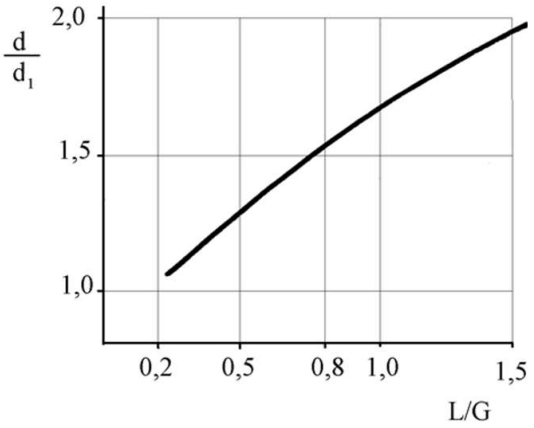

Figure 3.17 – Change in the droplet size of the sprayed liquid depending on the phase loads: d_1 – droplet diameter at L close to zero

However, it should be noted that a change in the cross-sectional area should not disturb the change in the free section along with the height of the mass transfer chamber, since the introduction of gas evenly over the entire height of the mass transfer chamber is one of the conditions for ensuring regular countercurrent phase movement.

On the other hand, an increase in the load on the liquid phase affects the picture of the movement of the droplet flow. In addition to a decrease in the interfacial surface and gas flow velocities, an increase in the radial velocity of the outflow of liquid jets into the gaseous medium increases the initial radial velocity of droplets to their rapid reaching the periphery of the mass transfer chamber.

This leads to a decrease in the residence time of the liquid in countercurrent movement along the radius (Figure 3.18) and a reduction in the path of droplets in the area where mass transfer

occurs (Figure 3.19). Simultaneously, this leads to a decrease in the efficiency of the mass transfer apparatus.

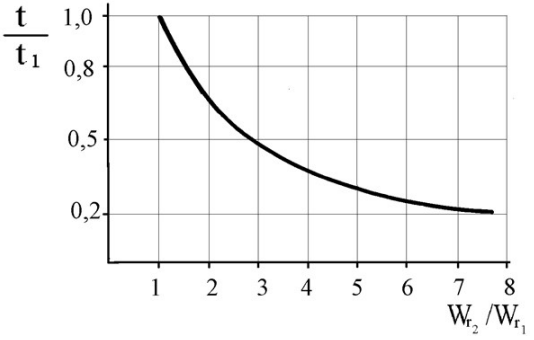

Figure 3.18 – The relationship between the residence time of droplets in the working chamber and the radial velocity of liquid supply to the gas: t_1 – the residence time of droplets at $W_{r2} = 0.7$ m/s

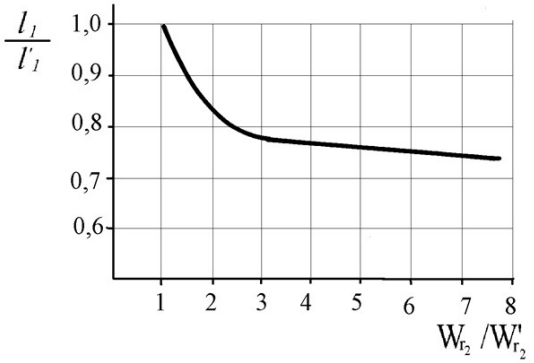

Figure 3.19 – The relationship between the length of the path of droplets in the working chamber and the radial velocity of the liquid supply to the gas

The calculation results are given for vortex mass-transfer chambers with dimensions $R_1 = 0.15$ m and $R_2 = 0.05$ m, assuming that spraying occurs at radius R_2. Then the minimum droplet path length is 0.15 m. Therefore, in Figure 3.19, after a sharp decrease in the path of movement in the mass transfer area, as the radial inlet velocity increases, there is a further slight decrease in the magnitude of this path.

The graph, which is given, only illustrates the very tendency of the droplet flight path to decrease in the mass-transfer chamber when the conditions of liquid injection change.

Thus, the given examples of the change in the pattern of motion of a two-phase gas-droplet medium from various factors clearly show the close relationship and mutual influence of velocities, phase loads, input characteristics of the gas flow and the liquid flow on each other.

4 Hydrodynamics of Flows in the Vortex Spraying Countercurrent Mass Transfer Apparatus

4.1 Methods for experimental studies on hydrodynamic parameters

Information about the movement of single-phase and two-phase flows in the vortex mass-exchange chamber of the vortex apparatus, given in the previous chapters, generally determines the range and tasks of experimental studies. The purpose of the experiments, which are described both in the literature sources of various researchers of any mass transfer equipment, and the authors of this monograph, was to study the nature of the movement, velocities, and pressure in a single-phase and two-phase medium in the mass-exchange chamber of a vortex spraying countercurrent mass-exchange apparatus.

Of considerable interest are studies of the hydrodynamics of devices in a vortex mass transfer chamber, whose dimensions are relatively large. The results obtained can be effectively used in actual industrial samples when designing the flow path of a new countercurrent spray mass transfer apparatus.

Since the gas (steam) flow forms the hydrodynamics of the vortex chamber, most of the research is the study of the motion of the vortex gas flow. Methods for studying the characteristics of a single-phase and multiphase flows are developed [72–74]. Considering the significant radial dimensions of the mass-exchange chamber, when studying the gas velocity and pressure fields in the mass-exchange chamber, most of the studies were carried out using the gas flow probing method. This paper presents results based on a 5 mm ball probe and 1 mm total and static pressure tubes.

Since the design scheme of connecting the probe is well known (Figure 4.1), only a brief description of the possibilities provided by the information obtained from such measurements is given.

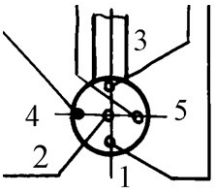

Figure 4.1 – Ball probe connection diagram: 1–5 – channels

The probe must first be calibrated on a special aerodynamic stand. After using a number of calibration curves, it is possible to determine such parameters as the magnitude of the total and static pressure, the velocity head and the velocity of the gas flow acting on the five-channel spherical probe, the direction of the total gas flow velocity vector, that is, the angle at which the gas flow flows onto the five-channel spherical probe.

According to the readings of the pressure gauges that are connected to the second, fifth and fourth holes, it is possible to determine the velocity head and the gas flow rate. By equalizing the pressure in the fourth and fifth holes, the probe can be set so that the vector of the total gas flow velocity will be in a plane that passes through the axis of the five-channel ball probe. The rotation angle is fixed according to the readings of the marks located on the coordinator. The angle of gas flow in the plane that passes through the axis of the five-channel probe, relative to the axis of the central hole under the second number, is determined using calibration curves according to the readings of pressure gauges connected to the first, second, and third holes.

Probing the flow with a five-channel spherical probe made it possible to study the spatial movement of the gas flow in the vortex chamber, that is, to accurately determine such hydrodynamic parameters as pressure, velocity, and its direction along the radius of the mass transfer chamber, along with the height and throughout the entire volume of this chamber.

In what follows, the following notation is used. Stand 1 – stand with vortex mass transfer chamber with R_c = 300 mm. Stand 2 has a radius of the vortex mass transfer chamber R_c = 1430 mm. In Stand 3, the radius of the swirl chamber is equal to R_c = 600 mm.

The study of the gas flow made it possible to study the spatial flow, determine the boundary of a flat vortex gas flow the magnitude and nature of the change in velocity and pressure in the gas flow along the radius of the mass transfer chamber.

In all three devices, radial diffusers were installed at the outlet of the vortex mass-exchange working chamber.

Energy losses at the entrance to the vortex mass transfer chamber, hydraulic energy losses during the spiral movement of the gas flow in the central region and at the exit from the vortex mass transfer chamber of the spraying apparatus are determined by the geometry of the vortex chamber and the mode of operation of the mass transfer apparatus.

The distribution of these hydraulic energy losses the allocation of a part of each loss from the total balance is complicated. Therefore, it seems appropriate to combine them as the total hydraulic energy losses of the vortex gas flow in the mass transfer chamber ΔP_c:

$$\Delta P_c = P_{in} - P_{out}, \tag{4.1}$$

where P_{in}, P_{out} – pressure in the gas flow at the inlet and outlet of the vortex chamber, Pa, respectively.

A "pinwheel" as a lattice of vertical plates was used to measure the energy of the vortex gas flow at the diffuser inlet. A dynamometer perceives the entire moment when gas is applied to the plates through the bushing and axle. Knowing the shoulder and the magnitude of the force (according to the readings of the dynamometer), it is possible to determine the value of the average circumferential velocity of the gas in the neck of the diffuser and, knowing the static pressure and the average axial velocity of the gas flow, determine the total pressure in the gas flow at the outlet of the vortex mass transfer chamber.

Three methods were mainly used when studying the hydrodynamics of two-phase flows in the vortex mass-exchange chamber of a spraying countercurrent apparatus. These are visual studies, flow probing using a probe with a constant purge, and studies of the effect of changing the parameters of a two-phase flow on the integral characteristics of the apparatus, such as, for example, hydraulic resistance.

The study of changes in energy losses in a vortex spraying countercurrent mass transfer apparatus at various loads in the liquid and gas phases and inlet gas velocities in tangential slots was carried out on all three stands. The amount of spray entrainment was determined as the difference between the amount of liquid supplied to the atomizer and the amount of liquid removed from the cylindrical walls of the vortex mass transfer chamber.

4.2 Operation of devices on experimental stands

To study the hydrodynamics of single- and two-phase flows in the apparatus, all three stands had different values of the main geometric dimensions of the vortex mass transfer chambers and their ratios, different designs of devices that divert gas and liquid flows, and the radial diffuser and nozzles for diverting gas.

The vortex mass transfer apparatus of Stand 1 (Figure 4.2) is made entirely of organic glass. The vortex spraying countercurrent mass transfer apparatus has a vortex mass transfer chamber diameter of 300 mm, and a gas outlet diameter of 100 mm.

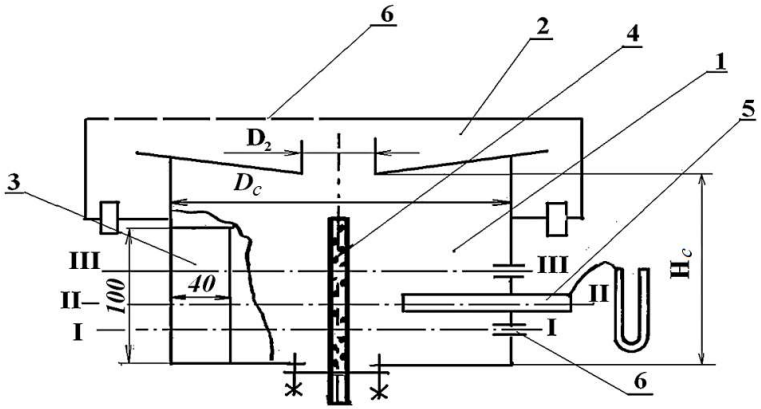

Figure 4.2 – The design scheme of Stand 1 (D_c = 300 mm): 1 – mass transfer chamber; 2 – radial diffuser; 3 – inlet tangential branch pipe; 4 – atomizer; 5 – pressure measuring device; 6 – places for measuring pressure

The gas removal from the vortex mass transfer chamber is carried out in the upper-end cap. The outer diameter of the radial diffuser is 380 mm. The gas is introduced into the vortex mass transfer chamber using a tangential branch pipe, which has a rectangular cross-section at the inlet to the mass transfer chamber. The cross-section area is 100 mm, and the width is 40 mm.

In the research process, the width of the rectangular inlet tangential branch pipe for introducing the gas flow into the vortex mass transfer chamber was changed. Structurally, this

was done by changing the width of the inserts directly in the tangential branch pipe, which made the flow area smaller.

The pressure points along the radius and the height of the vortex chamber are shown in Figure 4.2. The gas flow was studied in three sections in the mass transfer chamber. The bottom one is placed at 25 mm from the bottom end cap, the middle one is at 77 mm, and the top one is at a distance of 123 mm from the bottom end cap.

In the research process, the vortex mass transfer apparatus of Stand 1 was subjected to alteration, which consisted of reducing the height of the vortex mass transfer chamber from 250 mm to 100 mm.

The liquid was supplied to the gas flow in the central region of the vortex mass transfer chamber along with its entire height with the help of an atomizer. The diameters of the holes through which the liquid jets were introduced in the radial direction are 1.2 mm, and the outer diameter of the atomizer is 20 mm.

The liquid was removed from the vortex mass transfer chamber through a slot in the cylindrical wall at the periphery. The height of the slot for draining the flowing liquid is 100 mm, and the width is 5 mm.

The schemes presented in Figure 4.3 were used to study the velocity and pressure fields in a vortex two-phase gas-liquid flow.

The design scheme of Stand 2 is presented in Figure 4.4, and the flow directions – in Figure 4.5.

The diameter of the hole for gas removal from the vortex mass transfer chamber is 300 mm, and the height of the mass transfer chamber is 300 mm.

The cylindrical body of the mass transfer chamber is made in the form of six blades curved along the radius of the working chamber. Along with its entire height, on each of the blades is a

vertical slot connected to a chamber for draining liquid. The blades have axes around which they can be rotated. Under the chambers for draining liquid on the blades, in the lower end cap, holes are placed through which the device removing liquid from the blade is connected to a container for collecting liquid. The hole for gas removal from the vortex mass transfer chamber is made in the lower end cover.

The design scheme of flow measurements is presented in Figure 4.6.

Further, the gas flow is a radial diffuser. Unlike the vortex mass transfer apparatus in Stand 1, the vortex apparatus of Stand 2 also has a device for simulating the presence of a second stage in the apparatus, which is located behind the radial diffuser.

There was no vortex chamber in the second stage of the vortex apparatus of the second stand. The vortex gas flow is discharged through a tangentially located branch pipe beyond the boundaries of the mass transfer apparatus from the annular chamber behind the radial diffuser.

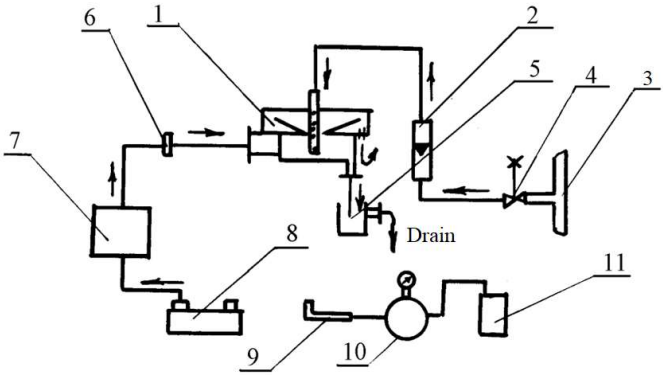

Figure 4.3 – The design scheme of flow measurements:
1 – vortex apparatus; 2 – rotameter; 3 – water supply line;
4 – valve; 5 – capacity for measuring the discharged liquid;
6 – flow meter; 7 – separating tank; 8 – blower; 9 – probe;
10 – expanding capacity; 11 – compressor

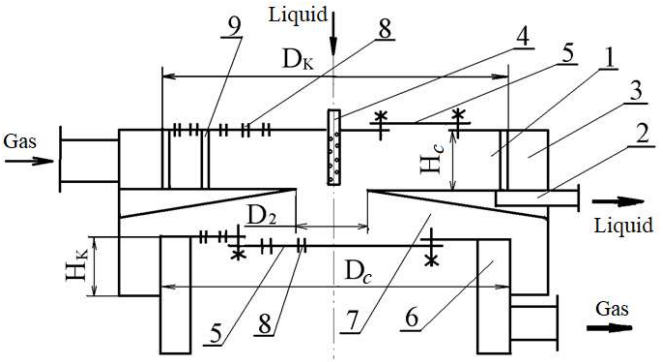

Figure 4.4 – The design scheme of Stand 2 (D_c = 1430 mm):
1 – mass transfer chamber; 2 – container for collecting liquid;
3 – inlet chamber; 4 – atomizer; 5 – windows for visual observations; 6 – mass transfer chamber of the second stage;
7 – radial diffuser; 8 – places of measurement;
9 – tangential slots for gas injection

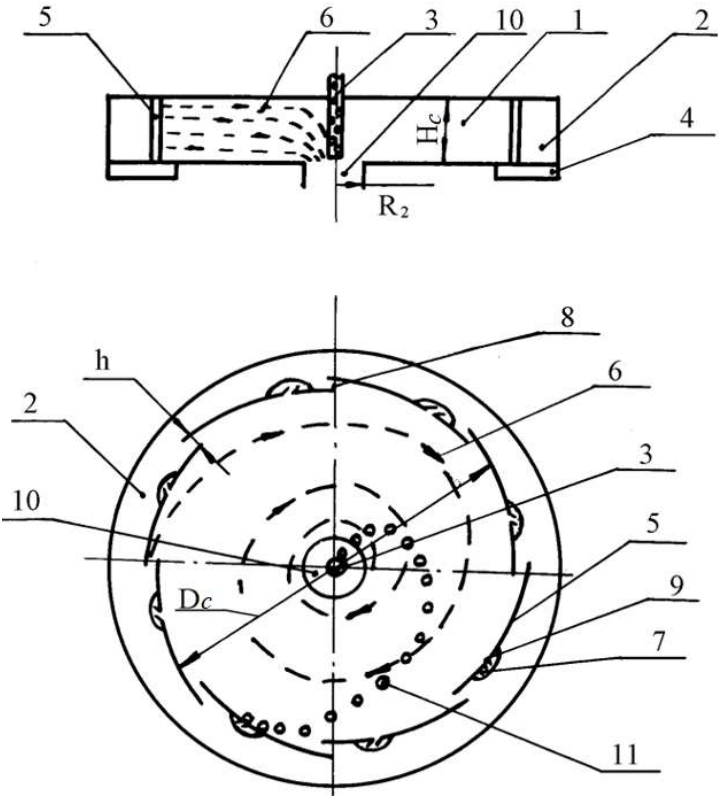

Figure 4.5 – Scheme of flow movement in the vortex apparatus of Stand 2: 1 – mass transfer chamber; 2 – annular chamber for gas supply; 3 – atomizer; 4 – an annular chamber for collecting and draining fluid from the apparatus; 5 – blades; 6 – gas flow; 7 – cavity for removing liquid from the mass transfer chamber; 8 – tangential slots for introducing liquid into the mass transfer chamber; 9 – slots for removing the liquid film from the cylindrical walls of the vortex chamber; 10 – gas outlet pipe; 11 – the flow of liquid droplets

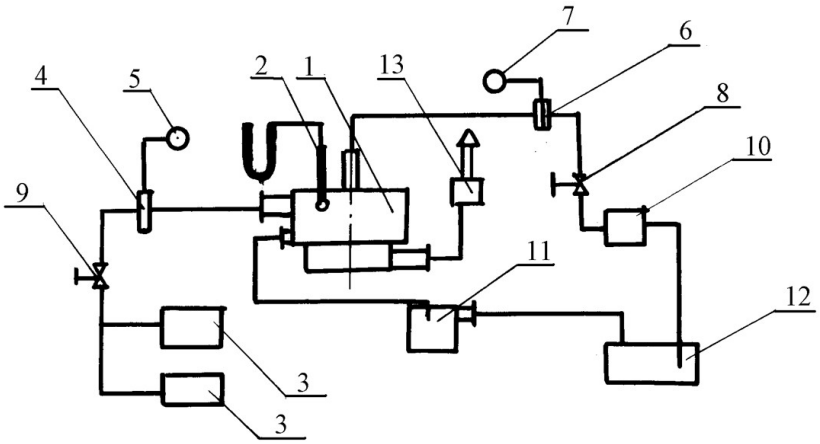

Figure 4.6 – The design scheme of flow measurements:
1 – vortex apparatus; 2 – probe; 3 – blower; 4 – air flow meter;
5, 7 – secondary devices; 6 – water flow meter; 8 – valve;
9 – valve; 10 – pump; 11 – measuring container;
12 – tank; 13 – splash guard

Thus, the lower cover of the radial diffuser and the inner cylindrical wall of the annular chamber behind the radial diffuser form a cylindrical void, which was used for visual observations and installation of a "turntable" for measuring the momentum and energy parameters of the gas flow behind the mass transfer chamber of the first stage of the vortex apparatus, since the lower the cover of the radial diffuser was removable and made of organic glass.

There are holes in which a coordinate for a ball probe is installed on the upper-end cover in two mutually perpendicular directions. Flow probing was carried out when the probe moved along the height of the vortex mass transfer chamber.

Air and water were used as working media. An intense air vortex was discharged through the gas outlet in the lower end cap of the vortex mass transfer chamber beyond the chamber

boundaries into a radial diffuser. Further, the gas was removed from the apparatus through the annular outlet behind the radial diffuser and the tangential branch pipe through the second stage. During the experiments, the liquid circulated in a closed cycle.

The diameter of the spray nozzle outlet is 1.2 mm. The amount of spray entrainment was determined by the difference in the flow rates of the liquid that is supplied and discharged from the apparatus, kg/s:

$$\Delta L = L_{in} - L_{out}, \tag{4.2}$$

where L_{in}, L_{out} – mass flow rate of a liquid supplied to and removed from the device, respectively, kg/s.

The design scheme of Stand 3 is presented in Figure 4.7.

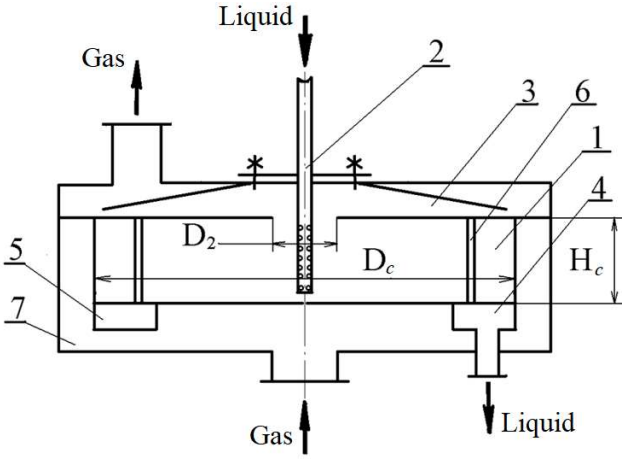

Figure 4.7 – The design scheme of Stand 3 (D_c = 600 mm): 1 – mass transfer chamber; 2 – atomizer; 3 – radial diffuser; 4 – container for collecting liquid; 5 – hole for draining liquid; 6 – tangential slots for gas injection; 7 – gas supply chambers

The vortex apparatus has a mass transfer chamber with a diameter of 600 mm. The diameter of the hole for gas removal in the end cap of the vortex mass transfer chamber is 120 mm, and the height of the mass transfer chamber is 200 mm. The hole for venting gas from the vortex mass transfer chamber is located in the upper-end cap of this mass transfer chamber. The dimensions of six slots were regulated by rods extended beyond the boundaries of the outer cylindrical body of the mass transfer chamber.

The liquid outlets from the working chamber of the vortex spraying countercurrent mass transfer apparatus were performed by 30 holes of 8 mm in diameter, drilled in the lower end cover at the base of the cylindrical walls of the vortex mass transfer chamber.

In this design of the vortex atomizing mass transfer apparatus, it is possible to study the change in hydraulic resistance depending on the loads in the liquid and gas phases the change in the input gas velocity in tangential slots. The pressure droplet carries out the measurements between the annular chamber for gas supply in front of the vortex mass transfer chamber and the annular chamber after the radial diffuser. The velocity of gas movement in these elements is close to zero, and the difference in static pressure determines energy losses. The amount of spray entrainment is determined by the amount of supplied and removed liquid difference.

When studying a two-phase gas-droplet flow, it is necessary to determine the effect of the ratio of loads by phases on their stable operation to identify the apparatus's optimal modes of operation.

The designs of the stands that are given allow, along with a visual study of the gas and droplet flows in the vortex chamber of a spraying countercurrent mass transfer apparatus, to study the local fields of velocities (both radial and circumferential) and

pressure in the gas flow, to study the effect of the droplet flow on gas hydrodynamics.

The stands also allow determining integral characteristics (e.g., the resistance of the apparatus) and studying the balance of energy losses as the distribution of hydraulic losses over the elements of a vortex countercurrent mass transfer apparatus (tangential slot, vortex or working chamber, branch pipe for draining gas, and radial diffuser).

Despite the design features that distinguish the apparatus designs, studies on stands for studying the hydrodynamics of vortex apparatuses have common approaches.

Studies of the hydrodynamics of vortex countercurrent mass transfer apparatuses were carried out on stands where air and water were used as working media. After using a gas blower, the air was supplied through an air duct into the annular chamber in front of the tangential slots (for the second and third stands) or directly through the tangential gas supply into the vortex chamber (for the first stand).

The gas flow rate was determined by calculation based on measuring the pressure droplet on both sides of the flow washer.

Further, the air was supplied through the tangential slots to the working vortex mass transfer chamber and was removed from it through the central hole in the lower or upper cover (depending on the design of the vortex spraying countercurrent mass transfer apparatus) from the mass transfer chamber. After the radial diffuser and separator, in which part of the liquid carried away by the gas flow was separated, the liquid was discharged into a measuring container. Here, its quantity was determined, and data on the liquid carried away by the gas from the mass-transfer chamber were used to determine the spray entrainment. After the separator, the air was released into the atmosphere.

The liquid was supplied to the vortex mass transfer chamber through a sprayer, located in the center of the mass transfer chamber in all three stands, in the radial direction evenly along with its entire height. In some cases, to study the effect of gas flow on liquid jets along with the height of the vortex mass transfer chamber, the number of jets was limited along with the height of the working chamber, which made it possible to identify a zone unfavorable for liquid dispersion, spraying in which can lead to an increase in spray entrainment. The flow rate of the supplied liquid was measured using a rotameter, which was calibrated in advance. When studying the integral characteristics, pressure sampling was carried out at places where the gas velocity is close to zero, and when measuring pressure droplets, these data were obtained at such points where the gas flow rates were the same. Thus, the repeated repetition of experiments, their reproducibility, and the use of standard research methods made it possible to obtain reliable results that characterize the operation of vortex spraying countercurrent mass transfer apparatuses.

4.3 Single-phase flow in a working mass transfer chamber

The main element of the vortex spraying countercurrent mass transfer apparatus is the vortex mass transfer chamber, in which the contact between liquid and gas takes place. The effective and stable operation of the mass-exchange apparatus depends on how the processes of liquid atomization, which moves countercurrently to the gas in the radial direction, and therefore, the movement of liquid droplets, are adequately organized in it.

To solve these problems, it is necessary:

– to determine the influence of the design of the vortex mass transfer chamber (e.g., the location of the gas supply, and changes in its dimensions and design) on the uniformity of the velocity field along with the height of the mass transfer chamber;

– to know the theoretical dependencies that allow the calculation of the hydrodynamic parameters of the apparatus with the possibility of creating between two cylindrical surfaces, with radiuses R_1 and R_2 (that is, between a cylindrical surface on which there are tangential slots for introducing a gas flow, and a cylindrical surface with a radius equal to the radius branch pipe for removing the gas flow (Figure 4.8) from the vortex mass transfer chamber), flat spiral gas flow;

– to identify the location of the maximum circumferential velocities of the vortex gas flow, which is very important for the correct location of the atomizing device or the introduction of droplets of the atomized liquid into the gas flow.

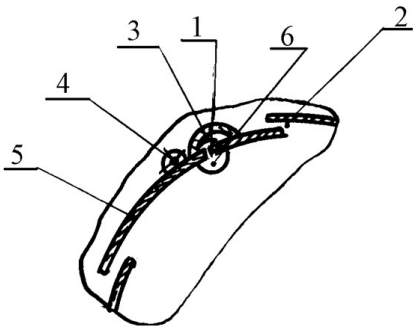

Figure 4.8 – Scheme of a device for draining fluid: 1 – vertical slot; 2 – tangential slot (introduces gas in the circumferential direction); 3 – cavity for liquid drain; 4 – blade axis; 5 – scapula; 6 – a hole in the bottom end cap

In addition, it is necessary to obtain quantitative data on the dependence of the change in the circumferential velocity of

the vortex gas flow along the radius of the mass-exchange chamber of the countercurrent apparatus. Also, it is necessary to find out the effect of the gas supply design, e.g., the relative value of the width of the tangential slots on the difference between the calculated average velocity in the tangential slots (defined as the ratio of the volume flow of gas and the area of the slots, and the circumferential velocity of the gas flow at a radius equal to R_1).

The next task in the experimental study of a single-phase vortex gas flow is to identify changes in the static pressure along the radius of the mass-exchange chamber of the vortex apparatus. The solution to this problem is necessary for the quantitative determination of the static pressure in a cylindrical section with a radius of R_2. Knowledge of the law of pressure change along the radius of the vortex mass transfer chamber allows one to consider the forces acting on the liquid film near the end cap to estimate the intensity of end flows that adversely affect the operation of the apparatus.

In Figure 4.9, the experimental data obtained with the height of the vortex mass transfer chamber equal to 250 mm are shown.

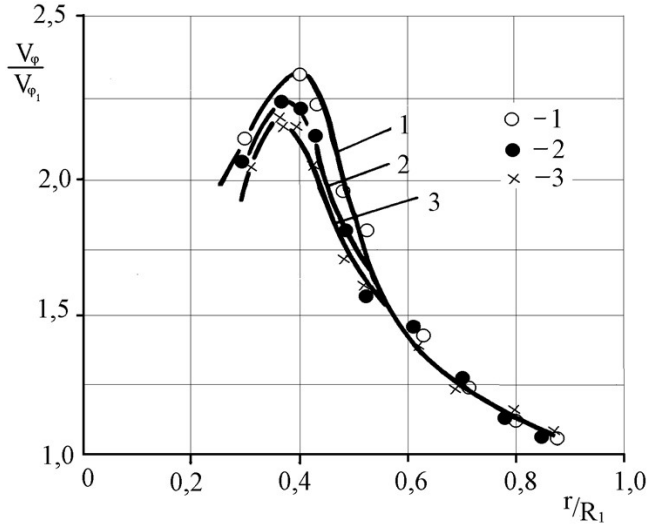

Figure 4.9 – Variation of the circumferential gas velocity along the apparatus height

The width of the inlet tangential slot was 40 mm, which, at a gas flow rate of 0.144 m^3/s, made it possible to obtain an inlet velocity V_{in} = 35.9 m/s. According to the results of measurements, the circumferential velocity at the cylindrical wall of the chamber turned out to be somewhat less ($V_{\varphi 1}$ = 32 m/s).

In general, the maximum circumferential velocities were located near a radius equal to the radius of the gas outlet opening.

In Figure 4.10, experimental data on the study of the presence of axial flows in the gas flow between cylindrical sections with radiuses R_1 and R_2.

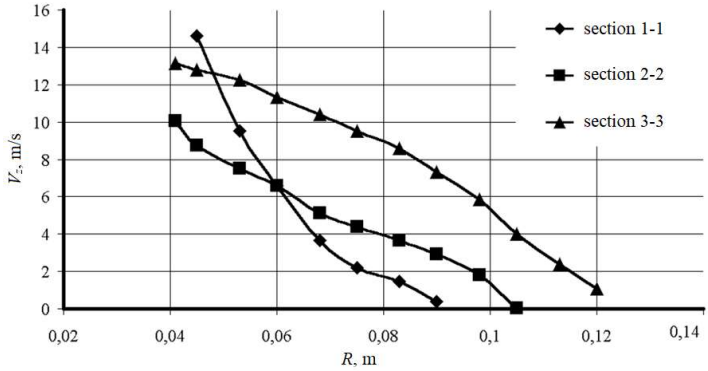

Figure 4.10 – Variation of the axial gas velocity along with the apparatus height

Cross-section 1-1 is near the bottom end cap, and cross-sections 2-2 and 3-3 are away from it.

Axial velocities in a gas with the vortex mass transfer chamber size of 150 mm were observed near the end cap already at a radius of 90 mm.

In section 3-3, which is more distant from the lower end cap than the height of the inlet tangential slot, axial velocities in the gas flow are already observed much closer to the wall of the mass transfer chamber in a cylindrical section with a radius of 120 mm.

Measurements of the vortex gas flow in a vortex mass transfer chamber with a height of 100 mm showed a significant change in the gas flow structure compared to the flow structure in a vortex chamber with a height of 250 mm. This difference mainly consists in the absence of axial velocities in the area limited by two cylindrical surfaces with radiuses R_1 and R_2. Axial velocities in the gas flow appear at r equal to $(1.2–1.5)R_2$.

Its magnitude is commensurate with the value of the axial or circumferential velocity in the branch pipe, which discharges

the gas flow, the axial velocity of the gas reaches only directly near the edge of the outlet pipe for gas removal.

In Figure 4.11, profiles of the relative circumferential velocities of the gas flow are given for various inlet gas velocities in tangential slots, which indicates the self-similarity of the velocity profiles in terms of flow and in countercurrent vortex atomizing mass transfer apparatuses.

After reaching a cylindrical section with a radius R_2 in the vortex mass-exchange chamber, the circumferential velocity of the gas begins to decrease to zero as it approaches the axis of the mass-exchange chamber. An example is the change in the absolute values of peripheral velocity in two different modes, given in Figure 4.12.

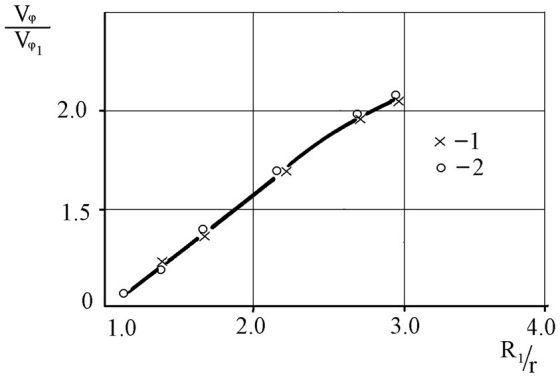

Figure 4.11 – Change in the relative circumferential velocity of the gas along the radius for different inlet velocities: 1 – V_{in} = 29.6 m/s; 2 – V_{in} = 49.9 m/s

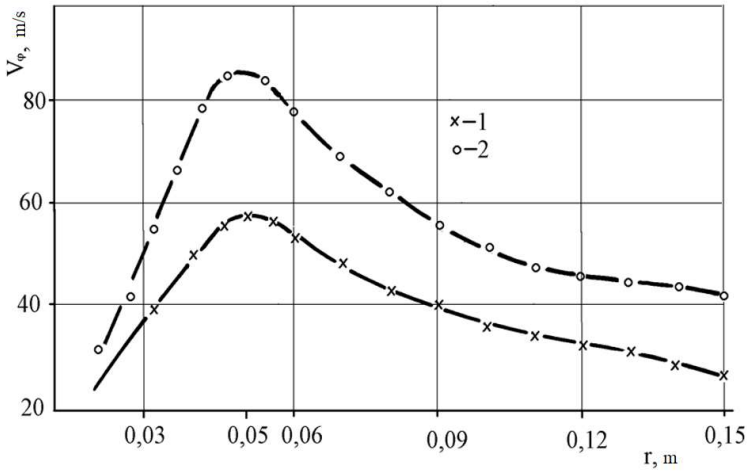

Figure 4.12 – Variation in peripheral velocity at different gas velocities at the inlet to the working chamber for different inlet velocities: 1 – V_{in} = 29.6 m/s; 2 – V_{in} = 49.9 m/s

Here can be seen the maximum circumferential gas velocity location near the radius r = 50 mm, which corresponds to the pipe pipe

Of practical interest is also the study of the effect of changing the width of the tangential slot on the hydrodynamics of the vortex chamber. It should be known to determine the value of $V_{\varphi 1}$.

In Figure 4.13, the change in relative velocity is shown for various tangential gaps for introducing a gas stream into a vortex mass transfer chamber.

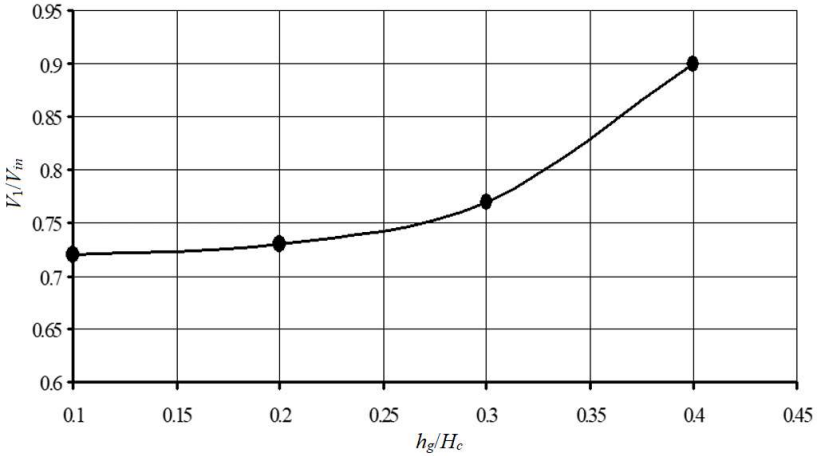

Figure 4.13 – Change in relative velocity at radius R_1 (experimental data and calculated values): h_g – tangential gap, m; H_c – channel height, m

The obtained points correspond to the empirical curve defined by the equation:

$$\frac{V_{\varphi_1}}{V_{in}} = 9.29\left(\frac{h_g}{H_c}\right)^4 + 0.47. \qquad (4.3)$$

In Figure 4.14, graphs of relative pressure change along the radius of the vortex mass transfer chamber are shown.

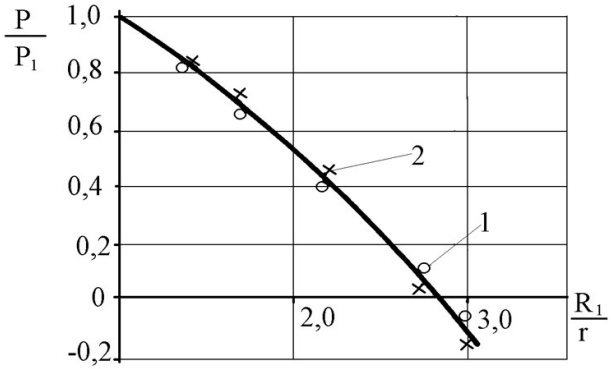

Figure 4.14 – Relative pressure change along the apparatus radius: 1 – V_{in} = 29.6 m/s; 2 – V_{in} = 49.9 m/s

These dependencies correspond to the above-presented circumferential velocities of the gas flow, i.e., the experimental data were obtained at inlet gas velocities V_{in} = 29.6 m/s (P_1 = 1.96 kPa), and V_{in} = 49.9 m/s (P_1 = 3.98 kPa).

The experimental studies carried out confirmed the absence of axial velocities in the gas flow, starting from the radius R1 to the diffuser neck. Axial velocities were noticed only at a radius equal to (1.0–1.2)R_2. Their value was of the same order of magnitude with the average axial velocity at the outlet of the vortex mass transfer chamber or with circumferential velocities, the same as in the vortex mass transfer apparatus, directly at the cylindrical section with radius R_2.

It was also fully confirmed the assumption that with a plane spiral motion of gas in the area between two cylindrical surfaces with radiuses R_1 and R_2, it is possible to create a gas flow uniform in the height of the vortex mass transfer chamber with the same circumferential velocities. Experimental data for one of the modes, confirming this assumption, are shown in Figure 4.15.

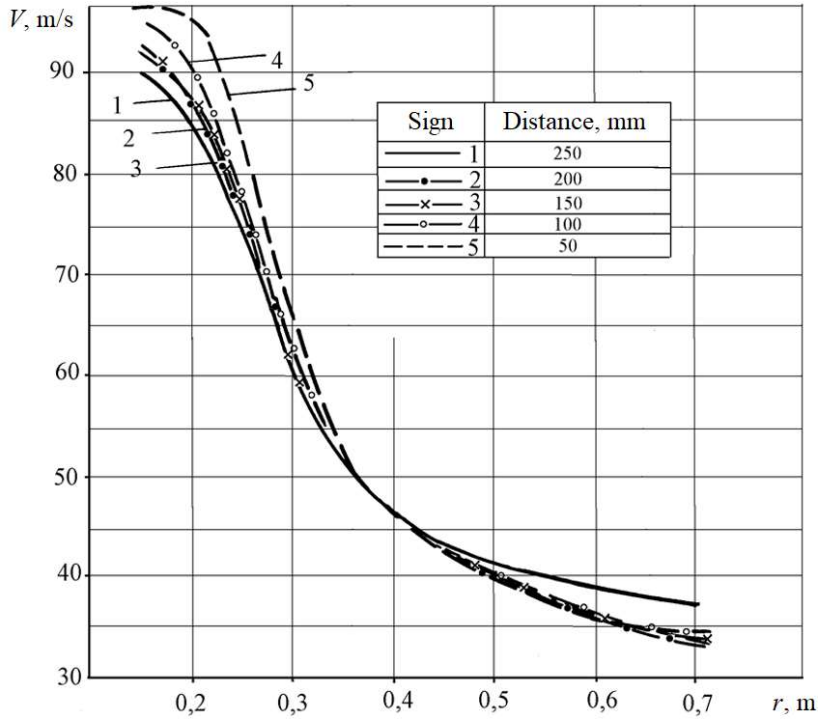

Figure 4.15 – Change in peripheral gas velocity at different heights *Z*, m

The velocities (Figure 4.16) and pressures (Figure 4.17) for Stand 2 are similar to the results obtained for the vortex mass transfer chamber of Stand 1.

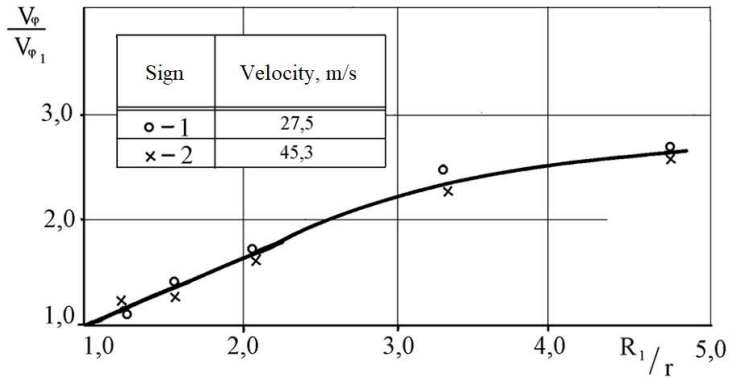

Figure 4.16 – Change in relative circumferential velocity for different inlet velocities: 1 – V_{in} = 29.6 m/s; 2 – V_{in} = 49.9 m/s

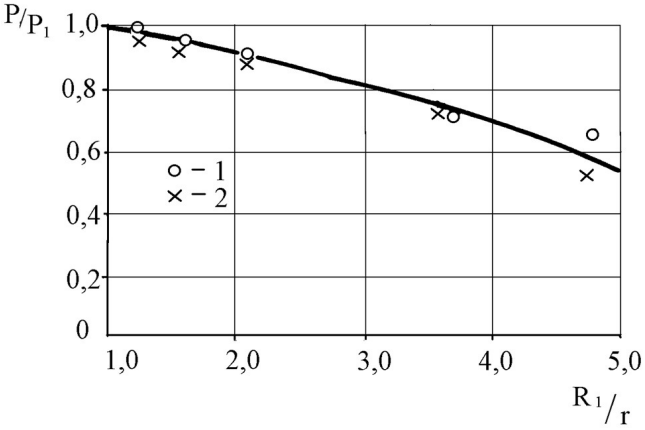

Figure 4.17 – Relative pressure change for different inlet velocities: 1 – V_{in} = 29.6 m/s; 2 – V_{in} = 49.9 m/s

However, the difference is as follows. The magnitude of the pressure droplet and the increase in the circumferential velocity in a flat gas flow near the diffuser neck is more significant since the vortex mass transfer chambers of both

stands differ significantly in geometric dimensions, as well as their ratios.

Ratio change $V_{\varphi 1}/V_{in}$ reduces depending on the change in inlet velocity. For example, $V_{\varphi 1}/V_{in} = 0.80$ for $V_{in} = 27.5$ m/s, and $V_{\varphi 1}/V_{in} = 0.73$ for $V_{in} = 45.3$ m/s.

In general, in changing the slot width from 5 mm to 15 mm, the ratio h/H_c changed from 0.017 to 0.050.

To estimate the droplet in the velocity at the exit from the tangential slots of the gas flow supply to the vortex mass transfer chamber, we can assume $V_{\varphi 1} = (0.72–0.80)V_{in}$.

Remarkably, when calculating the value of P_2 and the change in pressure along the radius of the vortex mass transfer chamber according to theoretical dependencies (3.32), it is necessary to set the quantity value as the boundary condition P_1. Notably, according to Figure 4.17, $P_1 = 10.33$ kPa for $V_{in} = 27.5$ m/s, and $P_1 = 13.29$ kPa for $V_{in} = 45.3$ m/s.

The pressure in the annular chamber, which supplies the gas evenly to the tangential slots located on the vortex mass transfer chamber's cylindrical wall, corresponds to the gas flow's total energy since the gas velocity is practically equal to 0. There is a relationship between the values of P_{in} and P_1:

$$P_{in} = \frac{\rho_g V_{\varphi_1}^2}{2} + P_1 + \Delta P_{in}, \qquad (4.4)$$

where ΔP_{in} – inlet pressure difference, Pa.

In turn, the value of $V_{\varphi 1}$ depends on velocity V_{in}, tangential gap h, and design of gaps.

In the series of carried out experiments, with a change h/H_c within the above limits, the value P_1/P_{in} was changed in the range of 0.72–0.81. Notably, smaller values of this ratio correspond to gas velocities in slots above 40 m/s and greater – for gas velocities less than 25 m/s.

4.4 Two-phase flow

The whole set of problems solved in the study of a two-phase flow in the working chamber of the vortex apparatus can be divided into several separate tasks, depending on the method used to study the flows. When studying a two-phase flow, visual studies are used, flow probing with a probe with a constant purge, the change in apparatus pressure, and the value of spray entrainment are studied depending on the ratio of phase loads.

In particular, visual observations were carried out in vortex apparatuses in Stands 1–2, which have a transparent body and observation windows. Pulsations and unstable device operation when probing a two-phase flow do not make it possible to carry out accurate quantitative measurements. Therefore, the task is usually set to show a qualitative change in the velocity field in a two-phase flow concerning the motion of a single-phase flow. Flow probing was carried out in Stand 1.

This chapter presents the influence of the ratio of loads by phases on the amount of spray carryover. These studies were carried out mainly in Stands 1, 3 since their design turned out to be more successful in organizing liquid drainage.

Firstly, let us consider the process of liquid spraying, characteristic of the operation of a countercurrent vortex mass transfer apparatus when jets are supplied in the central part. For this purpose, an atomizer with one hole was installed in the vortex mass-exchange chamber of Stand 1, from which the liquid flowed into the gas flow in the radial direction. After that, the atomizer moved along the axis, which led to the displacement of the hole and liquid jets and the height of the vortex mass transfer chamber. Sputtering took place at a distance of $(0.8–1.0)R_2$ from the chamber's center. Simultaneously, there was a sharp change in fluid direction from radial to circumferential (Figure 4.18).

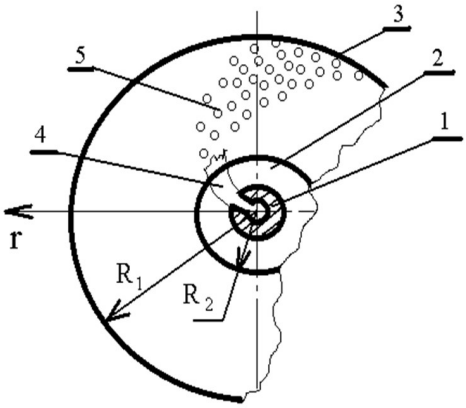

Figure 4.18 – Scheme of disintegration of the liquid jet:
1 – atomizer; 2 – gas outlet pipe; 3 – cylindrical wall;
4 – continuous jet of liquid; 5 – liquid droplets

When the sprayed jet was located near the lower end cap, a more active separation of droplets was observed on the cylindrical wall of the vortex mass transfer chamber near this end cap, but practically the entire wall was irrigated.

When the liquid jet was located at half the height of the vortex mass transfer chamber, irrigation of almost the entire surface of the cylindrical body was observed. The irrigation intensity of this surface near the end caps is approximately the same. It increases when approaching the plane in which the jet was injected.

After the jet breaks up into droplets, a rearrangement occurs in the two-phase flow structure. The liquid in axial motion tends to uniform distribution over the working volume of the vortex mass transfer chamber. This is an essential positive feature of the countercurrent vortex motion of a two-phase gas-droplet flow in the apparatus and confirms the possibility of carrying out the theoretical calculations described above, based on the assumptions of a uniform structure of a two-phase gas-

droplet flow along with the height of the vortex mass transfer chamber.

When the atomizer is located in the central region and liquid is introduced into the gas flow near the gas flow outlet in the end cap, the probability of increased spray entrainment increases sharply. This is especially true when spraying at a distance closer than $H_c/3$ from this end cap, which is associated with the presence in this zone of an axial gas flow with high axial velocities.

The flow rate of the airflow in Stand 2 is varied from 0.56 m^3/s to 1.11 m^3/s. The volumetric flow rate of liquid (water) varied from 0 to $2.5 \cdot 10^{-3}$ m^3/s. The ratio of loads in the liquid and gas phases was regulated by changing the amount of liquid supplied during the experiment.

As a result of visual observations, a two-phase flow was studied in the vortex mass-exchange chamber of the counter-current apparatus. The flow pattern is as follows.

At a constant airflow, the load ratio by phases varies from 0 to 3. As the liquid load increases, four intervals can be conventionally distinguished. The flow of a two-phase gas-droplet flow has its own characteristic features.

As the load on the liquid increases from 0 to 0.7, in the central zone of the vortex mass transfer chamber, a spray of liquid is observed almost at the outlet of the atomizer. After that, the droplets are entrained by the airflow into rotational motion. The blades that make up the cylindrical body of the vortex mass transfer chamber are covered with a thin liquid film. This film is entrained by the gas flow, parallel to the end caps, into the slots for liquid removal, located along with the entire height on each of the blades. The thickness of the liquid film along the height of the blades is approximately the same. The resistance of the vortex apparatus is considerable. The first signs of the end effect appear, expressed in the movement of droplets along with the

end cover to the center of the working chamber. On the lower cover of the vortex mass-transfer chamber, the end effect is more affected. Here, a jet spiral liquid flow from the blades to the center is formed.

In the next phase, load-interval from 0.7 to 1.5, a jet flow of liquid appears from the nozzles of the spraying device. In this case, the jet length reaches (0.12–0.40)R_2. The resistance of the device is noticeably reduced. The change in the spray pattern, the movement of droplets, and the droplet in resistance of the vortex spray countercurrent mass transfer apparatus indicate a decrease in the gas flow velocities in the working chamber in the spray zone. The liquid film, which moves under the action of the gas flow along with the blades of the cylindrical surface of the vortex mass transfer chamber, thickens towards the bottom. A noticeable water ring appears at the base of the blades on the lower end cap.

With a further increase in phase loads up to 2.5, there is an elongation of the liquid jets flowing from the spray device. The shape of the jets changes somewhat. A straight section appears at the nozzle outlets. In front of the entire spray zone, there is a sharp bend in the jet. The liquid film that moves along the blades partially slips over the slots to drain the liquid. Near the lower edge of the shoulder blades, the water ring increases significantly in size. The resistance of the vortex mass transfer chamber continues to decrease. The flow of liquid along with the lower end cap increases has a spiral character, but a decrease in the twist of the gas flow is noticeable. Wide jets appear on the upper-end cap, but the amount of liquid that moves along it towards the center is much less than the liquid that moves along the lower-end cap.

An increase in the phase load ratio up to 3 leads to a further droplet in the resistance of the vortex apparatus, which is a consequence of a decrease in the circumferential velocities of

the gas flow. In this case, the conditions for spraying the liquid into droplets deteriorate significantly. The liquid film flow along with the blades to the bottom is noticeable. The water ring near the blades on the lower end cap grows upward. The formation of spiral ridges is noticeable along with the lower end cap.

Thus, the third interval is already unfavorable from the point of view of creating a regular countercurrent movement of the gas flow and liquid microdroplets throughout the entire volume of the working chamber. Untimely removal of liquid leads to its concentration in the lower part, the appearance of the annular flow described above. This liquid flow intensively feeds the film on the lower end cap with liquid. As a result, the liquid entrainment along the end of the working chamber increases.

During studies, Stands 1–3 were installed so that the gas outlet hole was located in the upper-end cap. This prevented the liquid film from flowing down to this end cap from the cylindrical wall of the vortex mass transfer chamber.

The relative spray drift is defined as follows:

$$\delta_L = \frac{\Delta L}{L_{in}}, \tag{4.5}$$

where ΔL is determined by (4.2).

The graphical dependence of δL on the loads by phases and the change in the inlet velocity in the tangential input slots are given in Figure 4.19.

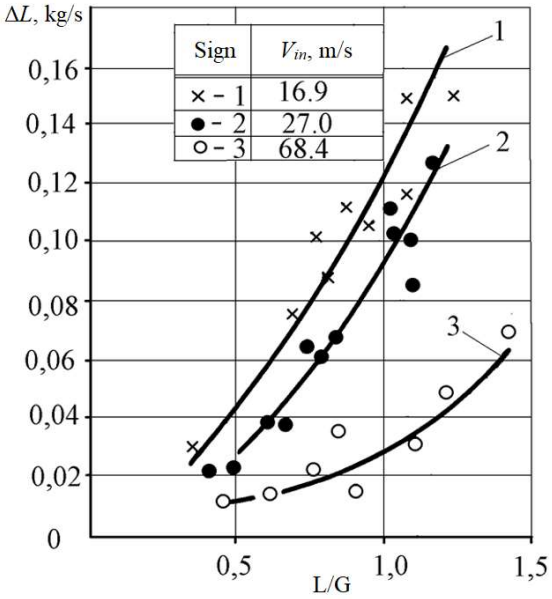

Figure 4.19 – Change in the relative value of spray entrainment from loads by phases at different inlet velocities: 1 – V_{in} = 16.9 m/s; 2 – V_{in} = 27.0 m/s; 3 – V_{in} = 68.4 m/s

In Stand 3, in a vortex mass transfer apparatus, in the range of loads for the liquid and gas phases from 0.3 to 1.5 and a change in the input gas flow velocity from 16.9 m/s to 68.4 m/s, spray entrainment, the relative value of which reaches 10 %, is observed at input gas velocities in tangential crevices less than 27 m/s. As these velocities increase, spray entrainment decreases, and at gas flow velocities in the inlet tangential slots Vin = 68.4 m/s – it does not exceed 7 % even if the load ratio is more significant than 1.0.

In Figure 4.20, the results of studying the change in the circumferential velocity of the gas flow in the mass transfer chamber in Stand 1 for the case of increased phase load ratios on

the radius of the vortex mass transfer chamber of 0.55 m are shown. The values are given concerning the peripheral velocity in this section in the absence of a liquid phase.

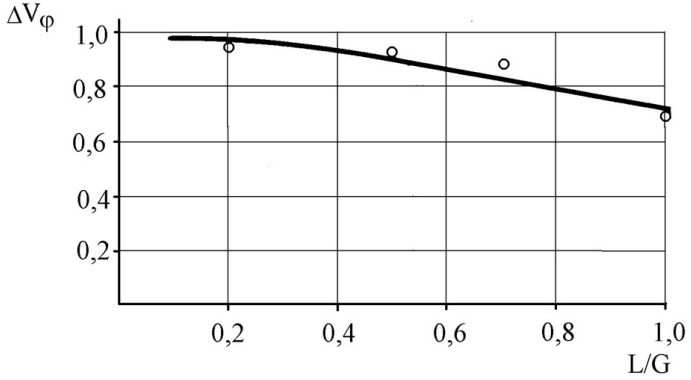

Figure 4.20 – Change in the relative circumferential gas velocity

The data indicate the presence of a droplet in the velocities, which confirms the theoretical conclusions presented in the previous chapter.

Thus, experimental studies of a two-phase vortex gas-droplet flow made it possible to get an idea about the features of the physical processes that occur in the vortex chamber of the vortex apparatus. These are the spraying of liquid into droplets in the central region of the vortex mass transfer chamber, the involvement of liquid droplets in rotational motion, and the movement of droplets from the center to the periphery of the vortex chamber under the action of centrifugal forces, the formation of liquid film flows on the cylindrical surface of the sidewall and along with the end caps, the effect of the load ratio on phases to reduce the circumferential velocities of the gas in the working chamber.

The information obtained allows us to correctly approach the development of the design of those elements of the vortex spraying countercurrent mass transfer apparatus that provide the supply and removal of the gas flow, the supply, spraying, and removal of liquid, and prevent the appearance of such undesirable phenomena as end flows.

For example, the implementation of the removal of the gas flow in the upper-end cap allows you to reduce spray entrainment because the liquid film that flows from the cylindrical walls to the lower end cap will not feed the end flow on the upper-end cap, and the amount of liquid that is carried away by the gas stream from the apparatus from this end cap, will droplet. Many other design solutions improve the operation of the vortex countercurrent mass transfer apparatus. They are described in the following sections.

4.5 Hydraulic resistance of the apparatus

4.5.1 Hydraulic resistance under the absence of a liquid phase

The conducted experimental and theoretical studies of vortex flows of gas and liquid droplets show the following. In the absence of any structural elements in the vortex mass transfer chamber like rotating atomizers or additional blades that change the direction of the gas flow, its hydrodynamic characteristics, i.e., hydraulic resistance, depends on the ratio of the main geometric dimensions, the gas velocity in the inlet tangential slots, and the ratio of loads in phases.

The hydrodynamics of the apparatus is determined by the motion of a single-phase gas flow. Therefore, the hydraulic resistance of the vortex mass transfer apparatus when working with two-phase media is determined by the hydrodynamic

resistance of the "dry" apparatus, that is, a vortex mass transfer apparatus in the absence of a liquid phase supply. The value of hydraulic resistance varies according to the load on the liquid phase. These facts are due to the changes in the structure and magnitude of velocities and the involvement of droplets in rotational motion.

For Stand 1, the change in the relative energy loss in the gas flow with a change in the inlet velocity of the gas flow at the inlet to the mass transfer chamber in the tangential slots of the vortex apparatus is shown in Figure 4.21.

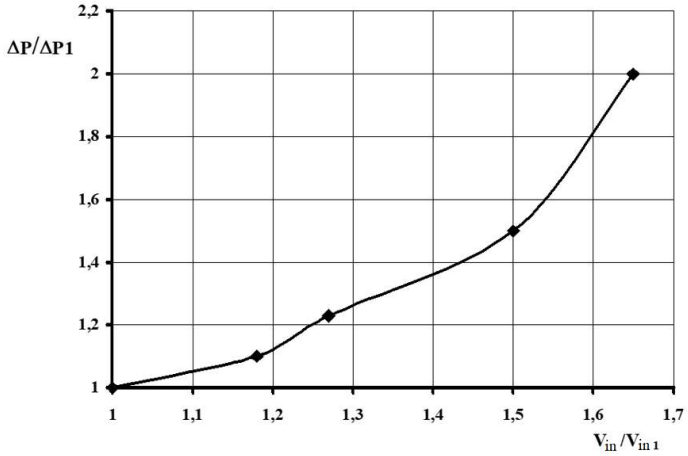

Figure 4.21 – Change in relative energy losses in Stand 1 with chamber diameter of 300 mm (inlet pressure P_{in} = 1.96 kPa; inlet velocity V_{in} = 29.6 m/s)

Here, the total pressure droplet determining the energy loss in the vortex spray countercurrent mass transfer apparatus was determined by as follows:

$$\Delta P = P_{in} - P_3, \tag{4.6}$$

where P_3 – pressure in annular chamber after the radial diffuser, Pa; P_{in} – total energy at inlet and total energy:

$$P_{in} = P_{st} + \frac{\rho_g V_{in}^2}{2}; \quad (4.7)$$

where P_{st} – static pressure, Pa.

Further, the minimum inlet velocity mode is taken as a reference point, and the following notations are introduced: ΔP_1 – pressure loss, Pa; V_{in1} – inlet velocity, m/s. Therefore, it is possible to determine the change in the drag coefficient ζ when changing flow regimes, where ζ_1 corresponds to the parameters ΔP_1 and V_{in1}.

In Figure 4.22, experimental data on the study of energy losses in a vortex countercurrent apparatus are given for Stand 2.

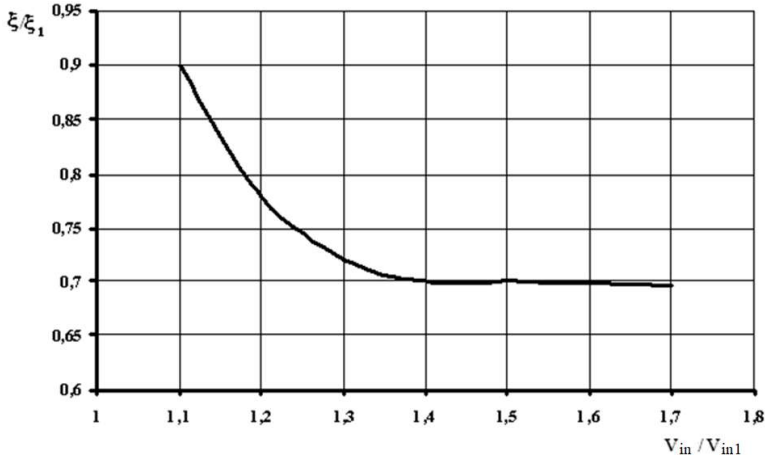

Figure 4.22 – Change in relative energy losses in Stand 2 with chamber diameter of 1430 mm (inlet pressure P_{in} = 3.95 kPa; inlet velocity 17.7 m/s)

In this case, the pressure difference was measured between the inlet chamber. Through it, the gas flow is supplied to the tangential slots and the annular region at the outlet of the radial diffuser.

A general increase in the hydraulic resistance ζ of the apparatus somewhat decreases, but the intensity of this decrease is several times less than the increase in gas velocity in the inlet tangential slots.

The ratio of drag coefficients is:

$$\frac{\zeta}{\zeta_1} = \frac{\Delta P}{\Delta P_1}\left(\frac{V_{in_1}}{V_{in}}\right)^2. \qquad (4.8)$$

The corresponding values of the drag coefficient in Stands 1–2 are summarized in Figures 4.23–4.24, respectively.

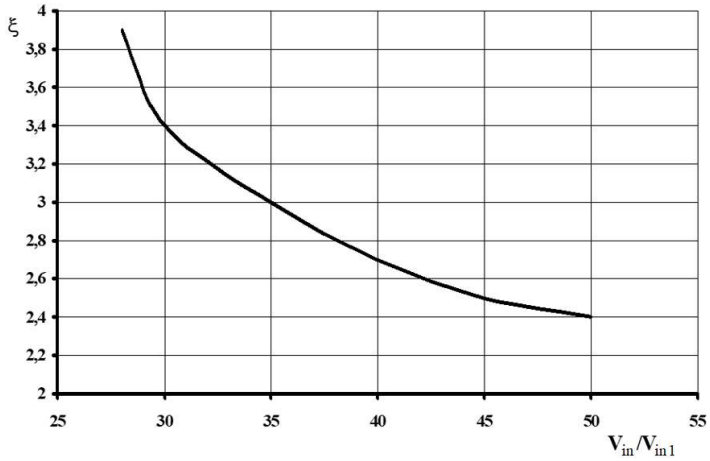

Figure 4.23 – Change in the coefficient of hydraulic resistance of the vortex apparatus in Stand 1

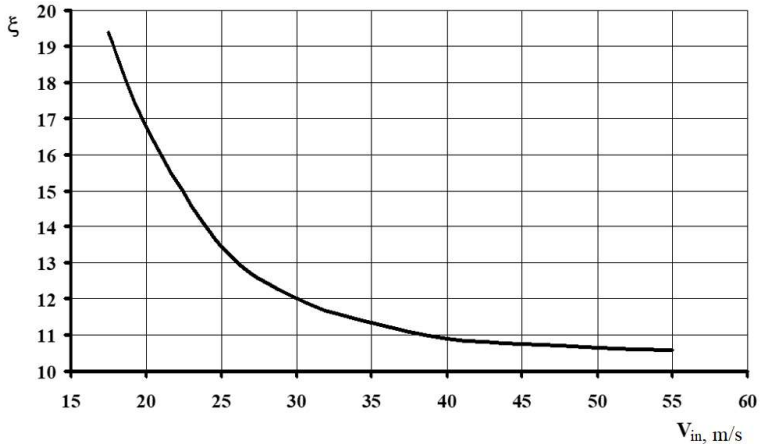

Figure 4.24 – Change in the coefficient of hydraulic resistance of the vortex apparatus in Stand 2

Remarkably, one stage of the vortex countercurrent mass transfer apparatus consists of two elements, which are the mass transfer chamber and the diffuser. These elements react differently to increases in gas velocity. It is essential to coordinate the operation of the vortex mass transfer chamber and the radial diffuser so that in the design mode, the gas flow passes through the mass transfer chamber and the radial diffuser with minimal energy losses in both elements.

Due to the hydrodynamic features in the vortex chamber of a countercurrent apparatus, it is necessary to calculate the diffuser and determine its geometry. The following chapter is devoted to studying the separation of energy losses in the mass-exchange chamber from the total balance of losses.

4.5.2 Distribution of energy losses in a vortex chamber and a radial diffuser

In studying energy losses during the gas movement in a radial diffuser after the apparatus, the property of a rotating flow to influence a lattice of plates was used. The last one is installed in the direction of the circumferential gas velocities at the entrance is directed normally to the plates' surface.

When passing through the channels formed by the "turntable" plates, the gas flow velocities change their direction and magnitude while influencing the grating itself in the circumferential direction. The density and width of the plates are chosen such that the gas flow at the exit from this grate has practically no circumferential velocity, which is a component of the total velocity of the gas flow.

By balancing the "turntable", that is, by applying a force opposite to the force from the gas flow and equal in magnitude to the moment from the gas flow, it is possible to determine the hydrodynamic parameters of the flow.

The scheme for measuring the angular momentum of the gas flow behind the vortex mass transfer chamber is shown in Figure 4.25.

Change in kinetic moment K_g, kg·m^2/s^2, when passing gas through a grid installed between the working chamber and the radial diffuser, is as follows:

$$\frac{dK_g}{dt} = \left[\left(rV_\varphi\right)_{av} - \left(rV_\varphi\right)_d\right]\dot{m}, \tag{4.9}$$

where t – time, s; r – radius, m; V_φ – angular velocity, m/s; "av" – average sign; "d" – derivative sign; $\dot{m}$ – mass flow, kg/s.

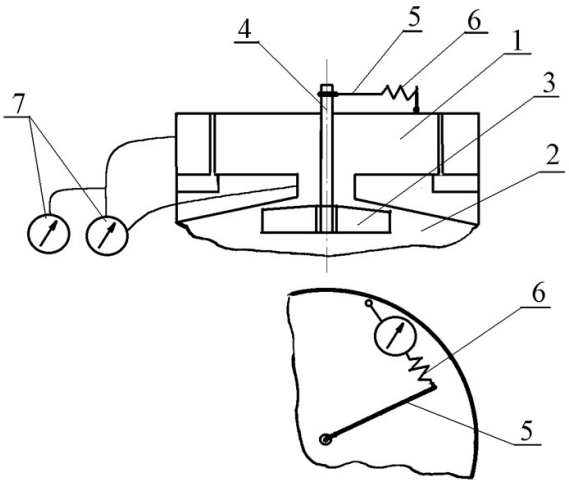

Figure 4.25 – Scheme of changing the kinetic moment of the gas behind the mass transfer chamber: 1 – mass transfer chamber; 2 – diffuser; 3 – turntable; 4 – axis; 5 – lever; 6 – dynamometer; 7 - manometers

Given the large density of the grating, that is, the ratio of the length of the channels to the pitch, sufficient for the complete unwinding of the gas flow and its exit in the radial direction, we can assume $(rV_\varphi)_d = 0$. Therefore, the last expression can be simplified as follows:

$$K_g = \rho_g Q_g r_{av} V_{\varphi_{av}}, \tag{4.10}$$

where ρ_g – gas density, kg/m^3; Q_g – gas flow rate, m^3/s; r_{av} – average radius, m; $V_{\varphi_{av}}$ – average velocity, m/s.

The moment from the force of the vortex gas flow, N·m:

$$M_F = F_g l_F, \tag{4.11}$$

where F_g – gas-dynamic force, N; l_F – lever length, m.

Due to the fundamental equation of rotational motion

$$\frac{dK_g}{dt} = M_F, \tag{4.12}$$

and considering expressions (4.10) and (4.11), the average velocity can be determined from the last equation:

$$V_{\varphi_{av}} = \frac{F_g l_F}{\rho_g Q_g r_{av}}. \tag{4.13}$$

Based on a linear law of change in the circumferential velocity of the gas flow from the radius of the branch pipe R_2 to the radius of a bushing R_b, on which the lattice plates are fixed, and the uniform distribution of the axial velocity of the gas flow over the cross-section of the branch pipe discharging the gas flow, we can obtain expressions for determining the average radius from the equality of the annular cross-sectional areas:

$$r_{av} = \sqrt{\frac{R_2^2 + R_b^2}{2}} \tag{4.14}$$

and average axial velocity, m/s:

$$V_{z_{av}} = \frac{Q_g}{\pi\left(R_2^2 + R_b^2\right)}. \tag{4.15}$$

Then the total pressure of the gas flow at the outlet of the vortex mass transfer chamber, Pa:

$$P_2 = P_{st_2} + \frac{\rho_g V_{av}^2}{2}, \tag{4.16}$$

where the average velocity is as follows:

$$V_{av} = \sqrt{V_{\varphi_{av}}^2 + V_{z_{av}}^2}\,. \qquad (4.17)$$

According to the known readings of the dynamometer and the length of the lever, which is constant during the experiments, it is possible to determine the total moment of impact from the vortex gas flow. The pressure value in the gas flow, which passes the neck of the radial diffuser, was measured by taking pressure from the wall of the branch pipe at the outlet of the vortex mass transfer chamber.

The change in the value of hydraulic losses in the vortex mass transfer chamber concerning the energy losses in the stage is shown in the form of a graphical dependence in Figure 4.26.

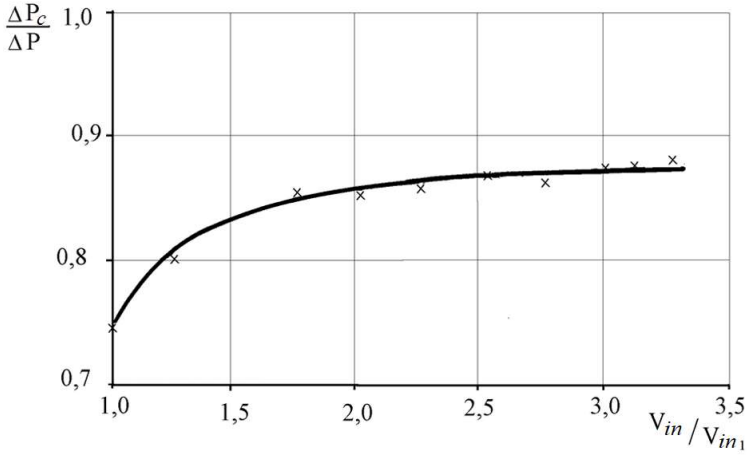

Figure 4.26 – Change in the relative value of hydraulic energy losses depending on the operating mode of the apparatus (V_{in1} = 17.7 m/s)

By analyzing the results obtained, certain conclusions can be formulated. Firstly, at low gas velocities in the inlet tangential

slots of the vortex mass transfer chamber and, consequently, low circumferential velocities of the gas flow at the inlet to the radial diffuser, part of the hydraulic energy losses in the radial diffuser is significant.

Secondly, as the circumferential velocities of the gas flow in the chamber increase, the role of the diffuse element increases, which is reflected in a decrease in the relative energy losses in the radial diffuser a decrease in the hydraulic resistance coefficient.

Thus, when operating with small peripheral gas velocities in the working chamber, it is possible to use a structural scheme without a radial diffuser.

Finally, the presence of high circumferential velocities of the gas flow in the mass-exchange chamber of the apparatus leads to the need to install a radial diffuser behind the working chamber. This makes it possible to reduce the intensity of the increase in energy losses with an increase in gas velocities in the vortex chamber, to increase the efficiency of the mass transfer apparatus as a whole.

4.5.3 Change in hydraulic resistance depending on phase loads

The theoretical studies of a two-phase gas-droplet flow with vortex countercurrent motion of liquid and gas droplets have shown that in the absence of any blades or rotating elements, the involvement of droplets in the rotational movement around the axis occurs due to the energy of the vortex gas flow.

In this case, the involvement of droplets of the sprayed liquid in rotational motion is accompanied by a decrease in peripheral velocity, which is a component of the total velocity of the gas flow. The magnitude of this influence, that is, the reduction of the tangential (circumferential) gas velocity, is proportional to the ratio of the phase loads.

On the one hand, reducing the circumferential velocities of the gas flow around the axis of the mass transfer chamber of the vortex spraying countercurrent mass transfer apparatus is a positive moment, as it also leads to a decrease in energy losses in the vortex chamber of the apparatus, the value of which is proportional to the square of the circumferential gas velocity at the outlet of the mass transfer chamber.

On the other hand, the drop in circumferential velocities of the gas may adversely affect the stable operation of the vortex spray countercurrent mass transfer apparatus for the following reasons.

Firstly, the gas flow velocities must be sufficient to entrain the liquid droplets in a rotating motion at the droplet velocities necessary to create a centrifugal force field that entrains the droplets in a countercurrent movement of the gas in a radial direction, from the center to the periphery. Otherwise, conditions may arise to disrupt the operation of the vortex countercurrent apparatus, which is expressed in the movement of droplets together with the gas flow to the exit from the mass transfer chamber, in an increase in spray entrainment.

Secondly, the interfacial surface depends on the dispersity of the droplets of the sprayed liquid. The size of droplets depends on the velocity of the gas flow in the spray zone. Reducing this gas velocity to a particular value can decrease the interfacial surface and the efficiency of mass transfer processes in the vortex chamber. In addition, droplets of a larger diameter will be less involved in rotational motion, which can also lead to an increase in spray entrainment due to a decrease in the magnitude of centrifugal forces acting on these droplets and reduce the efficiency of mass transfer.

Finally, one of the conditions for intensifying mass transfer processes in the working chamber of a vortex spraying countercurrent mass transfer apparatus is the presence of a gradient of circumferential gas velocities along the radius of the vortex chamber. Theoretical calculations show, the greater the value of this gradient, the more intense the circulation of liquid in droplets and the renewal of the interfacial surface, which affects the rate of mass transfer processes.

Therefore, the study of the hydraulic resistance depending on the phase loads makes it possible to obtain information for energy calculations, the choice of auxiliary equipment, and the analysis of the economic necessity of using the apparatus. Moreover, it also provides information on reducing peripheral gas velocities in the mass transfer chamber and on possible limits of loads in the liquid phase, under which it is necessary to operate the apparatus.

The study of the change in the hydraulic resistance of a vortex countercurrent spraying apparatus was carried out in Stands 2–3.

In Stand 2, measurements in the vortex apparatus were carried out by studying the change in the pressure difference between the chamber supplying the gas flow and the cavity at the outlet of the radial diffuser.

The change in the ratio of loads in phases was achieved by changing the amount of liquid supplied by the pump to the atomizer. The gas flow rate varied from 0.50 m^3/s to 1.11 m^3/s. The load range for the liquid supplied to the apparatus ranged from $1.6 \cdot 10^{-4}$ m^3/s to $2.1 \cdot 10^{-3}$ m^3/s.

The obtained experimental data on the change in hydraulic resistance depending on the ratio of loads in phases for five different values of gas velocity in the inlet tangential slots are shown in Figure 4.27.

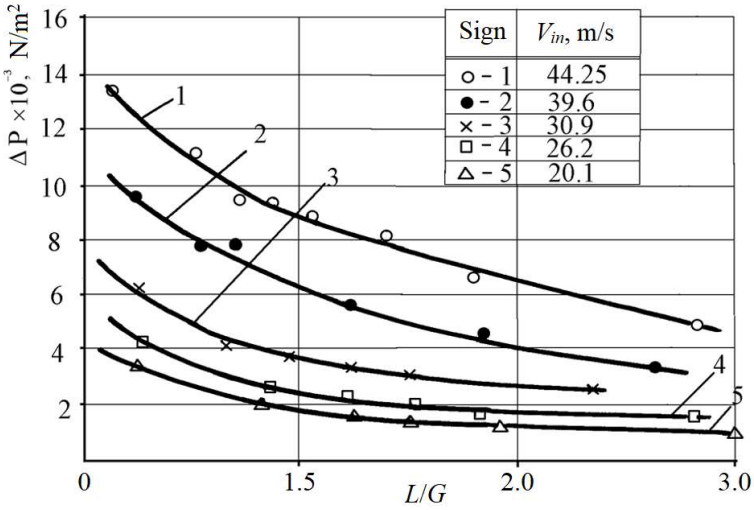

Figure 4.27 – Change in the hydraulic resistance of the apparatus depending on the phase loads

Maximum resistance of a "dry" vortex spraying countercurrent mass transfer apparatus, in the absence of a liquid phase and gas velocity in tangential slots V_{in} = 44.2 m/s is equal to 14.1 kPa. At a gas velocity in tangential slots V_{in} = 20.1 m/s, the resistance of the "dry" vortex countercurrent apparatus equals 4.1 kPa.

During the experiments, the vortex apparatus of Stand 3 (chamber diameter of 600 mm) has been included in the design scheme of Stand 1.

The change in the gas velocity in the inlet tangential slots was achieved by changing the width of these slots. The flow rate of the gas that passes through the vortex apparatus ranged from 0.16 m^3/s to 0.2 m^3/s. The range of fluid loads was within from $8.0 \cdot 10^{-5}$ m^3/s to $3.3 \cdot 10^{-4}$ m^3/s.

Graphical dependencies for the change in the hydraulic resistance of the vortex apparatus on the ratio of loads by phases are shown in Figure 4.28.

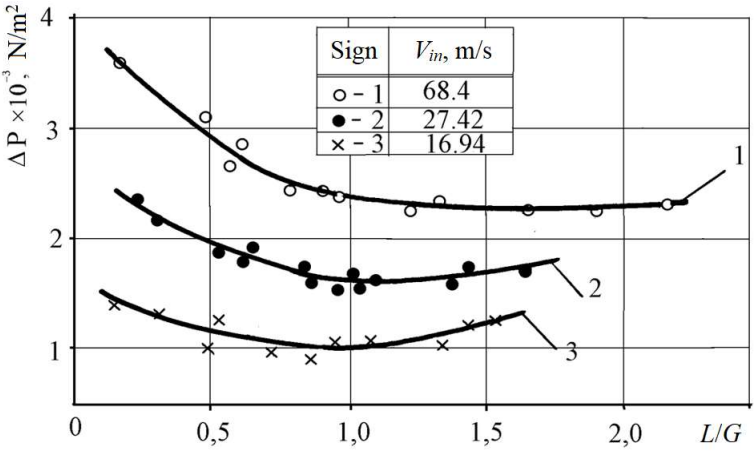

Figure 4.28 – Change in the hydraulic resistance of the apparatus depending on the phase loads

The resistance of the vortex apparatus in the absence of a liquid phase and the gas velocity in the tangential slots is equal to 4.0 kPa for inlet velocity V_{in} = 68.4 m/s, and 1.6 kPa – for inlet velocity V_{in} = 16.9 m/s. When changing the gas velocity in

the inlet tangential slots, the hydraulic resistance of the "dry" vortex apparatus did not exceed the indicated limits.

Considering the obtained graphic dependencies, one can note many essential features that characterize the operation of the apparatus. Firstly, an increase in the ratio of loads in phases leads to a decrease in the hydraulic resistance of the apparatus. Secondly, the decrease in hydraulic resistance is associated with a decrease in gas flow rates.

Finally, a further increase in the device's resistance speaks of the energy costs for transporting the liquid. It indicates the entrainment of droplets in a co-current movement with gas.

The latter phenomenon in a countercurrent vortex apparatus is highly undesirable. At low gas velocities, a weak field of circumferential velocities is also formed in the inlet tangential slots, which creates unfavorable conditions for the regular countercurrent movement of vortex gas and droplet flows.

For example, at the velocity in the tangential slots of about 16.9 m/s, the vortex spraying countercurrent mass transfer apparatus operates in the countercurrent mode as the phase loads increase up to their ratio equal to 0.9. A further increase in the load ratio leads to the appearance of increased spray entrainment, leading to a breakdown in the operation of the apparatus.

An increase in the gas velocity in the inlet tangential slots leads to an improvement in the operating conditions of the apparatus.

At the velocity of 24.4 m/s, the operation range of the apparatus in countercurrent mode moves to the right and reaches a phase load ratio of 1.1.

At a gas velocity in the inlet tangential slots of the mass transfer chamber of 68.4 m/s, the load ratio shifts even more to the right side and reaches a value of 1.7.

The stated conclusions are well confirmed by the experimental dependencies shown in Figure 4.19. There is a pronounced tendency to reduce spray entrainment and improve the operation of the apparatus in the counterflow mode with an increase in the peripheral gas velocities in the mass transfer chamber.

In addition to increasing gas velocities in the inlet tangential slots, an increase in the radial dimensions of the mass transfer chamber R_1 is essential for creating a field of circumferential velocities in the gas flow, organizing a regular counterflow in the mass transfer chamber. An increase in this radius from 0.300 m (Stand 3) to 0.715 m (Stand 2) made it possible to create a stable countercurrent phase motion at V_{in} = 20.1 m/s.

In Stand 2, with an increase in the gas velocity in the inlet tangential slots up to 44.3 m/s, a continuous decrease in the hydraulic resistance of the apparatus is observed throughout the entire range of changes in the phase load ratio (Figure 4.27). This fact indicates a decrease in peripheral gas velocities in the mass transfer chamber.

4.6 Analysis of the experimental results on hydrodynamics

The theoretical dependencies presented in the second and third sections of this work and a number of experimental data on the study of the vortex countercurrent motion of a gas-droplet flow in vortex spraying countercurrent mass transfer apparatuses make it possible to analyze and compare the calculated and experimental data on the circumferential and radial velocity of the gas flow along the radius of the vortex mass transfer chamber, and as well as pressure distribution along the radius.

One of the determining factors in the organization of countercurrent vortex motion of gas and liquid droplets in the mass-exchange chamber of the apparatus is the introduction of gas. Vortex contact stages and vortex mass transfer apparatuses with cross-phase current, it can be concluded that it is necessary to implement a tangential (in the circumferential direction) introduction of the gas flow through a number of slots located along with the entire height of the cylindrical body of the vortex mass transfer chamber.

In this case, with an appropriate ratio of the height, radius of the vortex mass-exchange chamber, and the radius of the pipe for removing gas from the mass-exchange chamber, it is possible to achieve a field of circumferential velocities uniform along with the height of the working chamber of the vortex mass-exchange apparatus. Then the intensity of the flow twist does not fall along with the height of the vortex mass transfer chamber. That is, in any cylindrical section, starting from the slots of the tangential input of the gas flow, at the periphery of the mass transfer chamber, and towards its central region, where the gas flow is removed, a field of gas velocities uniform along the height of the vortex chamber is achieved in the absence of axial flow.

The introduction of gas through a series of tangential slots along the entire height of the mass transfer chamber creates all the conditions for a countercurrent vortex motion of the gas, and liquid phases uniform along with the height of the working chamber, equalization of the mass transfer rates over the volume of the apparatus, which generally leads to a significant improvement in its operation. When calculating the gas flow parameters at the outlet of the tangential slots, it is advisable to use the dependence $V_{\varphi 1} = (0.7–0.9)V_{in}$. The value of the input gas velocity in the slots is defined as:

$$V_{in} = \frac{Q_g}{hH_cN_h}, \quad (4.18)$$

where N_h – the total number of gaps.

Experimental studies of various tangential inlets the ratio of their geometric dimensions have shown that the inlet velocity of the gas flow should be chosen close to 30 m/s. This is expedient from the point of view of optimizing such factors as hydraulic losses, the ratio of the radiuses of the cylindrical wall of the vortex mass transfer chamber and the branch pipe for gas removal from it, the value of the circumferential gas velocity in the spray zone.

A decrease in the inlet velocity of the gas flow in the inlet tangential slots leads to the need for an undesirable increase in the radial dimensions of the vortex mass transfer chamber of the apparatus, an increase in hydraulic resistance. An increase in the inlet velocity of the gas flow in the tangential slots at the entrance to the vortex mass transfer chamber over 30 m/s influences the increase in energy losses in the slots themselves and on friction against the cylindrical wall of the vortex mass transfer chamber, reduces the path length when liquid droplets move in the working chamber of the apparatus.

When determining the value of the circumferential velocity of the vortex gas flow near the cylindrical wall of the vortex mass transfer chamber $V_{\varphi 1}$, it must be considered that large inlet gas velocities in the tangential slots at the entrance to the mass transfer chamber and a smaller ratio of the width of the tangential slot to its height corresponds to a smaller coefficient.

The gas flow through the tangential slots in the cylindrical wall of the vortex mass transfer chamber is accompanied by energy losses and flow restructuring. Accounting for all factors determining the static pressure in the vortex gas flow at the exit from the inlet tangential slots is a complicated problem. Therefore, a simple relation $P_1 = (0.72–0.81)P_{in}$ can be recommended.

It shows the dependence of the static pressure in the gas flow at the entrance to the vortex mass transfer chamber on the total pressure in the annular chamber supplying the gas.

In the range of gas inlet velocities from 16 m/s to 50 m/s, it should be considered that higher inlet velocities correspond to a more significant pressure drop and vice versa. That is, at velocities of about 40 m/s, the P_1/P_{in} ratio approaches 0.72, and at velocities of 25–16 m/s, this ratio approaches 0.82.

To create a flat vortex gas flow, in addition to the conditions at the inlet to the vortex mass transfer chamber of a spraying countercurrent mass transfer apparatus, the ratio of the main geometric dimensions, such as the radius of the vortex mass transfer chamber, the height of the vortex mass transfer chamber and the radius of the gas outlet pipe in one of the end caps of the vortex chamber, has a significant influence. Of great importance is the ratio of the radius of the vortex mass transfer chamber to the radius of the branch pipe for gas removal from this mass transfer chamber as a factor that affects the magnitude of the circumferential velocity of the gas flow in the central region, which is the liquid spray zone.

Equation (3.18) can be used to determine the ratios of the main geometrical dimensions of the vortex mass transfer chamber to organize a flat spiral movement of the gas flow in it.

Experimental studies have shown the presence of a flat vortex gas flow between a cylindrical wall, on which tangential slots for the gas inlet are located, and a cylindrical section with a radius close to the radius of the gas outlet pipe in mass transfer chambers having a ratio of the main geometric dimensions close to that specified in equation (3.18).

In engineering calculations, when assessing the dimensions of vortex spraying countercurrent mass transfer apparatuses, their mode of operation, it is not always convenient to use, although analytical, rather cumbersome dependencies (3.29) to

determine peripheral velocities, as well as the maximum gas velocity at the radius at the inlet edge of the nozzle for gas removal from the vortex mass transfer chamber R2.

Vortex mass transfer chambers, the results of which have been published in various literature sources, cover a significant range both in terms of the circumferential velocities of the gas flow and in terms of the absolute value of geometric dimensions. Therefore, based on the research material, it is possible to obtain a simple empirical formula, for example, (1.4), suitable for carrying out reasonably accurate estimates of the circumferential velocities of the gas flow along the radius of the vortex mass transfer chamber.

The third section (3.22) shows that the coefficient n in formula (1.4) generally has a complex structure. It depends on the radius of the cylindrical wall of the vortex mass transfer chamber, the radius of the gas flow outlet pipe from it, the circumferential velocities of the gas flow at the inlet and outlet of the vortex mass transfer chamber, and varies along the radius of the mass transfer chamber.

According to the results of the available experimental studies of various mass-exchange chambers of vortex apparatuses with different dimensions, but a flat spiral flow of a gas flow in the zone of contact of the liquid and gas phases, using formula (1.5), specific values of the exponent *n* were determined for the studied vortex chambers.

The results are shown in Figure 4.29.

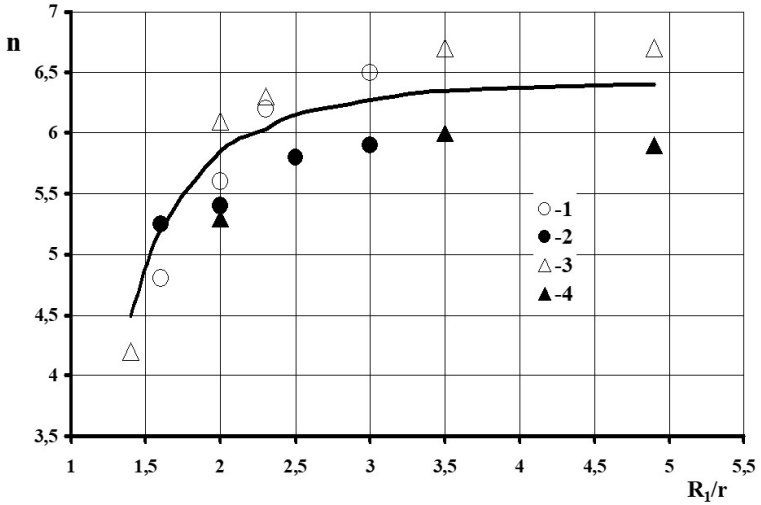

Figure 4.29 – Changing the exponent *n* along with the radius: 1, 2 – Stand 1; 3, 4 – Stand 2

The following function can approximate the change in the exponent *n* with sufficient accuracy for engineering calculations:

$$n = a - b\left(\frac{r}{R_1}\right)^c, \tag{4.19}$$

where initially, the following coefficients are applied: $a = 0.7$, $b = 0.4$, and $c = 3$.

This equation was obtained based on experimental data for vortex mass transfer chambers with specific geometric dimensions and ratios.

It should be noted that to calculate the vortex mass transfer chambers of counterflow spraying apparatuses with the ratio $R_1/R_3 \leq 3$, it is expedient to apply formula (4.19) with the coefficient $b = 0.6$.

For identifying more general patterns, verification calculations were carried out using equations (3.29) and (3.32). The calculation results are shown in Figure 4.30.

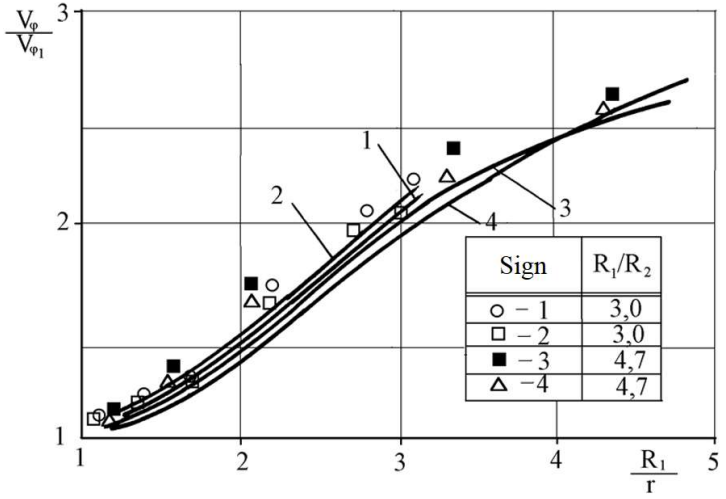

Figure 4.30 – Variation of velocities along with the radius of the working chambers

Notably, experimental studies on vortex flows [75] showed the presence of significant deviations in the value of the coefficient of turbulent viscosity along the radius. Empirical constant ζ^*, applied in the calculations, corresponds to the value of the turbulent viscosity coefficient near the cylindrical wall of the vortex elements.

Notably, the circumferential velocity of the gas flow of the gas reaches its maximum value, if in the vortex mass transfer chamber there is a flat vortex movement of the gas flow from the inlet to the outlet, at the cut of the outlet for gas removal in the center of one of the end caps of the vortex mass transfer chamber.

It is possible to significantly improve the structure of flows in the apparatus vortex chamber with an increase in its relative height by organizing a vortex mass transfer chamber of gas removal that is uniform in height. A structural diagram of a possible gas outlet is shown in Figure 4.31.

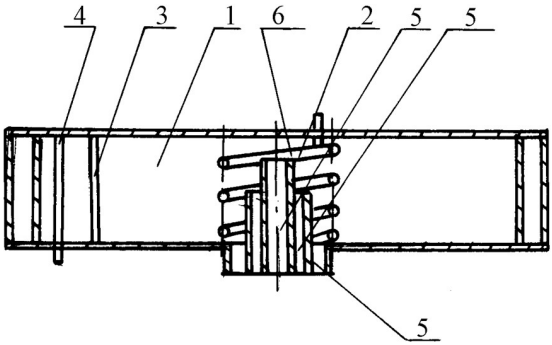

Figure 4.31 – Scheme of gas removal for eliminating unevenness in the flow along with the height of the device: 1 – mass transfer chamber; 2 – atomizer; 3 – tangential slots for gas inlet; 4 – liquid outlets; 5 – annular channels for gas removal; 6 – branch pipes for gas removal

Here, by changing the size of the annular channels formed by the annular nozzles of the atomizer, on the outer side of which nozzles for liquid atomization are installed, it is possible to change the amount of gas discharged from different heights of the working chamber. This allows achieving a velocity field uniform in height in the vortex mass transfer chamber itself.

In the present work, theoretical and experimental studies, the designs of the gas flow removal from the vortex mass transfer chamber in the form of a branch pipe located in one of the end caps were considered. The dimensions of its flow section should be chosen from the condition of achieving an average flow rate within 30–40 m/s along the axis.

This value of the axial velocity of the gas flow does not lead to sizeable hydraulic energy losses. The choice of a lower gas flow rate in the gas outlet pipe from the vortex mass transfer chamber is undesirable since, in this case, the radius of the inlet edge of this branch pipe R_2 will increase. This leads to the need to increase the radius of the cylindrical surface of the vortex mass transfer chamber R_1 to obtain the required values of the circumferential velocities of the gas flow in the spray zone and apparatus dimensions (Figure 4.32).

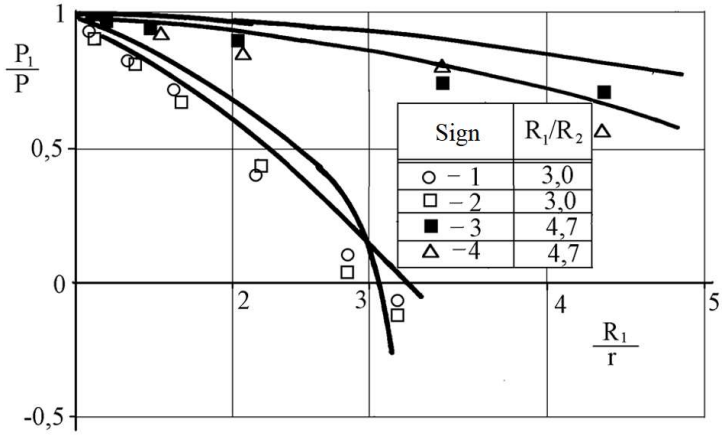

Figure 4.32 – Change in pressure along the radius of the working chamber

Dispersion of liquid into droplets must be organized near a cylindrical section with a radius R_2 equal to the radius of the gas flow outlet pipe from the vortex mass transfer chamber, which has an explanation since it is at this section that the circumferential gas velocities reach the highest values, and the relative velocities of the gas and liquid phases are sufficient to achieve fine spray.

Thus, when spraying a liquid, it is advisable to inject the liquid directly at the cylindrical surface with a radius R_2 and supply the liquid at low radial velocities since this increases the residence time of the droplets in the mass transfer chamber.

The introduction of liquid in the circumferential direction, one directed with the movement of the gas flow, makes it possible to increase the field of circumferential velocities, restore the regular vortex countercurrent movement of the gas-droplet flow, and improve the operation of the vortex spraying countercurrent mass transfer apparatus.

Much attention in the design and development of apparatus should be given to devices that divert the fluid flow. The liquid should be removed from the cylindrical wall of the vortex mass transfer chamber along with its entire height and intensively. Otherwise, the tangential slots for introducing the gas flow are blocked by a liquid film that moves along the periphery. There is a secondary crushing of the liquid film into droplets and entrainment of the droplets together with the gas flow in the center of the vortex mass transfer apparatus, which requires additional energy costs and worsens the conditions for intensive mass transfer. The liquid accumulates on the periphery of the vortex mass transfer chamber near the cylindrical wall in the form of a rotating ring.

When the axis of the vortex atomizing countercurrent mass transfer apparatus is located vertically during operation, there is a danger of the appearance of end currents, which leads to increased spray entrainment. To prevent such flows, it is advisable to place a hole for gas removal from the vortex mass transfer chamber in the upper-end cap. This leads to the termination of the feed of the end flow with liquid flown under gravity and prevents the end flow.

One of the possible design solutions for removing liquid from the vortex mass transfer chamber is the location of the axis

of the vortex countercurrent mass transfer apparatus in the working position horizontally.

This prevents the liquid from draining from the cylindrical wall to any of the end caps creating conditions for the uniform height of the vortex mass transfer chamber to remove the liquid and enter the gas flow. With this arrangement of the apparatus, it is advisable to drain the liquid in the form of vertical slots along with the entire height of the mass transfer chamber in its lower part.

The accumulated experimental material on the study of the hydraulic resistance of various mass transfer chambers of the apparatus makes it possible to predict the possible hydraulic resistance of the vortex apparatus for preliminary calculations of newly created structures of the vortex mass transfer technology.

Under the design and velocity similarities for the vortex countercurrent apparatus, the nomogram presented in Figure 4.33 can be used.

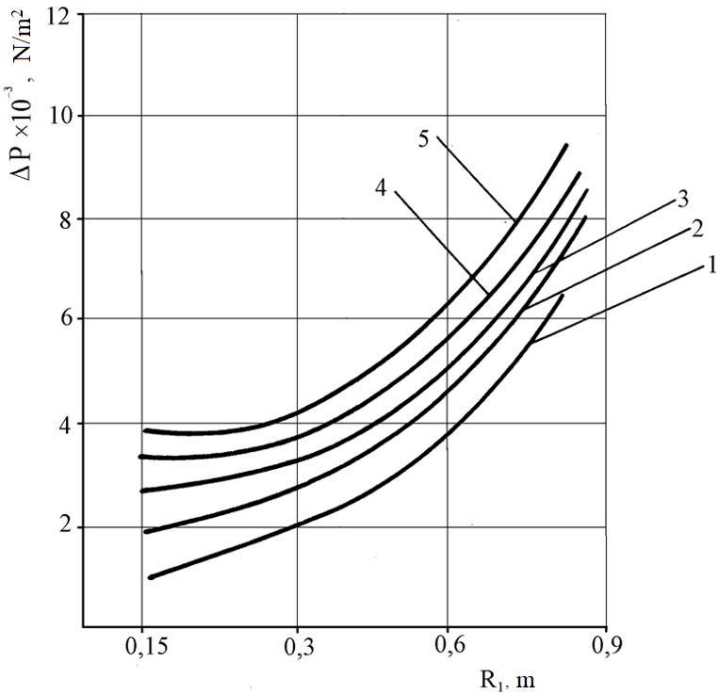

Figure 4.33 – Change in the resistance of the vortex apparatus depending on the size of the mass transfer chamber for different inlet velocities: 1 – V_{in} = 20 m/s; 2 – V_{in} = 30 m/s; 3 – V_{in} = 40 m/s; 4 – V_{in} = 50 m/s; 5 – V_{in} = 60 m/s

Here, the radius of the vortex mass-transfer chamber and the inlet velocity are preselected from the condition of achieving the required circumferential velocity in the area where the liquid is sprayed. After that, according to the nomogram, the resistance of the apparatus is approximately determined. If this value is included in the requirements of the auxiliary equipment, further refined calculation of hydrodynamics, droplet velocities, and time of their stay in the chamber is carried out. Also, the outlet velocity of the gas due to the introduction of the liquid phase,

the hydraulic resistance, and the geometric dimensions of the radial diffuser are determined.

Overall, due to the analysis of experimental studies of the hydrodynamics of the apparatus, it is possible to calculate the geometric and hydrodynamic characteristics of the vortex spray mass transfer apparatus and determine the geometry of the flow path when developing new designs of such devices.

5 Mass Transfer Characteristics of the Vortex Spraying Countercurrent Mass Transfer Apparatus

5.1 Mass transfer characteristics during absorption (desorption)

When studying the mass transfer characteristics of various contact devices, the method of determining the mass transfer coefficient has proven itself well [76]. Determining the mass transfer coefficient directly from experience is complicated since there are no reasonably reliable methods to measure the concentration at the phase boundary. Therefore, to find the mass transfer coefficient based on experimental data, it is advisable to use an indirect method. In addition, it is considered that the diffusion coefficients in liquids are several orders of magnitude smaller than in gases.

In the studies of the vortex-type apparatus, to find the mass transfer coefficient of the liquid phase, experiments were carried out on the desorption of poorly soluble CO_2 gas in water. In this case, we can neglect the resistance of the gas phase and assume that the mass transfer coefficient, which is determined in the liquid phase, is equal to the mass transfer coefficient.

The data presented in this section are based on the results of experimental studies, where the saturation of water with carbon dioxide was carried out in a packed column with a direct-flow movement of the phases from bottom to top. After the column, a degasser was installed to remove carbon dioxide from the water, which remained insoluble. The flow rate of the liquid saturated with CO_2 was measured using a rotameter.

The amount of gas supplied to the vortex countercurrent atomizing mass transfer apparatus was determined from the data

of instruments in which a flow washer was used in the same way as in the study of hydrodynamic characteristics. Spray entrainment was measured as the difference between liquid supplied for irrigation and discharge from the vortex spraying countercurrent mass transfer apparatus. The amount of CO_2 contained in the water supplied to the atomizer of the vortex mass transfer apparatus was determined by titration using an automatic titration unit. The method for determining CO_2 in water is based on a carbon dioxide solution titration with a 0.01–0.05 % NaOH solution. Titration is carried out using a pH meter to a pH value of 8.3. In such a solution, the carbon dioxide content is practically zero.

The concentration of CO_2 is determined by calculation as:

$$x = 44\frac{V_1}{V_2}N_0K_N \tag{5.1}$$

where 44 – gram equivalent of CO_2; V_1 – a volume of the solution used for titration, ml; V_2 – sample volume, ml; N_0 – solution normality; K_N – correction factor.

The content in the water at the outlet of the apparatus was determined by a similar method.

Due to the low concentrations of CO_2 in the gas and the large phase equilibrium constant in the carbon dioxide-water mixture, the influence of the gas phase on the driving force of the desorption process can be neglected, and the efficiency can be calculated using the equation:

$$E_{M_x} = \frac{\Delta x}{x}, \tag{5.2}$$

where E_{Mx} – desorption efficiency; x, Δx – concentration and its difference, respectively.

Then the number of transfer units at low concentrations of the component is equal to:

$$N_x = ln\frac{x}{x+\Delta x}, \tag{5.3}$$

or in the following form:

$$N_x = \frac{\beta_{xV} V_a}{Q_l}, \tag{5.4}$$

where β_{xV} – volume mass transfer coefficient, s^{-1}; V_c – the volume of the working chamber of the vortex spraying countercurrent mass transfer apparatus, m^3; Q_l – liquid flow rate, m^3/s.

From the last equation, the volumetric mass transfer coefficient in the liquid phase is equal to:

$$\beta_{x_V} = \frac{N_x Q_l}{V_c}. \tag{5.5}$$

The number of transfer units in expression (5.5) is determined by equation (5.3). Under experimental conditions, the liquid temperature usually changes, so the value β_{x_V} should be reduced to the temperature of 20 °C. When CO_2 is desorbed from water within the limits of liquid temperatures from 5 °C to 40 °C, $\beta_{X_V} \approx exp(0.023t_l)$, where t_l – liquid temperature, °C.

Thus, the volumetric mass transfer coefficient in the liquid phase for the apparatus, corrected for temperature, can be determined from the equation:

$$\beta_{x_V} = \frac{N_x Q_l}{\pi R_1^2 H_c} e^{0.023(20-t_l)}. \tag{5.6}$$

Figure 5.1 presents the design scheme of the stand for determining the mass transfer characteristics of the apparatus.

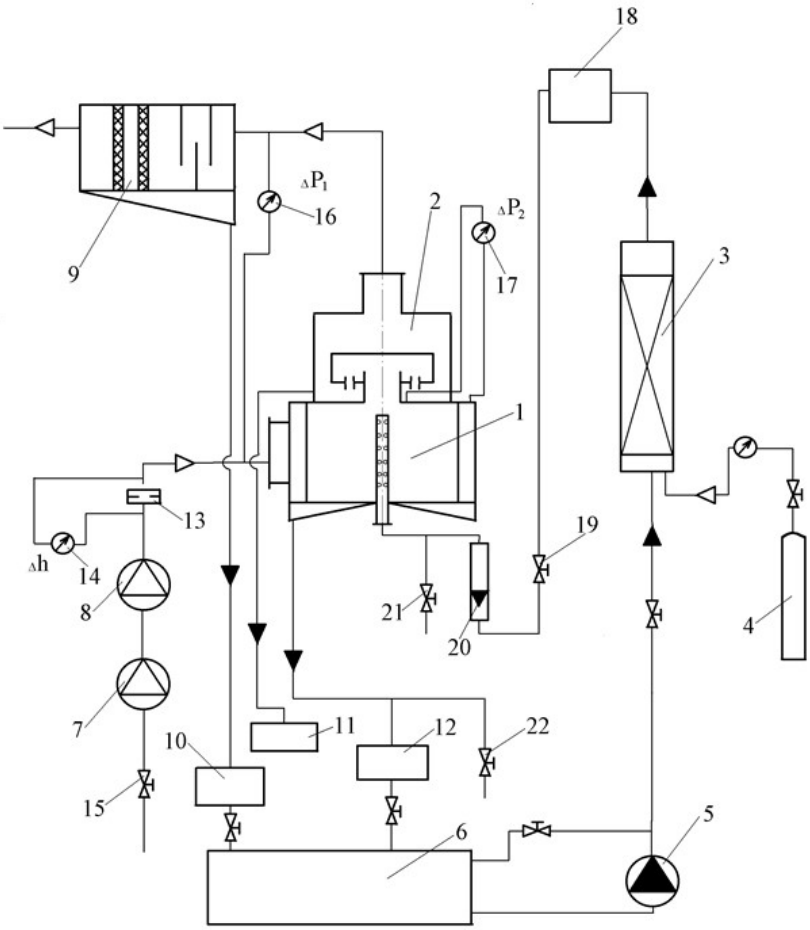

Figure 5.1 – Design scheme of the experimental setup: 1 – vortex apparatus; 2 – separator; 3 – absorption column; 4 – cylinder with pressure reducer; 5 – pump; 6, 11, 12 – liquid collectors; 7, 8 – high pressure fans; 9 – labyrinth mist trap with fine filters; 10 – liquid container; 13 – air flowmeter; 14 – differential pressure gauge; 15, 19, 21, 22 – valves; 16, 17 – manometers; 18 – degasser; 20 – liquid rotameter

5.2 Mass transfer characteristics during rectification

According to the results of theoretical and experimental studies of the hydrodynamics of the apparatus, carried out in various designs of vortex mass transfer chambers, two vortex apparatus were designed and manufactured to study the efficiency of mass transfer processes under rectification conditions. During the development, the features of the movement of the phases were considered and the identified shortcomings of the existing structures. Since the main task of the research was to study the mass transfer characteristics, the design of the tested apparatus was somewhat simplified, which led to a slight increase in hydraulic resistance.

In particular, the apparatus did not have a radial diffuser, and the hole for gas removal from the mass transfer chamber was somewhat smaller than required to ensure low hydraulic losses. The gas outlet had a diameter of 80 mm. The scheme of the studied countercurrent mass transfer apparatus is shown in Figure 5.2.

The axis of the device in the working position is horizontal. The mass transfer chamber is a cylindrical container with a diameter and height of 0.8 m and 0.15 m, respectively. Steam is introduced at the periphery in the upper part of the chamber through three tangential slots. A container is attached to the end cap, in which there is an opening for steam removal from the mass transfer chamber. This container removed steam from the apparatus through a tangential branch pipe located on the periphery of this container. Steam is supplied to the apparatus through a tangential branch pipe into the gas supply chamber, located in the upper part of the apparatus in front of the tangential slots.

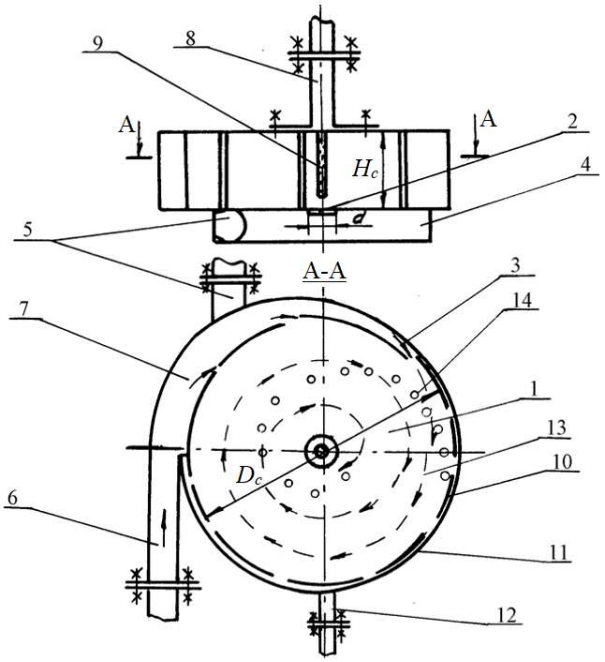

Figure 5.2 – Design scheme of the vortex countercurrent apparatus: 1 – mass transfer chamber; 2 – gas removal from the mass transfer chamber; 3 – tangential slots; 4 – container for gas removal; 5 – branch pipe for gas removal from the apparatus; 6 – branch pipe for supplying gas to the apparatus; 7 – chamber for gas supply; 8 – branch pipe for supplying liquid to the atomizer; 9 – atomizer; 10 – liquid outlet slots; 11 – container for liquid; 12 – branch pipe for draining liquid from the apparatus; 13 – direction of gas movement; 14 – the trajectory of the movement of droplets

The liquid is fed into the apparatus through a sprayer mounted on the end cap opposite to the one with an opening for removing steam from the mass transfer chamber. The atomizer is a branch pipe with a diameter of 10 mm, plugged on one side.

On the other hand, the liquid was injected into the nebulizer. On the entire surface of the branch pipe, there are 200 holes 1.2 mm in diameter, through which liquid jets are introduced into the vapor flow, moving in the vortex chamber in the radial direction. On the periphery of the mass transfer chamber, in the lower part of the cylindrical body, there is a number of tangential slots for draining liquid from the vortex chamber, connected along the entire length to a container for collecting liquid. The liquid is removed from the apparatus through the nozzle from this container.

The device works as follows. Steam, introduced into the mass transfer chamber through three tangential slots, moves towards the center. It creates powerful vortex flow with a significant increase in circumferential velocity to the central region, where the liquid is introduced into the mass transfer chamber in the radial direction. Liquid jets are involved in rotational movement around the apparatus axis and move towards the cylindrical wall of the chamber, settling on it and in the form of a film. The liquid is removed from the apparatus through the slots in the lower part of the housing.

Testing the effectiveness of vortex atomizing mass transfer apparatuses was carried out at the “hot” stand of the Severodonetsk branch the State Institute of Nitrogen Industry (Severodonetsk, Ukraine) under the conditions of rectification of a methanol-water mixture, mainly with a total return of reflux to the still, that is, with an infinite reflux number. The installation (Figure 5.3) contains a bottom in which the mixture was evaporated, a lower vortex apparatus, an upper vortex apparatus (the apparatuses are installed in series), a condenser, rotameters, refrigerators in the steam and reflux sampling lines.

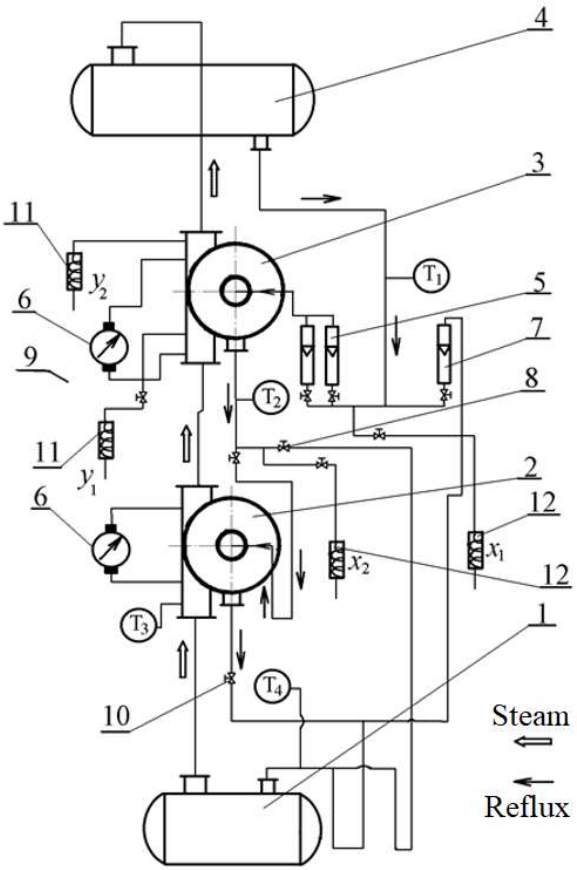

Figure 5.3 – The design scheme of the experimental stand: 1 – bottom; 2 – lower vortex apparatus; 3 – upper vortex apparatus; 4 – capacitor; 5 – rotameters; 6 – pressure gauges for measuring the pressure drop; 7 – rotameter to control the flow of reflux into the bottom; 8 – valve for dropping reflux into the bottom; 9 – valve for supplying reflux to the lower apparatus; 10 – valve for removing reflux from the lower apparatus; 11 – refrigerators for vapor phase sampling; 12 – refrigerators for sampling the liquid phase

Usually, the study of the effectiveness of contact devices, in particular plates of various designs, is carried out in a column that contains about tens of such elements. In some cases, if we exclude the mutual influence of the plates on one another, the entrainment of liquid to the higher located elements, then the dependencies on the volumetric mass transfer coefficient and the number of transfer units for one contact stage can, under certain conditions, be extended to the entire column.

Given that one of the goals of creating a vortex apparatus with phase counterflow in the contact zone is replacing column equipment, which contains several trays, with one apparatus, it is advisable to investigate the effectiveness of one vortex apparatus.

One of the study's objectives was to refute or confirm the above justifications about the possibility of achieving several theoretical levels of concentration change in one hollow apparatus, where the vortex countercurrent movement of the contacting phases is organized. Valves (Figure 5.3, pos. 8–10) are provided in the scheme of the experimental setup to turn off the lower apparatus and prevent reflux from entering it. Reflux from the upper apparatus, bypassing the lower apparatus, flowed directly into the bottom. This made it possible to determine the effectiveness of one device.

In addition, in the scheme of the stand, there is a line with a rotameter (Figure 5.3, pos. 7), through which it is possible to divert part of the reflux, bypassing the upper apparatus, into the bottom, that is, to work with a finite reflux ratio.

The efficiency of mass transfer processes in a vortex countercurrent apparatus is generally determined by the change in the vapor phase concentrations before and after the apparatus and the liquid phase at the inlet and outlet. When working with an infinite reflux ratio, the processes are stabilized under the equality of the phase concentrations x_1, y_2, and x_2, y_1. The vapor

phase is taken through glass coolers (Figure 5.3, pos. 11), where the vapor is condensed.

Reflux sampling was carried out from the walls of the pipes in the hydraulic lock in front of the rotameters. Through it, the reflux is supplied to the atomizer. At the outlet of the upper apparatus, that is, in places where filling the volume with fresh flowing liquid is guaranteed.

Further, the reflux is cooled in glass refrigerators (Figure 5.3, pos. 12), from where they are already taken into test tubes.

The analysis of the methanol content in the samples is carried out using a refractometer. The measurements taken by the refractometer are selectively controlled by analyzes carried out by specific gravity.

Temperatures are measured at three points. The reflux temperature is measured at the inlet and the outlet of the vortex apparatus. The steam temperature at the bottom outlet is controlled too.

The calculation of the volume flow rate of steam through a vortex spraying countercurrent mass transfer apparatus considers the complete return of reflux to the system, that is, according to the readings of rotameters and the equality of mass flow rates.

Figure 5.3 explains the operation of the experimental setup. Vapor from the bottom was fed through the lower vortex apparatus to the apparatus, passed through the mass transfer chamber, where contact with the liquid phase took place and removed to the condenser. The reflux from the condenser is fed to the atomizer introduced into the mass transfer chamber, where liquid jets are sprayed into droplets, which were involved in rotational motion and, under centrifugal forces, moved countercurrently relative to the vapor along the radius of the vortex chamber. Then the droplets are settled on the cylindrical

walls, and the liquid is removed from the apparatus into the bottom.

Sampling was carried out with an interval of 40–60 min until the concentration equalized. Selectively, to control the measurements of y_1 and x_2, samples were taken from the bottom. When the process stabilized, these measurements coincided.

An example of data on the experimental determination of the efficiency of a vortex mass transfer apparatus is given in Tables 5.1–5.2.

Table 5.1

Dataset for carrying out experimental studies

Steam flow, m^3/s	Concentration in the liquid phase, %		Concentration in the steam phase, %	
	X_1	X_2	Y_1	Y_2
2	3	4	5	6
0.236	89.6	85.4	86.3	96.5
	99.5	85.6	85.0	98.5
	99.7	86.6	85.6	99.7
0.044	89.6	80.1	79.5	92.0
	94.4	82.2	81.5	93.3
	96.5	82.8	82.8	96.5
0.089	96.7	59.5	57.0	94.4
	97.0	59.0	57.5	96.7
	98.5	59.0	59.0	98.5
0.144	95.4	62.8	59.5	93.5
	96.5	59.0	59.5	96.1
	98.7	58.0	58.0	98.7
0.211	90.0	78.4	85.6	86.5
	90.7	76.1	86.0	88.0
	91.0	75.4	86.5	91.0

Table 5.2
Experimental results data

Temperature, °C			Resistance, N/m^2	Theoretical stages number	Reflux number
t_1	t_2	t_2			
7	8	9	10	12	13
49	72	78	5488	8	∞
53	72	81			
53	72	80			
58	69	83	2450	2	∞
61	70	83			
61	70	84			
48	72	74	2940	4.5	∞
52	72	79			
59	72	83			
53	74	77	3920	5	∞
59	73	80			
60	73	81			
55	74	81	3185	5	0.85
55	73	82			
59	74	82			

The study of the sequential operation of two apparatuses and their operation with nozzles of various designs is not considered. However, the stand and apparatuses design provide such work, which is an essential step in developing and subsequent improvement of such vortex apparatuses with phase counterflow in the zone contact.

The apparatus resistance is measured by the pressure difference between the inlet pipe for gas supply and the branch pipe for a gas outlet from the apparatus. The diameters and the

steam velocities in these nozzles are equal to each other. The total energy losses in all elements are measured.

5.3 Experimentally obtained mass transfer characteristics during absorption (desorption)

Three vortex apparatuses were designed and manufactured for an experimental study of mass transfer characteristics. They are characterized by the following parameters (Figure 5.1). Two devices had a radius and height of the mass transfer chamber of 380 mm and 80 mm. The atomizers of both devices were a branch pipe with six holes 1 mm in diameter for irrigating the mass transfer chamber in the radial direction.

The difference was in the following layout of the apparatus. One was mounted in such a way that the axis was vertical. The gas outlet was located in the upper part of the apparatus, and the liquid outlet was carried out from the cylindrical walls through the holes in the lower end cap.

The second apparatus had a horizontal axis. The gas was removed through a hole in the end cap located vertically. The liquid was drained through a number of tangential slots in the lower part of the cylindrical body of the mass transfer chamber. The design of the apparatus is similar to that of the apparatus tested during the rectification process (Figure 5.2).

The third apparatus had a mass transfer chamber diameter and height $D_c = 1000$ mm and $H_c = 250$ mm. The axis of the device was located vertically.

Tables 5.3–5.4 summarize the experimental results in determining the effectiveness of the apparatus with a vertical axis.

In Tables 5.5–5.6, the results of the experimental determination of the effectiveness of the apparatus are given ($D_c = 1000$ mm).

Table 5.3
Dataset for carrying out experimental studies for apparatus with vertical axis

Consumption, m^3/s		Phase loads ratio, L/G	Relative брызгоунос δ_L	Hydraulic resistance ΔP, kPa	Concentration in the liquid phase x_1, g/l
Gas Q_g	Liquid Q_l				
0.043	0.6	0.107	0.018	1.42	1.87
0.043	1.3	0.233	0.028	1.40	1.92
0.043	2.0	0.258	0.021	1.37	2.30
0.043	2.7	0.483	0.015	1.28	1.89
0.043	3.4	0.609	0.010	1.23	1.73
0.043	4.1	0.734	0.015	1.22	1.71
0.061	0.6	0.076	0.018	2.81	1.60
0.061	1.3	0.165	0.028	2.78	1.95
0.061	2.0	0.254	0.034	2.75	1.88
0.061	2.7	0.343	0.045	2.73	1.57
0.061	3.4	0.432	0.059	2.65	1.50
0.061	4.1	0.521	0.029	2.55	1.83
0.075	0.6	0.062	0.034	4.02	1.63
0.075	1.3	0.134	0.039	3.97	1.64
0.075	2.0	0.206	0.053	3.92	1.76

Table 5.4
Experimental results data for apparatus with vertical axis

Concentration in the liquid phase x_1, g/l	Inlet velocity, m/s		Recovery rate	Theoretical stages number	Mass transfer coefficient β_{X_V}, 10^3 s^{-1}
	Gas V_{in}	Liquid W_{in}			
0.087	9.0	1.27	0.95	3.05	1.60
0.246	9.0	2.76	0.87	2.07	2.36
0.269	9.0	4.24	0.87	2.00	3.53
0.269	9.0	5.73	0.87	2.06	4.87
0.403	9.0	7.21	0.82	1.70	5.06
0.265	9.0	8.69	0.87	2.05	7.36
0.088	12.7	2.76	0.96	3.18	3.64
0.040	12.7	4.24	0.98	3.91	6.81
0.135	12.7	5.72	0.93	2.63	6.22
0.152	12.7	7.21	0.93	2.60	7.74
0.133	12.7	8.69	0.93	2.71	9.13
0.039	15.58	2.76	0.98	3.92	4.46
0.111	15.58	4.24	0.94	2.88	5.04
0.085	15.58	5.72	0.95	3.03	7.16
0.094	15.58	7.21	0.94	2.80	8.34

Table 5.5
Dataset for carrying out experimental studies of the efficiency (Dc = 1000 mm)

Consumption, m^3/s		Phase loads ratio, L/G	Concentration of the liquid phase, g/l	
Gas Q_g	Liquid Q_l		x_1	x_2
0.127	1.33	0.080	7.20	0.52
0.127	1.70	0.103	3.58	0.21
0.127	2.06	0.125	4.60	0.27
0.127	2.43	0.147	9.50	0.51
0.127	2.79	0.170	8.00	0.46
0.127	3.14	0.192	2.00	0.17
0.127	3.52	0.214	1.67	0.19
0.129	1.33	0.079	1.60	0.13
0.129	1.70	0.101	1.48	0.09
0.129	2.06	0.122	1.81	0.132
0.129	2.43	0.144	2.08	0.17
0.129	2.79	0.166	1.42	0.17
0.129	3.16	1.188	1.84	0.20
0.129	3.89	0.231	1.58	0.17

Table 5.6
Experimental results data of the efficiency (*Dc* = 1000 mm)

Inlet velocity, m/s		Recovery rate	Theoretical stages number	Mass transfer coefficient β_{xy}, 10^3 s^{-1}
Gas V_{in}	Liquid W_{in}			
12.99	1.88	0.93	2.63	1.41
12.99	2.40	0.94	2.83	1.94
12.99	2.92	0.94	2.83	2.36
12.99	3.43	0.95	2.92	2.87
12.99	3.95	0.94	2.85	3.22
12.99	4.47	0.91	2.44	3.12
12.99	4.98	0.89	2.18	3.11
13.29	1.88	0.92	2.51	1.35
13.29	2.39	0.94	2.79	1.92
13.29	2.91	0.93	2.62	2.18
13.29	3.43	0.92	2.51	2.47
13.29	3.25	0.88	2.12	2.39
13.29	4.46	0.89	2.22	2.84
13.29	5.49	0.89	2.21	3.48

The obtained numerical characteristics indicated the high efficiency of the devices and confirmed the theoretical dependencies on the effect of the transverse gradient of gas flow velocities on the number of theoretical stages of concentration change in one spray stage. The number of theoretical stages in one spraying stage exceeded 1.2. In cases of operation of the devices at modes close to optimal (finely dispersed spray and minor spray entrainment), the number of theoretical stages of concentration change exceeded 4.0. The conducted studies revealed the relationship between spray entrainment and a decrease in the efficiency of the apparatus.

5.4 Experimentally obtained mass transfer characteristics during rectification

In almost all modes, the reduction in mass transfer efficiency coincides with an increase in the relative droplet removal (Figures 5.4).

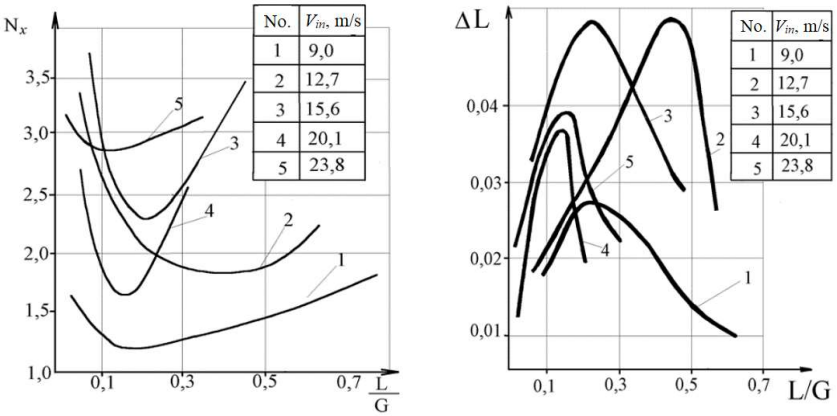

a b

Figure 5.4 – Number of transfer units (a) and relative spray removal (b) for apparatus with the vertical axis (D_c = 380 mm)

The presence of such an increase in the amount of liquid that is carried away by the gas from the apparatus is explained by the design features of the apparatus and their hydrodynamics. Since the atomizer was located in the center of the mass transfer chamber, where there is an axial gas movement at a velocity of about 20–40 m/s, at a relatively low outflow velocity (small L/G ratio), a finely dispersed liquid atomization is observed due to high relative phase velocities.

Large centrifugal forces act on droplets. Therefore, the liquid "skips" the dangerous zone of axial gas velocities.

Further, with an increase in the liquid load, the gas velocities decrease, which affects the force effect of the gas on the droplets and leads to some increase in the spray entrainment.

The subsequent increase in the load on the liquid and the velocity of the outflow of jets from the holes of the atomizer change the movement of the liquid phase in the central region. Spraying of jets occurs near a radius close to the radius R_2, near the border of the dangerous zone of axial velocities and high circumferential gas velocities, which has a positive effect on reducing spray entrainment.

The main result of research into the effectiveness of a vortex spray mass transfer apparatus with phase counterflow in the contact zone is to confirm the possibility of achieving several theoretical stages of changing concentrations in one spray stage.

The studies generalize the experimental material to obtain criterion equations, according to which it is possible to calculate the mass transfer coefficients since the range of studies covered a relatively wide range of the vortex apparatus with different geometric dimensions of vortex chambers, their ratio, and intervals of gas and liquid flow rates.

According to the results of experimental studies, calculating the number of theoretical stages of concentration change in one spraying stage can be performed graphically and from tabular values using the equilibrium line of the methanol-water mixture.

In the apparatus, the vapor and liquid phases contact in a small volume. This is due to the size of the mass transfer chamber. To identify the advantages of a vortex countercurrent apparatus, it is advisable to apply criteria that characterize the efficiency of using a unit volume of the mass transfer chamber in which the countercurrent movement of phases occurs. One of these criteria is the volumetric mass transfer coefficient, s^{-1}:

$$\beta_{xV} = \frac{GN_x}{V_c}. \quad (5.7)$$

The expediency of defining this criterion, for example, is because the expression of the intensity of mass transfer in the form of volumetric mass transfer coefficients is very indicative for assessing the effectiveness of the inter-tray volume or the volume of the column as a whole.

Another essential criterion that characterizes the energy intensity of mass transfer equipment is the value of specific hydraulic resistance, which falls on a single theoretical stage of concentration change or transfer unit.

Using this criterion for evaluating the energy qualities of various designs of contact elements makes it more transparent when analyzing the advantages or disadvantages of the considered tray designs. In addition, knowledge of the specific hydraulic resistance is essential when calculating newly designed equipment or reconstructing existing columns, as it allows you to determine the change in pressure along with the height of the apparatus or column, which can lead to a change in temperature, concentration, and affect the mass transfer processes.

The steam flow rate through the apparatus reached values up to 1000 kg/hr, which corresponds to the steam velocity in the tangential slots up to 50 m/s.

Figure 5.5 presents the experimentally obtained dependence of the change in the volumetric mass transfer coefficient on the operating mode of the vortex apparatus.

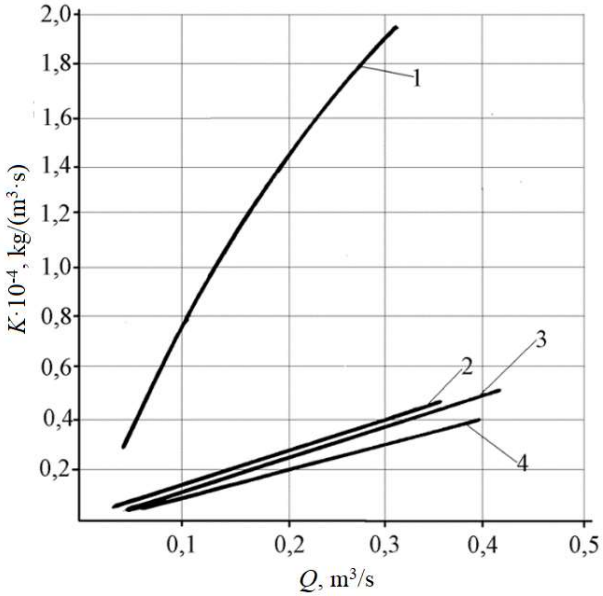

Figure 5.5 – Comparative characteristics: 1 – vortex apparatus; 2 – sieve plate; 3 – cap plate; 4 – valve plate

For comparison, three characteristics of the change in the volumetric mass transfer coefficient for three types of mass transfer devices are plotted. These are a sieve, cap, and valve plates. The size of the volumetric coefficient for the apparatus is an order of magnitude higher than in tray equipment.

A graphical dependence of resistivity per theoretical concentration step is shown in Figure 5.5, which shows similar dependencies for various types of trays [77].

The above analysis of the characteristics obtained allows us to draw a number of conclusions about the features of a vortex mass transfer apparatus with phase counterflow in the contact zone.

With a low flow rate of the vapor phase through the apparatus and, accordingly, low steam velocities in the inlet tangential slots in the spray area, large droplets appear due to a low value of the relative velocity of the phases. The small size of the interfacial surface and low circumferential gas velocities along the radius of the mass transfer chamber lead to the fact that the apparatus operates inefficiently in these modes. The change in concentrations is about two theoretical stages.

A further increase in the flow rate and steam velocities in the mass transfer chamber creates conditions for a more finely dispersed liquid atomization, an increase in the interfacial surface due to a decrease in droplets, the small size of which at high circumferential gas velocities makes it possible to organize countercurrent movement with low spray entrainment and more intensive circulation of currents in droplets. All this leads to the intensification of mass transfer, which makes it possible to achieve 7–8 theoretical stages of concentration change in one spray stage.

Simultaneously, an increase in gas velocity leads to an increase in the hydraulic resistance of the apparatus, which is proportional to the squared gas velocity. The cumulative effect of the increase in efficiency and hydraulic resistance leads to a decrease in resistivity, which falls on a single theoretical stage of changing the concentration. The resistivity is about 70 mm of water in the optimal operating mode region.

Figure 5.6 shows that the value is less than similar characteristics for some trays and is comparable to the resistivity value in the optimum region for trays with more economical performance.

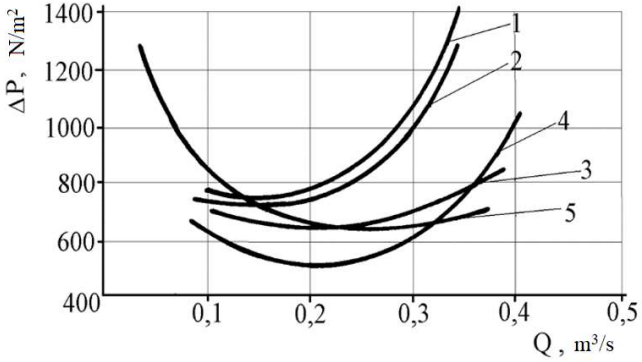

Figure 5.6 – Resistivity change per theoretical stage of concentration change for different devices: 1 – standard S-like plate; 2 – S-like plate with baffle elements ; 3 – direct-flow valve plate; 4 – sieve plate with baffle elements; 5 – vortex apparatus

Considering the replacement of several plates with one apparatus and a decrease in the amount of reflux supplied for irrigation, which leads to a decrease in energy costs during operation, the use of vortex-type apparatuses with phase counterflow in the contact zone provides a significant economic effect, the rationale for which is described in the next chapter. The presented experimental results are a critical step in developping vortex devices of this type.

5.5 Calculation of mass transfer characteristics

As shown in the previous sections, the calculation of the mass transfer coefficients and other parameters that characterize the efficiency of the apparatus operation theoretically encounters many difficulties, in connection with which, for engineering

calculations, according to the data of experimental studies, a dependence of the form:

$$Nu = Nu(Re, Pe, R_1, R_2), \tag{5.8}$$

where *Nu*, *Re*, *Pe* – Nusselt, Reynolds, and Peclet numbers, respectively.

Considering that the bulk of the experimental data was obtained under conditions of desorption of the poorly soluble CO_2, when obtaining such dependencies, we can assume that the mass transfer coefficient is practically equal to the mass transfer coefficient. In turn, the relationship between the volumetric mass transfer coefficient β_X and the mass transfer coefficient β_{X_V} are expressed by the relation:

$$\beta_{x_V} = \beta_x a_s, \tag{5.9}$$

where a_s – specific interfacial surface, m^2/m^3:

$$a = F_s/V_c; \tag{5.10}$$

F_s – the interfacial surface as a total surface of liquid droplets, m^2; V_c – the volume of the camera.

$$F_s = S_0 n_0 = \frac{6V_l}{d_0} = \frac{3d_n^2}{2d_0} n_a \pi (R_1 - R_2), \tag{5.11}$$

where S_0 – liquid droplet surface, m^2; n_0 – number of droplets; V_l – the volume of liquid in the working volume of the mass transfer chamber, m^3; n_n – number of nozzles; d_0, d_n – diameters of a droplet and a nozzle, respectively, m (Figure 5.7).

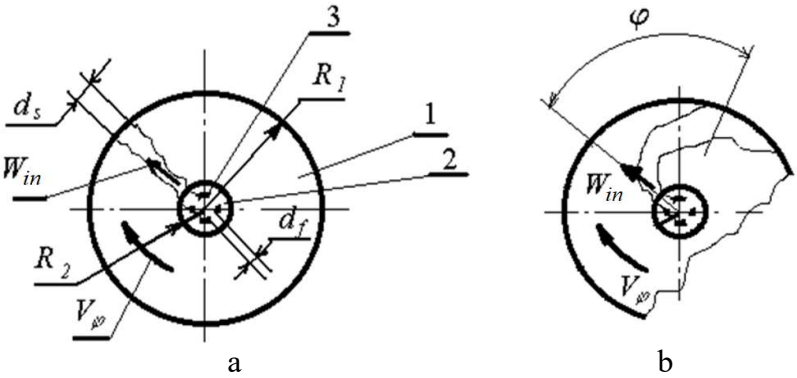

Figure 5.7 – Scheme of liquid jet movement: a – without gas rotation ($V_\varphi = 0$); b – under gas rotation ($V_\varphi \neq 0$); 1 – mass transfer chamber; 2 – gas outlet; 3 – atomizer; R_1 – the radius of the mass transfer chamber; R_2 – gas outlet radius; d_n – nozzle diameter, m; d_j – diameter of a liquid jet, m; W_{in} – inlet velocity of a liquid, m/s; φ – deviation angle of the liquid flow about the axis of the nozzle hole, rad

Thus, the relationship between these two mass transfer coefficients is represented by the following dependence:

$$\beta_x = \frac{\beta_{x_V}}{a_s} = \frac{\beta_{x_V} V_c}{F_s} = \frac{2\beta_{x_V} V_c d_0}{3\pi(R_1 - R_2) n_0 d_n^2}. \qquad (5.12)$$

In addition, given that the droplet diameter is affected by the gas velocity in the spray zone, which in turn depends on the ratio of the radiuses R_1 and R_2 (Chapter 3.4) and input gas velocity (V_{in} depends on the area of the tangential slots and the height of the mass transfer chamber), the dependence (5.8) can be simplified. The functional dependence of the Nuselt criterion *Nu* on the Peclet *Pe* and Reynolds *Re* criteria:

$$Nu = 1.124 - 1.24\frac{R_1 - R_2}{R_1} Pe^n e^{\left(2.47\frac{R_1 - R_2}{R_1} - 2.40\right)\cdot 10^{-4} Re}, \quad (5.13)$$

where n = 0.78–0.84.

Thus, the obtained results can be used for practical calculations of the vortex mass-transfer chamber of newly designed apparatuses.

To do this, it is necessary, by determining from the material balance equation the amount of a substance that passes from gas to liquid and determining the mass transfer coefficient from equation (5.14), it is possible to calculate the volume of the mass transfer chamber of the designed apparatus:

$$V_c = \frac{M_l}{\beta_{x_V} \Delta x_{av}}, \quad (5.14)$$

where Δx_{av} – average concentration difference.

Refining calculations of the geometry, hydrodynamic characteristics, and conditions for spraying liquid jets into droplets are needed.

Further, based on the results of the refined hydrodynamic parameters, adjustments are made to the geometric dimensions of both the vortex mass transfer chamber itself and auxiliary elements, and the final calculation of the mass transfer characteristics of the apparatus is carried out.

6 Designing of Vortex Spraying Mass Transfer Apparatuses and Areas of Their Application

6.1 The rationale for the use of vortex spraying mass transfer apparatuses

The data presented in the previous chapters, confirming the efficiency (in a unit volume of the mass transfer chamber, a more significant change in concentration is achieved than in other contact devices) of vortex countercurrent mass transfer devices, indicate the expediency of their use in various industries. But, before giving recommendations for their implementtation in industry, let us consider the economic side of the issue. Due to changes in what factors, is it economically beneficial to introduce the considered devices in various technological processes.

The costs associated with the creation and implementation of the leading chemical equipment can be divided into two groups:

– the cost of manufacturing the apparatus and the materials used in this case.

– essential cost item is the cost of energy resources during operation.

The design of the vortex spraying mass transfer apparatus in general consists of two shells located one in one. Several tangential slots for gas supply and vertical slots for liquid output are made in the inner shell and its entire height. In the manufacture of the apparatus, the inner cylindrical chamber is made of several metal sheets curved along the radius of the vortex chamber, which is connected by welding or in another way to two end caps. The assembly of the vortex apparatus does

not require special precision. Quite simple technological operations are used in the manufacture.

The manufacture of vortex atomizing mass transfer apparatus, for example, for testing on industrial mixtures at the State Institute of Nitrogen Industry (Severodonetsk, Ukraine), and JSC "Sumy Machine-Building Science and Production Association" (Sumy, Ukraine) required a unit cost of 1.83 USD/kg. Simultaneously, for example, manufacturing a sieve plate with fender elements in the same period required a unit cost of 2.42 USD/kg. Here and below, prices are given according to these data, but it is not so much the absolute figures that are important, but the comparison of prices with the manufacture of other contact mass transfer devices.

Table 6.1 presents comparative cost data for material consumption for various plates.

Table 6.1

Comparative characteristics for various contact elements

Type of the contact element	Specific cost, USD/kg	Specific resistance, mm H_2O
Cap plate	2.18	150
S-type plate	1.50	145
Direct-flow valve plate	1.81	77
Sieve plate with baffle elements	1.45	50
Vortex spraying countercurrent mass transfer apparatus	1.10	70

Here, information is given on the material costs for creating a mass-exchange apparatus equivalent to a vortex counterflow apparatus, in which a change in concentrations corresponding to seven theoretical stages would be achieved.

For comparison, the operating mode was chosen according to the test data of the vortex apparatus. Its productivity is 1000 kg/hr.

The above results show that the use of vortex spraying countercurrent mass transfer apparatus leads to a significant reduction in metal consumption. Accordingly, the costs are also reduced, which is proportional to the decrease in material consumption.

In addition, there are other advantages of vortex countercurrent devices:

– a relatively small height, which entails the possibility of using pumps of low power when pumping reflux in the rectification processes from the reflux condenser to the upper part of the apparatus;

– reduction in the size of the vortex mass transfer apparatus, when operated under conditions of rectification, leads to a decrease in the outer surface of the apparatus and, as a result, heat losses to the environment are reduced;

– reduction in the amount of reflux supplied for irrigation of the distillation vortex apparatus, which leads to a significant reduction in energy costs for the operation of pumping equipment for pumping reflux;

– capital investments to create the various base fastening and ancillary equipment are reduced.

Thus, the use of vortex countercurrent apparatuses, from the point of view of reducing manufacturing costs and capital investments in construction, is of great interest.

The countercurrent movement of the phases stable operation in the countercurrent mode suggests the most efficient use of the considered vortex apparatus in the rectification processes, which is confirmed by the experimental data obtained, which indicates the possibility of using the vortex apparatus in these processes.

Let us consider how the economic effect is formed from the use of apparatus during the operation of the equipment. In the general case, the heat balance of the column is the equality between the heat supplied with the original product to evaporate the mixture in the bottom and the heat removed from the condenser. Under the invariance of the auxiliary equipment, the costs for the mixture evaporation in the bottom are of interest. This heat is spent on the evaporation of the mixture and on overcoming the hydraulic resistance of the column or apparatus itself. The specific hydraulic resistance (per theoretical concentration step) of a vortex countercurrent mass transfer apparatus (Tables 6.1–6.2) is close to various trays. Therefore, the resistance of the equipment does not increase when replacing the plates with a vortex apparatus.

Table 6.2

Parameters of the contact device to achieve a concentration difference corresponding to seven theoretical concentration stages

Number of elements	Diameter, m	Height, m	Materials/ producing costs ratio
9	0.42	2.7	2.6
9	0.42	2.7	2.4
9	0.42	2.7	2.0
12	0.42	3.6	3.0
1	0.80	0.7	N/A

Typically, the reflux ratio is chosen from the condition of the ratio of the height of the column. It is associated with the number of disc contact elements and their efficiency, factors of the yield of the finished product, and the cost of evaporation of

the mixture. With a decrease in the reflux ratio and, accordingly, the cost of evaporation of the mixture in the bottom, it becomes necessary to increase the number of real contact mass-transfer elements in the form of plates, increase the height of the column and the associated costs.

Using highly efficient apparatuses makes it possible to reduce the reflux ratio and the cost of evaporating the reflux that circulates in the column. Reducing the reflux number by only 20 % gives annual savings with a distillation apparatus capacity of 25,000 kg/hr, which will amount to annual savings in the workshop of 37,000 USD, for example, at the PJSC "Azot" (Severodonetsk, Ukraine), where five columns are installed (185,000 USD). These figures are calculated assuming a reflux reduction of 20 %. Given the significant constant rise in the price of energy resources at the beginning of the 21st century, the economic effect increases tenfold.

The considered economic effect, which is formed from reducing energy costs for the evaporation of reflux circulating in the apparatus, clearly shows the advantages of using vortex spraying countercurrent mass transfer apparatuses and reducing the cost of their operation. To this economic effect, one should also add financial savings from reducing the material consumption of the apparatus by 5–7 times.

Another essential characteristic of mass transfer equipment is removing products from one cubic meter of the apparatus.

In Table 6.3, data are presented comparing various designs of mass transfer apparatus.

As can be seen from the data analysis on the removal of products from a unit volume of the mass transfer chamber, this indicator also confirms the efficiency of using the usable volume in the mass transfer chamber of the vortex apparatus.

Table 6.3
Specific productivity of the apparatus

Type of the apparatus/column	Specific productivity, $m^3/(s \cdot m^3)$
A column with plane-parallel packing (nozzle height – 24 mm)	8.0
A column with plane-parallel packing (nozzle height – 7 mm)	7.7
A column with capped plates	2.4
A column with sieve plates (free cross-section – 15 %)	2.7
A column with sieve plates (free cross-section – 27 %)	1.7
A column with sieve plates (free cross-section – 36 %)	3.3
A column with valve plates	2.6
A column with Kittel's plates	2.6
Nozzle in film mode	2.0
Packed emulsification column	11.0
Liquid dispersion injector	6.6
Vortex countercurrent apparatus	11.7

In some cases, this value is an order of magnitude higher than a similar criterion in individual designs of contact devices, which indicates the expediency of using vortex countercurrent apparatuses in processes where it is necessary to separate a large amount of product.

The general scheme of a multi-stage vortex apparatus with phase counterflow in the contact zone is shown in Figure 6.1.

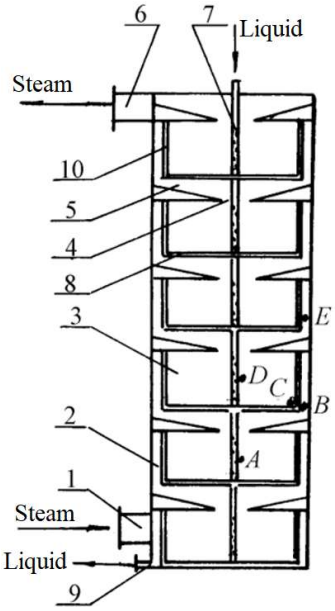

Figure 6.1 – Multistage vortex atomizing mass transfer apparatus: 1 – steam supply pipe; 2 – chamber for supplying steam to tangential slots; 3 – mass transfer chamber; 4 – steam removal from the chamber; 5 – radial diffuser; 6 – branch pipe for removing steam from the apparatus; 7 – atomizer; 8 – liquid collection chamber; 9 – removal of liquid from the apparatus; 10 – the cylindrical wall of the mass transfer chamber with tangential slots for steam supply

The inner part of the column's design is greatly simplified compared to tray equipment. The consumption of materials decreases because the mass transfer chambers are made in the form of hollow cylinders.

Since the specific hydraulic resistance of the vortex apparatus is somewhat lower than that of the replaceable trays,

a decrease in the overall resistance of the column and associated energy costs follows.

Note that in the spray zone, due to the achievement of high gas velocities, the size of the static pressure is significantly reduced, improved conditions are created for the rectification process, similar to the vacuum rectification process.

The liquid from flow next to the previous stage in a multistage vortex apparatus, in the direction of gas (steam) movement, occurs due to the difference in static pressures, and the height of the stages' location is explained by Figure 6.2.

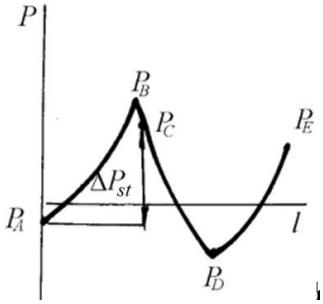

Figure 6.2 – Change in static pressure: l – the steam path; ΔP_{st} – pressure difference between the atomizing zone and the liquid outlet area resulting from the change in a steam velocity

Other layouts of the vortex stages are possible. Particularly, an industrial design of the apparatus with three parallel-connected devices was installed in JSC "Svema" (Shostka, Ukraine). The diameter of each of the devices is 3.3 m. They are designed to clean industrial emissions from dimethylformamide (dimethylacetamide).

Thus, a number of these factors indicate the prospects for the development and use of vortex apparatus with phase counterflow in the contact zone in various industries.

6.2 Rational choice of the design

The design features of the apparatus design in the general case depend on many factors such as the physical composition of the media, the consumption of gas (steam) and liquid (reflux), the location of the axis of the apparatus in the working position, the gas velocity at the outlet of the mass transfer chamber. But you can highlight the main features and give recommendations that must be considered in the development process.

The mass transfer chamber consists of two covers and a cylindriccal body. A tangential slot is made in the body for supplying liquid. It is advisable to provide several tangential slots to create a symmetrical gas flow. Suppose fluctuations in gas flow rate are possible during operation, then due to changes in inlet velocity and circumferential velocity in the spray area. In that case, it is possible to change the dispersion of the spray cone, which entails changes in the composition of the resulting products, reducing the apparatus's efficiency.

In this case, it is possible to install special control dampers or valves in the tangential slots to regulate the slots' width. This will lead to a change in the inlet velocity of the gas flow, which in turn will increase the gas velocity in the spray area since the value of this velocity is related to the value of the gas flow velocity in the inlet tangential slots. The diameter of the resulting droplets depends on the tangential velocity of the gas in liquid spraying. It is possible to provide for automatic control of inlet velocity depending on changes in flow parameters, which is achieved by installing, for example, spring-loaded shutters in the input slots or other similar devices.

When choosing the geometric dimensions, the ratio of the height of the vortex mass transfer chamber to its radius, on which tangential slots are installed for the input of the gas flow, must be less than one. This is necessary to create a flat vortex

flow of gas (steam) even at significant ratios of the radius on which these blades are installed with tangential slots R_1 and the radius of the gas outlet pipe from the apparatus R_2, usually located in one of the end caps.

In a single-stage apparatus design, to create a symmetrical gas outlet from the vortex working chamber and equalize the flow along with the height of the mass transfer chamber, it is possible to perform a gas outlet in the form of two holes both end caps.

In the gas outlet, to reduce the intensity of the end currents, a cylindrical protrusion should be located, facing the inside of the mass transfer chamber.

After the gas outlet from the mass transfer chamber, there is a radial diffuser, after which the gas outlet from the apparatus or a chamber for supplying gas to the tangential slots of the vortex mass transfer chamber of the next stage follows. When performing gas removal in a single hole in the mass transfer chamber, it must be in the upper-end cap.

Much attention should be paid to the correct design and location of the liquid outlets from the mass transfer chamber.

The location of the axis in the working position horizontally contributes to the uniform removal of liquid from the cylindrical walls of the chamber. In this case, the slots for draining liquid are in the lower part of the body. Behind them, there is a chamber for collecting liquid, from where the liquid will be removed from the device.

If the axis of the apparatus in the working position is located vertically, then the design of the liquid outlets becomes somewhat more complicated. Such a withdrawal can be made in vertical slots located along with the entire height of the cylindrical body on the inner side of this body. The slots are connected to cavities on the outer side, along with the entire height. In the lower part, holes are provided for draining liquid

into the chambers for collecting liquid. After, the liquid is removed from the apparatus. Each slot has its cavity for draining liquid, or they can be combined.

In addition, at the base of the cylindrical body, in the lower end cap, it is necessary to provide holes connected to the chamber for collecting liquid. The need for such holes is due to the liquid downflow on the cylindrical wall and the refill of the end flow.

The design of the spraying device, which is installed in the central region of the vortex mass transfer chamber, is possible in three main design options (e.g., a cylindrical atomizer in the center of the apparatus). Here it is necessary to consider the possibility of increasing spray entrainment when spraying liquid at 1/3 of the height of the vortex working chamber from the end cover, in which the gas outlet is located.

The second possible design is an outer surface diameter close to the gas outlet diameter. Nozzles for introducing liquid into the gas flow are located on the outer surface and the chamber's entire height.

And the third, more complex in terms of implementation and operation, is the design of a rotating atomizer. Its shell, from which the liquid flows into the gas flow, is in the central region of the mass transfer chamber. The drive for rotation is a lattice of plates located in the radial diffuser and is connected by a shaft to the atomizer shell. In this design, the energy of the rotating gas flow at the outlet of their mass transfer chamber is additionally used to atomize the liquid into droplets.

These are, in brief, the main requirements for the design of a vortex spraying countercurrent mass transfer apparatus.

6.3 Calculation of the main geometric dimensions of the flow path

A sequence for calculating mass transfer and hydrodynamic characteristics, which in turn determine the dimensions of the apparatus, its resistance, and the layout of individual elements are recommended below:

1. The amount of transferred substance is determined from the material balance equation.

2. Given the required spray dispersion (liquid droplet diameter) and phase load ratio ($L/G < 1$), the volumetric mass transfer coefficient and the required relative phase velocities in the spray zone (3.18) are determined (5.13).

3. According to equation (5.14), the working volume of the mass transfer chamber is approximately determined.

4. Choose sprayer design.

5. According to the flow rate of the gas (steam) flow and the recommended velocity, the size of the gas outlet from the mass transfer chamber is found.

6. Based on the known gas velocities, given by the value of the gas velocity at the chamber inlet, in the spray zone, and the radius of the gas outlet pipe, the estimated radius of the mass transfer chamber (4.19) and (1.4) is determined using an empirical dependence.

7. If spraying is performed by introducing a jet in the central region, the deviation of the jet direction from the radial direction, the acquisition of circumferential velocity by the liquid, and the decrease in the relative velocity of the phases are evaluated. In this case, a correction is introduced in Chapter 4 under the assumption that spraying occurs near a cylindrical surface with a radius equal to the radius of the gas outlet from the chamber. The necessary relative velocities are also determined in that chapter.

8. The decrease in circumferential velocities of the gas due to the introduction of the liquid phase is calculated. In this case, the ratio of loads in the gas and liquid phases (3.42) is considered.

9. The value of the relative phase velocities in the spray area is corrected.

10. Starting from #6, the results are recalculated. Simultaneously, the refined size of the working chamber is determined, and the theoretical dependencies (3.29), (3.67), and (3.48) are used. The calculations are repeated until the results converge.

11. Known radiuses of the vortex mass transfer chamber, gas outlet, and gas velocities at the inlet and outlet determine the field of gas flow velocities (3.29), the velocities of liquid droplets (3.49), and their residence time in the mass transfer chamber.

12. The height of the vortex mass transfer chamber is determined by (3.18).

13. The supply tangential slots' design, area, and number are chosen. This considers the decrease in the gas velocity at the exit from the slots by (4.3) and $V_{\varphi 1} = (0.7–0.9)V_{in}$.

14. The value of the static pressure at the outlet of the mass transfer chamber is determined by (3.32).

15. According to the known parameters, its geometry is calculated at the entrance to the radial diffuser.

16. Energy losses are determined in the mass transfer chamber, diffuser, and the apparatus as a whole.

17. Calculation of liquid outlets, their throughput.

18. A verification calculation of hydrodynamics is performed, consisting of the following. From the known gas velocity near the cylindrical wall and the circumferential velocity of the gas flow not perturbed by the liquid, the field of velocities and pressures of a single-phase flow in the mass

transfer chamber is determined. These velocity and pressure fields are corrected considering the presence of a liquid phase. And according to the results of such calculations, the parameters of the droplet flow are determined.

19. By changing the ratio of loads by phases, they determine the zone of stable operation find the boundary of a possible transition to the cocurrent mode by phases (dangerous mode of disruption of the apparatus).

20. The design development of the apparatus is being carried out, corrections that arise during the design process are introduced into the hydrodynamic calculations due to possible special requirements that are imposed on the dimensions of the apparatus and its location.

Subject Index

References

1. Petrov, S., Nosova, A., Bashkirtseva, N., Fakhrutdinov, R. (2019). Features of heavy oil spraying with single evaporation. IOP Conference Series: Earth and Environmental Science, Vol. 282(1), 012004, doi: 10.1088/1755-1315/282/1/012004.

2. Panda, A., Kumar, A., Mohapatra, S.S. (2020). Water soluble polymer added high mass flux spray: A novel approach for the attainment of enhanced heat transfer rate in transition boiling regime. International Journal of Heat and Mass Transfer, Vol. 157, 119838, doi: 10.1016/j.ijheatmasstransfer.2020.119838.

3. Jia, P., Chen, J., Cai, X., Kong, L., Wang, C., Shang, C., Zhang, M., Shi, Y. (2021). Study on oil-water separation characteristics of hydrocyclone based on CFD-PBM numerical simulation. Journal of Petrochemical Universities, Vol. 34(4), pp. 58–65, doi: 10.3969/j.issn.1006-396X.2021.04.010.

4. Sklabinskyi, V., Pavlenko, I. (2021). Intensification of mass transfer processes through the impact of the velocity gradient on hydrodynamics and stability of liquid droplets in a gas flow. Chemical Engineering Science, Vol. 235, 116470, doi:10.1016/j.ces.2021.116470.

5. Leont'ev, A.I., Kuzma-Kichta, Y.A., Popov, I.A. (2017). Heat and mass transfer and hydrodynamics in swirling flows (review). Thermal Engineering, Vol. 64(2), pp. 111–126, doi: 10.1134/S0040601517020069.

6. Moskalev, L.N., Ponikarov, S.I. (2016). Use of a vortex-type contact condenser in absorption of methanol and formaldehyde from a contact gas. Journal of Engineering

Physics and Thermophysics, Vol. 89(5), pp. 1179–1185, doi: 10.1007/s10891-016-1481-x.

7. Savelyeva, A.V., Nemudraya, A.A., Podgornyi, V.F., Laburkina, N.V., Ramazanov, Y.A., Repkov, A.P., Kuligina, E.V., Richter, V.A. (2017). Analysis of the efficiency of recombinant Escherichia coli strain cultivation in a gas-vortex bioreactor. Biotechnology and Applied Biochemistry, Vol. 64(5), pp. 712–718, doi: 10.1002/bab.1527.

8. Yeshzhanov, A., Volnenko, A., Zhumadullayev, D., Korganbayev, B. (2019). Calculation of hydrodynamic characteristics of combined apparatuses with a regular-suspended packing. International Review of Mechanical Engineering, Vol. 13(7), pp. 382–389, doi: 10.15866/ireme.v13i7.16645.

9. Antipov, S.T., Drannikov, A.V., Poymanov, V.V., Pribytkov, A.V., Yurova, I.S. (2019). Mathematical model of the drying process of capillaryporous materials particles in the apparatus with a suspended-swirled flow of heat-carrying medium. EurAsian Journal of BioSciences, Vol. 13(2), pp. 1051–1056.

10. Naumov, I.V., Kashkarova, M.V., Mikkelsen, R.F., Okulov, V.L. (2020). The structure of the confined swirling flow under different phase boundary conditions at the fixed end of the cylinder. Thermophysics and Aeromechanics, Vol. 27(1), pp. 89–94, doi: 10.1134/S0869864320010084.

11. Abdelghfar, M.M., Beshay, K.R., Elhariry, G., Khalil, E.E. (2020). Swirling flow patterns through refrigerator vortex tubes. *AIAA Scitech 2020 Forum*, Vol. 1, Part F, pp. 1–13, doi: 10.2514/6.2020-1935.

12. Koshlak, H., Pavlenko, A. (2020). Mathematical model of particle free settling in a vortex apparatus. Rocznik Ochrona Srodowiska, Vol. 22(2), pp. 727–734.

13. Xue, Y., Binns, J. R., Arjomandi, M., Yan, H. (2019). Experimental investigation of the flow characteristics within a vortex tube with different configurations. International Journal of Heat and Fluid Flow, Vol. 75, pp. 195–208, doi: 10.1016/j.ijheatfluidflow.2019.01.005.

14. Kuzmin, A.O. (2021). Confined multiphase swirled flows in chemical engineering. Reviews in Chemical Engineering, Vol. 37(1), pp. 31–68, doi: 10.1515/revce-2019-0019.

15. Tutubalina, V.P., Korotkova, E.G., Maminov, O.V. (1983). Hydraulic resistance of an apparatus with tangential plate swirlers. Chemical and Petroleum Engineering, Vol. 19(7), pp. 278–280, doi: 10.1007/BF01156395.

16. Lemenand, T., Durandal, C., Della Valle, D., Peerhossaini, H. (2010). Turbulent direct-contact heat transfer between two immiscible fluids. International Journal of Thermal Sciences, Vol. 49(10), pp. 1886–1898, doi: 10.1016/j.ijthermalsci.2010.05.014.

17. Moskalev, L.N., Ponikarov, S.I. (2016). Use of a vortex-type contact condenser in absorption of methanol and formaldehyde from a contact gas. Journal of Engineering Physics and Thermophysics, Vol. 89(5), pp. 1179–1185, doi: 10.1007/s10891-016-1481-x.

18. Ren, W., Jin, N. (2021). Nonlinear interaction underlying flow structure transition of inclined oil–water two-phase countercurrent flow. European Physical Journal Plus, Vol. 136(5), 560, doi: 10.1140/epjp/s13360-021-01555-0.

19. Romanyuk, R.V., Lagutkin, M.G., Danilenko, N.V. (2020). Influence of the design of the upper vortex swirl on hydrodynamics of a vortex dust collector. Chemical and Petroleum Engineering, Vol. 56(7-8), pp. 548–553, doi: 10.1007/s10556-020-00808-6.

20. Fedoreiko, V.S., Rutylo, M.I., Iskerskyi, I.S., Zahorodnii, R.I. (2020). Optimization of heat production processes in the biofuel vortex combustion systems. Naukovyi Visnyk Natsionalnoho Hirnychoho Universytetu, Vol. 6, pp. 83–88, doi: 10.33271/NVNGU/2020-6/083.

21. Belinskaia, I., Zainetdinov, R., Evdokimov, K. (2020). On the issue of reducing the negative impact of nitrogen oxides in the system recirculation of diesel exhaust gases on applying the vortex effect. E3S Web of Conferences, Vol. 221, 165905, doi: 10.1051/e3sconf/202022102006.

22. Khmelev, V.N., Shalunov, A.V., Nesterov, V.A. (2020). Improving the separation efficient of particles smaller than 2.5 micrometer by combining ultrasonic agglomeration and swirling flow techniques. PLoS ONE, Vol. 15(9), doi: 10.1371/journal.pone.0239593.

23. Mahotkin, A.F., Mahotkin, I.A., Starkova, A.V. (2019). Technology for cleaning off-gases from dust in vortex devices with closed water circulation. IOP Conference Series: Earth and Environmental Science, Vol. 288(1), 012016, doi: 10.1088/1755-1315/288/1/012016.

24. Pitak, I., Shaporev, V., Briankin, S., Komarysta, B., Nechyporenko, D. (2019). Development of a highly efficient combined apparatus (A combination of vortex chambers with a bin) for dry dedusting of gases. Eastern-European Journal of Enterprise Technologies, Vol. 3(10-99), pp. 49–55, doi: 10.15587/1729-4061.2019.170134.

25. Kulkarni, S.R., Vandewalle, L.A., Gonzalez-Quiroga, A., Perreault, P., Heynderickx, G.J., Van Geem, K.M., Marin, G.B. (2018). Computational fluid dynamics-assisted process intensification study for biomass fast pyrolysis in a gas-solid vortex reactor. Energy and Fuels, Vol. 32(10), pp. 10169–10183, doi: 10.1021/acs.energyfuels.8b01008.

26. Brand, J.F., Van Dyk, J.C., Waanders, F.B. (2018). Conceptual use of vortex technologies for syngas purification and separation in UCG applications. Journal of the Southern African Institute of Mining and Metallurgy, Vol. 118(10), pp. 1029–1039, doi: 10.17159/2411-9717/2018/v118n10a3.

27. Voynov, N.A., Zhukova, O.P., Kozhukhova, N.Y., Bogatkova, A.V. (2018). Vortex gas-liquid separator. Khimiya Rastitel'nogo Syr'ya, Vol. 2, pp. 217–223, doi: 10.14258/jcprm.2018023448.

28. Sklabinskij, V.I., Kholin, B.G. (1992). Intesification of internal currents in drop moving in gas flow with cross velocity gradient. Teoreticheskie Osnovy Khimicheskoi Tekhnologii, Vol. 26(5), pp. 741–745.

29. Alekseenko, S., Kuibin, P., Okulov, V., Shtork, S. (1999). Helical vortices in swirl flow. Journal of Fluid Mechanics, Vol. 382, pp. 195–243, doi: 10.1017/S0022112098003772.

30. Evdokimov, O., Prokhorov, D., Guryanov, A., Veretennikov, S. (2022). Transient numerical simulations of a cold-flow bidirectional vortex chamber. Physics of Fluids, Vol. 34(1), doi: 10.1063/5.0079224.

31. Samruaisin, P., Chuwattanakul, V., Pimsarn, M., Promthaisong, P., Saysroy, A., Chokphoemphun, S., Kumar, M., Eiamsa-ard, S. (2021). Influence of a double vortex chamber on temperature reduction in a counter-flow vortex tube. Case Studies in Thermal Engineering, Vol. 28, doi: 10.1016/j.csite.2021.101662.

32. Gonzalez-Quiroga, A., Shtern, V., Perreault, P., Vandewalle, L., Marin, G.B., Van Geem, K.M. (2021). Intensifying mass and heat transfer using a high-g stator-rotor vortex chamber. Chemical Engineering and Processing - Process Intensification, Vol. 169, doi: 10.1016/j.cep.2021.108638.

33. Tukmakov, A.L., Tukmakova, N.A. (2021). A model of polydisperse vapor–droplet mixture flow in a vortex chamber. Journal of Engineering Physics and Thermophysics, Vol. 94(4), pp. 910–918, doi: 10.1007/s10891-021-02367-w.

34. Chen, L., Shanbhogue, S., Pannala, S., Shtern, V., Ghoniem, A., West, D. (2021). A nonpremixed annular jet vortex chamber reactor for methane pyrolysis under oxygen-enriched conditions. Industrial and Engineering Chemistry Research, Vol. 60(19), pp. 7443–7453, doi: 10.1021/acs.iecr.1c00131.

35. Vikulin, A.V., Yaroslavtsev, N.L. (2020). Investigation of thermohydraulic characteristics of vortex chambers. Thermal Engineering, Vol. 67(8), pp. 554–559, doi: 10.1134/S004060152008008X.

36. Wang, J., Du, C., Wu, F., Li, L., Fan, X. (2019). Investigation of the vortex cooling flow and heat transfer behavior in variable cross-section vortex chambers for gas turbine blade leading edge. International Communications in Heat and Mass Transfer, Vol. 108, doi: 10.1016/j.icheatmasstransfer.2019.104301.

37. San, Y. K., Thien, R., Lee Chieng Chen, V. (2019). Numerical study on erosion of a pipe bend with a vortex chamber. Particulate Science and Technology, Vol. 37(2), pp. 200–206, doi: 10.1080/02726351.2017.1360973.

38. Dutta, S., Loha, C., Chatterjee, P.K., Kumar Sadhukhan, A., Gupta, P. (2018). Numerical investigation of gas-particle hydrodynamics in a vortex chamber fluidized bed. Advanced Powder Technology, Vol. 29(12), pp. 3357–3367, doi: 10.1016/j.apt.2018.09.014.

39. Pitsukha, E.A. (2018). On numerical simulation of the hydrodynamics and mixing of gas flows in a vortex chamber. Journal of Engineering Physics and Thermophysics, Vol. 91(5), pp. 1127–1137, doi: 10.1007/s10891-018-1840-x.

40. Voronin, D.V. (2017). Gas self-ignition in a plane vortex chamber. Combustion, Explosion and Shock Waves, Vol. 53(5), pp. 510–516, doi: 10.1134/S0010508217050033.

41. Verma, V., Li, T., De Wilde, J. (2017). Coarse-grained discrete particle simulations of particle segregation in rotating fluidized beds in vortex chambers. Powder Technology, Vol. 318, pp. 282–292, doi: 10.1016/j.powtec.2017.05.037.

42. Abdrakhmanov, R.K., Dvornikov, N.A., Lukashov, V.V. (2017). Dynamics of two-phase swirling flow in a vortex chamber with a lower end swirler. Thermophysics and Aeromechanics, Vol. 24(3), pp. 339–346, doi: 10.1134/S0869864317030027.

43. Trujillo, W.R., De Wilde, J. (2017). Influence of solids outlets and the gas inlet design on the generation of a gas-solids rotating fluidized bed in a vortex chamber for different types of particles. Chemical Engineering Science, Vol. 173, pp. 74–90, doi: 10.1016/j.ces.2017.07.031.

44. Abdrakhmanov, R.K., Lukashov, V.V., Makarov, M.S., Naumkin, V.S. (2016). Dynamics of the end-face boundary layer and hydraulic resistance of a vortex chamber with a side swirler. Journal of Engineering Physics and Thermophysics, Vol. 89(5), pp. 1202–1211, doi: 10.1007/s10891-016-1483-8.

45. De Wilde, J., Richards, G., Benyahia, S. (2016). Qualitative numerical study of simultaneous high-G-intensified gas–solids contact, separation and segregation in a bi-disperse rotating fluidized bed in a vortex chamber. Advanced Powder Technology, Vol. 27(4), pp. 1453–1463, doi: 10.1016/j.apt.2016.05.005.

46. Xu, Q., Wang, J., Xie, J. (2021). 3D numerical simulation and performance analysis of CO_2 vortex tubes. Applied Sciences, Vol. 11, 9386, doi: 10.3390/app11209386.

47. Wang, J., Du, C., Wu, F., Fan, X., Li, L. (2018). Effects of jet nozzle circumferential position and vortex chamber draft angle on the flow and heat transfer characteristics of vortex cooling. Journal of Xi'an Jiaotong University, Vol. 52(11), pp. 65–72, doi: 10.7652/xjtuxb201811010.

48. Rogovyi, A., Khovanskyy, S. (2017). Application of the similarity theory for vortex chamber superchargers. IOP Conference Series: Materials Science and Engineering, Vol. 233(1), doi: 10.1088/1757-899X/233/1/012011.

49. Baumert, H.Z. (2013). Universal equations and constants of turbulent motion. Physica Scripta, Vol. 88(T155), doi: 10.1088/0031-8949/2013/T155/014001.

50. Bai, X.-D., Zhang, W. (2022). Machine learning for vortex induced vibration in turbulent flow. Computers and Fluids, Vol. 235, doi: 10.1016/j.compfluid.2021.105266.

51. Ochowiak, M., Włodarczak, S., Pavlenko, I., Janecki, D., Krupińska, A., Markowska, M. (2019). Study on interfacial surface in modified spray tower. Processes, Vol. 7(8), doi: 10.3390/pr7080532.

52. Markadeh, R.S., Arabkhalaj, A., Ghassemi, H., Azimi, A. (2020). Droplet evaporation under spray-like conditions. International Journal of Heat and Mass Transfer, Vol. 148, doi: 10.1016/j.ijheatmasstransfer.2019.119049.

53. Lin, C.-H., Kuo, C.-W., Sun, C.-L. (2022). Performance enhancement of intermittent spray cooling with a self-rewetting fluid for relatively high-temperature applications. International Journal of Heat and Mass Transfer, Vol. 183, doi: 10.1016/j.ijheatmasstransfer.2021.122101.

54. Lübbert, C., Peukert, W. (2018). The mass transfer at taylor cones. Journal of Aerosol Science, Vol. 123, pp. 39–51, doi: 10.1016/j.jaerosci.2018.05.014.

55. Rayleigh, F.R.S. (1878). On the instability of jets. Proceedings of the London Mathematical Society, Vol. s1-10(1), doi: 10.1112/plms/s1-10.1.4.

56. Nukiyama, S., Tanasawa, Y. (1939). An experiment on the atomization of liquid : 3rd report, on the distribution of the size of droplets. Transactions of the Japan Society of Mechanical Engineers, Vol. 5(18), pp. 131–135, doi: 10.1299/kikai1938.5.131.

57. Lewis H.C., Edwards D.G., Goglia M.J., Rice R.J., Smith L.W. (1948). Atomization of liquids in high-velocity cas stream. Industrial and Engineering Chemistry, Vol. 40(1), pp. 67–74.

58. Bitron, M.D. (1955). Atomization of liquids by supersonic air jets. Industrial and Engineering Chemistry, Vol. 47(1), pp. 23–28, doi: 10.1021/ie50541a019.

59. Pavlenko, I., Sklabinskyi, V., Doligalski, M., Ochowiak, M., Mrugalski, M., Liaposhchenko, O., Liaposhchenko, O., Skydanenko, M., Ivanov, V., Włodarczak, S., Woziwodzki, S., Kruszelnicka I., Ginter-Kramarczyk, D., Michałek, B. (2020). The mathematical model for the secondary breakup of dropping liquid. Energies, Vol. 13(22), doi: 10.3390/en13226078.

60. Bordás, R., Roloff, C., Thévenin, D., Shaw, R.A. (2013). Experimental determination of droplet collision rates in turbulence. New Journal of Physics, Vol. 15, doi: 10.1088/1367-2630/15/4/045010.

61. Yang, J.-C., Chang, K.-C. (2001). Investigation on droplets' turbulence characteristics of hollow-cone spray in far downstream region. Transactions of the Aeronautical and Astronautical Society of the Republic of China, Vol. 33(3), pp. 193–199.

62. Liu, R., Zhang, B., Feng, W. (2013). A new model of critical liquid carrying in gas wells. Advanced Materials

Research, Vol. 616–618, pp. 730–736, doi: 10.4028/www.scientific.net/AMR.616-618.730.

63. Brennen, C.E. (2005). Fundamentals of Multiphase Flows. Cambridge University Press, Cambridge, UK.

64. Gal-or, Benjamin, Padmanabhan, Lakshminarasimha (1968). Coupled energy and multicomponent mass transfer in dispersions and suspensions with residence time and size distributions. AIChE Journal, Vol. 14(5), pp. 709–714, doi: 10.1002/aic.690140506.

65. Ishii, M., Zuber, N. (1979). Drag coefficient and relative velocity in bubbly, droplet or particulate flows. AIChE Journal, Vol. 25(5), pp. 843–855, doi: 10.1002/aic.690250513.

66. Elizarov, D.V., Elizarov, V.V., Kamaliev, T.S., D'yakonov, S.G. (2016). Mathematical modeling of mass transfer in laminar motion of a droplet in a liquid medium. Journal of Engineering Physics and Thermophysics, Vol. 89(2), pp. 305–316, DOI: 10.1007/s10891-016-1380-1.

67. Kupershtokh, A.L. (2018). Droplet flow along the wall of rectangular channel with gradient of wettability. AIP Conference Proceedings, Vol. 1939, doi: 10.1063/1.5027358.

68. Scapin, N., Dalla Barba, F., Lupo, G., Rosti, M.E., Duwig, C., Brandt, L. (2022). Finite-size evaporating droplets in weakly compressible homogeneous shear turbulence. Journal of Fluid Mechanics, Vol. 934, doi:10.1017/jfm.2021.1140.

69. Adzhemyan, L.T., Vasil'ev, A.N., Grinin, A.P., Kazansky, A.K. (2006). Self-similar solution to the problem of vapor diffusion toward the droplet nucleated and growing in a vapor-gas medium. Colloid Journal, Vol. 68(3), pp. 381–383, doi: 10.1134/S1061933X06030173.

70. Al-Sharafi, A., Yilbas, B.S., Sahin, A.Z., Al-Qahtani, H. (2020). Heating analysis of a water droplet in between multi-wall hydrophobic surfaces. Journal of Thermal

Science and Engineering Applications, Vol. 12(5), doi: 10.1115/1.4046609.

71. Al-Sharafi, A., Yilbas, B.S. (2019). Thermal and flow analysis of a droplet heating by multi-walls. International Journal of Thermal Sciences, Vol. 138, pp. 247–262, doi: 10.1016/j.ijthermalsci.2018.12.048.

72. Demianenko, M., Liaposhchenko, O., Pavlenko, I., Luscinski, S., Ivanov, V. (2020). Methodology of experimental research of aeroelastic interaction between two-phase flow and deflecting elements for modular separation devices. Advanced Manufacturing Processes. InterPartner 2019. Lecture Notes in Mechanical Engineering. Springer, Cham, pp. 489–499, doi: 10.1007/978-3-030-40724-7_50.

73. Lukashov, V.K., Kostiuchenko, Y.V., Timofeev, S.V., Ochowiak, M. (2020). An experimental study of heat and mass transfer in a falling liquid film evaporation into a crossflow of neutral gas. Journal of Engineering Sciences, Vol. 7(1), pp. F30–F38, doi: 10.21272/jes.2020.7(1).f3.

74. Czernek, K., Ochowiak, M., Janecki, D., Zawilski, T., Dudek, L., Witczak, S., Krupińska, A., Matuszak, M., Włodarczak, Hyrycz, M., Pavlenko, I. (2021). Sedimentation tanks for treating rainwater: CFD simulations and PIV experiments. Energies, Vol. 14(23), doi: 10.3390/en14237852.

75. Zahari, N.M., Zawawi, M.H., Ng, F.C., Sidek, L.M., Abas, A., Nurhikmah, F., Aziz, N.A., Hao, T.L., Radzi, M.R.M. (2022). Particle image velocimetry dynamic analysis on the penstock vortex flow for the dam reliability study. Lecture Notes in Civil Engineering, Vol. 202, pp. 493–501, doi: 10.1007/978-981-16-6978-1_38.

76. Ramm, V.M. (1976). Absorption of Gases. Chemistry Publishing House, Moscow, Russia.

77. Molokanov, Y.K. et al. (1973). Comparative performance characteristics of modern high-performance tray

designs. 3rd All-Union Conference on the Theory and Practice of Rectification. Severodonetsk, Ukraine, Vol. 2, pp. 65–68.

Sklabinskyi Vsevolod Ivanovych,
Pavlenko Ivan Volodymyrovych,
Pitel' Ján

Monitoring of Hydrodynamics and Mass Transfer in Vortex Flows

First edition
Number of pages: 244
Number of figures: 78
Number of tables: 8
Number of formulas: 181
Number of copies: 100

Publisher: RAM-Verlag
Stüttinghauser Ringstr. 44
D-58515 Lüdenscheid
Germany
RAM-Verlag@t-online.de
http://www.ram-verlag.eu

ISBN 978-3-96595-021-4